Flow Properties of Fully Nonlinear Model Equations for Surface Waves

Zahra Khorsand

Thesis for the degree of philosophiae doctor (PhD)
at the University of Bergen

2017

Date of defence: 03.11.2017

Preface

This dissertation is submitted for the degree of Doctor of Philosophy in Applied Mathematics at the Department of Mathematics, University of Bergen. The work on the thesis started in August 2012. The working environment has been the Department of Mathematics in Bergen. The work supervised by Prof. Henrik Kalisch from the Department of Mathematics at the University of Bergen.

The thesis consists of two parts. General background information and a summary of the papers are found in Part I of the thesis. Part II consists of 4 papers written during the work with the thesis. The titles, authors and publishers of these papers are:

Paper A: Particle trajectories in the Serre equations. Zahra Khorsand. Published in *Applied Mathematics and Computation* 230, 2014.

Paper B: Mechanical balance laws for fully nonlinear and weakly dispersive water waves. H. Kalisch, Z. Khorsand and D. Mitsotakis. Published in *Physica D* 333, 2016.

Paper C: A kinematic conservation law in free surface flow. S. Gavrilyuk, H. Kalisch and Z. Khorsand. Published in *Nonlinearity* 28, 2015.

Paper D: On the shoaling of solitary waves in the KdV equation. Z. Khorsand and H. Kalisch. Published in *Proc. 34th Conf. Coastal Engng, Seoul*, 2014.

Acknowledgements

I would like to express my sincere gratitude to my supervisor, Prof. Henrik Kalisch, for the patient guidance, encouragement and advice he has provided to me throughout my time as his student.

I would also like to thank all the professors and all the other members of staff at the Department of Mathematics, the University of Bergen who have been kind enough to advise and help me in their respective roles. I take this opportunity to thank Prof. Sergey Gavrilyuk for the great joint work we have done.

My appreciation goes to Tomas Torsvik and Ira Didenkulova for having me in the field work at the island Aegna, Estonia. This experience gave me a good knowledge about wave measurements in the coastal zone and I will never forget the pain of mosquitos' bite in beautiful Aegna island.

I am grateful for the opportunity that I had to visit the University of California, Merced and I would like to express my gratitude for their hospitality and support. I also acknowledge the support by the Research Council of Norway on grant number RCN: 213474/F20. My deep appreciation goes out to Prof. Dimitrios Mitsotakis and his lovely wife, Maria, for their friendship, hospitality and the warmth extended to me during my time in Merced and for always making me feel so welcome. I am also grateful to Prof. Dimitrios Mitsotakis for his invaluable advice and feedback on my work.

I would like to thank my officemate, Amutha Senthilkumar, for all the good times we shared together. A very special thanks to Vincent Teyekpiti for encouraging me and inspiring me and I really appreciate his can-do spirit. I am indebted to all my friends in Bergen who were always so helpful in numerous ways. Special thanks to Novin Balafkan, Sadaf Ghorbani, Laeya Najmi, Nematollah Zamani, Abolpour sisters Samaneh and Asiye.

My heartfelt thanks to my mother and father for always believing in me and encouraging me to follow my dreams. They have taught me about hard work and self-respect, about persistence and about how to be independent. My mother, especially, was a great role model of resilience, strength and character. Special thanks to my sisters, brothers and their families and my parents-in-law, brothers-in-law and their families for their good wishes.

And finally to my sweet and caring husband Mahdi, who has been by my side throughout this PhD program, living every single minute of it, and without him, I would not have had the courage to embark on this journey in the first place. And to my darling Rastin for being such a precious little baby that past one year and filling my heart with joy, and making it possible for me to complete what I started.

Abstract

The focus of this thesis is wave motion in shallow water. In particular, we investigate some properties of flows underneath long waves in shallow water and present the results in two parts. The first part contains a systematic derivation of four balance equations, namely mass, momentum, energy and tangent velocity at the free surface. The asymptotic derivation of the conservation laws is obtained due to the surface motion of long, fully nonlinear water waves. We use the Serre-Green-Naghdi system, which is an asymptotic, fully nonlinear, weakly dispersive wave model to describe the considered waves. It is found that the derived conservation equations are satisfied exactly by the solution of the Serre-Green-Naghdi system when the bottom is flat.

In the case of varying depth, mass and momentum conservation equations are satisfied exactly and the energy conservation is satisfied in an approximate sense. Moreover, they all reduce correctly to the equivalent derivations in both the Boussinesq and the shallow water scalings.

In the case of flat bottom, we find what appears to be a new conservation law in the full Euler system. This conservation laws involves the tangential velocity, and reduces to the well known fourth conservation law in the Serre-Green-Naghdi system.

We also describe particle trajectories in the Serre-Green-Naghdi approximation, and we find that the particles associated with the Serre-Green-Naghdi equations experience a backward drift which is in conflict with the Stokes drift.

In the second part, we apply balance laws associated with the Korteweg-de Vries equation to study the evolution of a shoaling wave. The employed nonlinear expression for energy flux eliminates the discontinuity of wave height which normally appears in such studies. The results show an increase in wave height due to the decrease in water depth and they are in good agreement with the numerical results based on full Euler computations.

Contents

Part I

Introduction

Chapter 1

General Background

Among the most impressive phenomena in nature are surface waves in the ocean. These waves range from the chaotic motions in a violent hurricane to calm and gentle swell on a tropical beach. These natural occurrences are of great interest to scientists and engineers. Scientists are interested in the dynamics and kinematics of the waves and explore how they are generated by the wind, why they break and how they interact with currents and sea bottom. Predicting wave heights and the occurrences of breaking waves along the shoreline are important for an engineer who has to design, operate or manage structures.

The propagation of gravity waves on the surface of an incompressible, inviscid and homogeneous fluid is widely studied and described by the Euler equations coupled with nonlinear boundary conditions at the free surface and at the bottom. This problem is extremely difficult to solve both theoretically and numerically. The complexity of this problem prompted scientists to derive simpler type of systems to model specific physical regimes. The linear theory of surface gravity waves has been the basic theory for water waves and is based on mass balance equation, momentum balance equation and three simple boundary conditions which describe certain kinematic and dynamic aspects of the waves. However, as waves travel into shallow water the steepness of these waves increase and the waves profiles become nonlinear hence, the linear wave theory is no longer valid.

The aim of this thesis is to extend some properties of the linear theory to the weakly nonlinear and fully nonlinear theory. Studies of long wave phenomena such as undular bores (a transition between two uniform flows of different depth) have been studied by researchers for decades. One comprehensive study was conducted by Favre [22] who classified bores into different types depending on the strength of the bore. In particular, if the difference in flow depths is less than 0.28 times the undisturbed depth, then the bore will feature a laminar flow.

One of the aspects of bores that has inspired some researchers is the well known energy loss, first discovered by Rayleigh [44]. Indeed it can be shown that

since mass and momentum are conserved through the bore, the classical shallow-water theory leads to a finite energy loss. In undular bores, this energy is thought to be radiated by the increasing number of oscillations created at the bore front.

Lemoine [38] used the linear theory to investigate the rate of energy radiation, but his findings were not in good agreement with the experiments conducted by Favre [22]. Benjamin and Lighthill [7] matched a cnoidal solution of the KdV equation with a uniform stream, and found that energy is not conserved, which led them to conclude that an additional dissipation mechanism is needed. Sturtevant [50] employed a cnoidal wave approximation and Favre's experiments and argued that both momentum and energy are not preserved due to the existence of a bottom boundary layer beneath the bore.

Recently, Ali and Kalisch [2, 3] argued that the energy loss predicted by shallow water theory is not due to a dissipation mechanism. They have shown that the energy loss is entirely due to surface oscillations if a higher-order approximation of the energy functional is employed. However, the energy density and flux used in these works does not quite match the expressions obtained in [4] using a more fundamental approach.

One of the main objectives of this thesis has been to extend the method introduced in [4] to the fully nonlinear Serre-Green-Naghdi (SGN) system. In particular, using the SGN framework gives a completely satisfactory explanation that no additional dissipation mechanism is needed to explain the energy loss in an undular bore in the shallow-water theory. As shown in paper B, in contrast to most Boussinesq-type systems, the SGN system features exact energy conservation since the differential energy balance is a direct consequence of the evolution equations. Therefore, the energy loss in weak bores is completely due to the development of surface oscillations, since the energy in the SGN system with a horizontal bottom is exactly conserved.

In addition, in paper B, we extend the method of [4] to the case of non-constant bathymetries and in paper C we also include some work on a balance law in the two-dimensional SGN system. Using the method first proposed in [11], we study numerical simulation of particle trajectories associated with the passage of solitary and periodic solutions of the SGN system. An interesting result here is that periodic waves feature a negative drift apparently in conflict with the well known Stokes drift seen in the linear approximation.

Water waves propagating from deep water into shallower water experience significant changes in height, speed and direction which lead to considerable changes in free surface profiles. Therefore, the wave profile is no longer sinus like. Wave shoaling is the process that starts at the time when the waves feel the effect of the bottom and proceed until they break. If the depth-induced changes in amplitude and direction are sufficiently small, then the linear wave theory with a horizontal bottom can be used locally. However, sometimes the variations in amplitude are

not small and the linear theory requires to be expanded. A great deal of research attempts to predict the waveheight change of shoaling waves considering the linear approximation of energy density and flux in the nonlinear situation. Svendsen and Brink-Kjær [52] found that the variation of the cnoidal wave height is connected to deep water data by assuming the energy flux is the same for the waves described by the linear theory and the cnoidal theory at the matching point between these two theories, which gives a discontinuity in wave height. A part of this thesis has been devoted to compute waveheight of a cnoidal wave solution of the Korteweg-de Vries (KdV) equation and in this study, a nonlinear energy conservation is used and the discontinuity in wave height is eliminated.

The disposition of this thesis is as follows. In this chapter, a kinematic conservation law in the context of the full Euler equations is described. In the next chapter, a brief resume of the linear wave theory and some important features of this theory are given. In the third chapter, the nonlinear waves including the derivation of the Serre-Green-Naghdi equations and the Korteweg-de Vries equation are reviewed. In addition, a study of particle trajectories associated with the propagation of periodic wave solutions of the SGN equations is given. Next, the derivation of balance laws in the asymptotic order of the SGN equations is put forward. Then, the energy loss in undular bores is discussed. Finally, a shoaling theory based on the energy flux corresponding to the Korteweg-de Vries equation is presented.

1.1 Euler equations

It was Leonhard Euler who first formulated the general equations describing the motion of a perfect fluid. The general compressible Euler equations first appeared in published form in 1757 [21]. However, he presented the equations of motion in the incompressible case to the Berlin Academy in 1752 [17]. The incompressible Euler equations consist of conservation of mass and momentum combined with the assumption that the density of the fluid is constant. In this section, we review the derivation of the Euler equations and drive a kinematic conservation law associated with the Euler equations. Firstly, we recall the Reynolds' transport theorem which is needed to derive the Euler equations.

Reynolds' transport theorem

Let F be a function of $(\mathbf{x},t)$ and $\mathcal{V}_t$ be a material volume whose bounding surface moves with the fluid and $\mathbf{u}$ be the velocity field. The Reynolds' transport theorem states that

$$\frac{D}{Dt}\int_{\mathcal{V}_t} F(\mathbf{x},t)\,d\mathcal{V} = \int_{\mathcal{V}_t}\left\{\frac{\partial F}{\partial t} + \nabla\cdot(F\mathbf{u})\right\}d\mathcal{V}, \tag{1.1}$$

where $\frac{D}{Dt} = \frac{\partial}{\partial t} + \mathbf{u} \cdot \nabla$ is the material derivative.

Mass balance

The mass conservation of fluid passing through an element is stated as follows:

the rate of mass accumulation within element =
transport rate of mass in - transport rate of mass out .

We consider a fluid of density $\rho(\mathbf{x},t)$. The mass contained in a material volume $\mathcal{V}(t)$ is given by

$$\int_{\mathcal{V}_t} \rho \, d\mathcal{V}.$$

We assume that the mass of the material volume does not change with time, thus

$$\frac{D}{Dt} \int_{\mathcal{V}_t} \rho \, d\mathcal{V} = 0.$$

Using (1.1) the conservation of mass can be written in local form as

$$\frac{\partial \rho}{\partial t} + \nabla \cdot (\rho \mathbf{u}) = 0,$$

which is called the continuity equation.

Using the product rule $\nabla \cdot (\varphi \mathbf{F}) = (\nabla \varphi) \cdot \mathbf{F} + \varphi(\nabla \cdot \mathbf{F})$, the continuity equation becomes

$$\frac{1}{\rho} \frac{D\rho}{Dt} + \nabla \cdot \mathbf{u} = 0.$$

If the fluid density does not change with pressure, then the fluid is called incompressible and in this case the continuity equation reduces to

$$\nabla \cdot \mathbf{u} = 0.$$

Momentum balance

Wave momentum is a vector property which is the product of the mass and the wave induced velocity of the water particles. Per unit volume, the momentum of a fluid is defined to be $\rho\mathbf{u}$. The total momentum of a material volume $\mathcal{V}(t)$is

$$\int_{\mathcal{V}_t} \rho \mathbf{u} \, d\mathcal{V}.$$

The conservation of momentum states that:

rate of momentum accumulation = rate of momentum in -
rate of momentum out + sum of forces acting on the system .

Let us assume that the only forces acting on the material volume are the surface force P and the gravity force $\rho\mathbf{g}$. Therefore, the momentum equation is given by

$$\mathbf{u}_t + (\mathbf{u}\cdot\nabla)\mathbf{u} = -\frac{1}{\rho}\nabla P - \mathbf{g}.$$

Hence, the incompressible Euler equations consist of momentum equations and the continuity equation:

$$\begin{aligned} \mathbf{u}_t + (\mathbf{u}\cdot\nabla)\mathbf{u} &= -\frac{1}{\rho}\nabla P - \mathbf{g}, \\ \nabla\cdot\mathbf{u} &= 0. \end{aligned} \tag{1.2}$$

The linearized momentum balance equations for the $x-$, $y-$ and $z-$directions are

$$\frac{\partial u}{\partial t} = -\frac{1}{\rho}\frac{\partial p}{\partial x},$$

$$\frac{\partial w}{\partial t} = -\frac{1}{\rho}\frac{\partial p}{\partial y},$$

$$\frac{\partial v}{\partial t} = -\frac{1}{\rho}\frac{\partial p}{\partial z} - g.$$

1.2 Kinematic balance law

The governing equations of a homogeneous, inviscid and incompressible fluid with a free surface over a flat bottom are the incompressible Euler equations with appropriate boundary conditions. In this section, we present a kinematic balance law for the two-dimensional Euler equations (1.2). To begin with, we review some tools to drive this balance law.

Vorticity and circulation

The vorticity ω is defined as the curl of the velocity field

$$\omega = \nabla\times\mathbf{u},$$

and the flow is irrotational when $\omega = \nabla\times\mathbf{u} = 0$.
The circulation around a closed contour C is defined as the line integral of the

velocity along that contour

$$\Gamma = \oint_C \mathbf{u} \cdot d\mathbf{r}.$$

Kelvin-Stokes Theorem

$$\int_S \nabla \times \mathbf{F} \cdot d\mathbf{S} = \oint_{\delta r} \mathbf{F} \cdot d\mathbf{r}. \tag{1.3}$$

This theorem states that the surface integral of the curl of a vector field over a surface S is related to the line integral of the vector field over the boundary of S, called δr.
Applying this theorem to the circulation Γ, we see that

$$\Gamma = \oint_C \mathbf{u} \cdot d\mathbf{r} = \int_S \nabla \times \mathbf{u} \cdot d\mathbf{S} = \int_S \omega \cdot d\mathbf{S} = \int_S \omega \cdot \hat{\mathbf{n}} \, dS, \tag{1.4}$$

where $\hat{n}$ is the unit vector normal to the surface S. Thus, we see that the circulation is an integral measure of the vorticity of the flow.

Kelvin's Circulation Theorem

Kelvin's circulation theorem states that under certain circumstances, the fluid is barotropic (i.e. $P = P(\rho)$) and the forces acting on the flow are conservative, the circulation around a material fluid parcel is conserved. To prove this theorem, we calculate the material derivative of the circulation

$$\begin{aligned}
\frac{D\Gamma}{Dt} = \frac{D}{Dt} \oint \mathbf{u} \cdot d\mathbf{r} &= \oint \left(\frac{D\mathbf{u}}{Dt} \cdot d\mathbf{r} + \mathbf{u} \cdot \frac{D(d\mathbf{r})}{Dt} \right) \\
&= \oint \left(\frac{D\mathbf{u}}{Dt} \cdot d\mathbf{r} + \mathbf{u} \cdot d\mathbf{u} \right) \\
\{\text{using Euler equations}\} &= \oint \left((-\frac{\nabla P}{\rho} - \nabla \Phi) \cdot d\mathbf{r} + \frac{1}{2} d\mathbf{u}^2 \right) \\
&= \oint (-\frac{\nabla P}{\rho}) \cdot d\mathbf{r} \\
\{\text{using Kelvin-Stokes theorem}\} &= \int_S \frac{\nabla \rho \times \nabla P}{\rho^2} \cdot \hat{\mathbf{n}} \, dS,
\end{aligned}$$

where $\nabla\Phi$ and $\frac{1}{2} d\mathbf{u}^2$ vanish because they are exact differentials integrated around a closed loop. For a barotropic fluid the gradient of P is always parallel to the gradient of ρ. Thus, we obtain

$$\frac{D\Gamma}{Dt} = \frac{D}{Dt} \oint \mathbf{u} \cdot d\mathbf{r} = 0.$$

Derivation of a kinematic balance law

We apply the proof of Kelvin's circulation theorem to derive a kinematic balance law for the Euler equations along an open curve which is embedded in the free surface. At the time of this work we have not found a derivation of the kinematic balance law along an open curve, and to the best of our knowledge the derivation presented here is new. We consider the two-dimensional Euler equations (1.2) in the domain

$$\{(x,z)|x \in \mathbb{R}, 0 < z < h_0 + \eta(x,t)\},$$

where $\eta(\mathbf{x},t)$ is the surface elevation and h_0 is the undisturbed fluid depth. Let us consider $\mathcal{L}_t$ as a material arc lying entirely in the free surface with ending points $A(t) = (x_A(t), z_A(t))$ and $B(t) = (x_B(t), z_B(t))$. Let us parametrize the initial arc $\mathcal{L}_0$ by the parameter s ($s_A \leq s \leq s_B$). Then we obtain the description of the arc $\mathcal{L}_t$ in the form

$$\mathbf{x} = \phi(t,s) = (\phi^x(t,s), \phi^z(t,s)), \quad s_A \leq s \leq s_B,$$

where $\dfrac{d\mathbf{x}}{dt} = \mathbf{u}(t,\mathbf{x})$. We define the total drift γ along $\mathcal{L}_t$ in the form

$$\gamma = \int_{\mathcal{L}_t} \mathbf{u} \cdot d\mathbf{x}.$$

Now the time evolution of γ along $\mathcal{L}_t$ is obtained by applying the proof of Kelvin's circulation theorem on a contour which is not necessarily closed, $\mathcal{L}_t$, by using the Euler equations (1.2) and the Reynolds' transport theorem (1.1). At the free surface, $z = h(t,x)$, the pressure vanishes and we get the conservation law

$$\frac{d}{dt}\int_{\mathcal{L}_t} \mathbf{u}\cdot d\mathbf{x} = \Big(\frac{|\mathbf{u}|^2}{2} - gh\Big)\Big|_{A(t)}^{B(t)}.$$

Using the relation

$$\int_{\mathcal{L}_t} \mathbf{u} \cdot d\mathbf{x} = \int_{\mathcal{L}_0} \mathbf{u} \cdot \frac{\partial \phi}{\partial s} ds,$$

the above conservation law can be written in local form in the Lagrangian coordinate as

$$\frac{\partial(\mathbf{u} \cdot \frac{\partial \phi}{\partial s})}{\partial t} + \frac{\partial}{\partial s}\Big(gh - \frac{|\mathbf{u}|^2}{2}\Big) = 0.$$

Introducing $K(t,x)$ defined along $\mathcal{L}_t$ by

$$\mathbf{u}(t,s) \cdot \frac{\partial \phi}{\partial s}(t,s) = K(t,x)\frac{\partial \phi^x}{\partial s}(t,s),$$

we obtain the following conservation law in the Eulerian coordinate (t,x)

$$\frac{\partial K}{\partial t}+\frac{\partial}{\partial x}\Big(uK+gh-\frac{1}{2}(u^2+w^2)\Big)=0, \tag{1.5}$$

which is an exact conservation law for representing the evolution of the tangent velocity K along the free surface. This conservation law holds also for the three-dimensional water wave problem, but in this case, the derived expression is not a pure conservation law. For more details, the reader is referred to [23].

Chapter 2

Linear wave theory

For about 170 years, the linear wave theory also referred to as Airy wave theory [1] has been the fundamental theory for ocean waves. The essential requirement for the linear theory is that the amplitude of the wave is small compared with the wave length and water depth. To develop the linear theory for surface gravity waves, the water is assumed to be incompressible with a constant density and no viscosity. Also, water particles may neither leave the surface nor penetrate the bottom. The particle velocities and wave-induced pressure in the water are presented by a mathematical concept which is known as velocity potential function. To employ this function, the motion of the water particles needs to be irrotational. By using the expressions of particle velocities and wave-induced pressure, one can find expressions for other wave characteristics and phenomena such as shoaling and set-down. The linear theory is based on mass balance equation and momentum balance equation, which can be expressed in terms of the velocity potential function.

2.1 Modeling linear waves

In what follows, we will deal with waves that are two-dimensional, (x,z), where the x-axis is the direction of wave propagation and the z-axis points vertically upwards. let $\mathbf{u} = (u(x,z,t), v(x,z,t))$ be the velocity field of the flow over the flat bottom $z = 0$ and $\eta(x,t)$ denote the free surface of the water and h represent the water depth. Since the motion is irrotational, $\nabla \times \mathbf{u} = 0$, a velocity potential $\phi(x,z,t)$ can be found such that $u = \dfrac{\partial \phi}{\partial x}$ and $v = \dfrac{\partial \phi}{\partial z}$. Substitution into the continuity equation gives an elliptic partial differential equation which is known as

Laplace's equation and is written as

$$\frac{\partial^2 \phi}{\partial x^2} + \frac{\partial^2 \phi}{\partial z^2} = 0, \quad \text{for } x \in \mathbb{R}, \quad -h < z < \eta(x,t).$$

From the linearized momentum balance equation we get the linearized Bernoulli equation

$$\frac{\partial \phi}{\partial t} + \frac{P}{\rho} + gz = 0,$$

where ρ is the water density and P is the pressure. Related to the motions of the water particles and forces acting on the water particles there are three boundary conditions. At the free surface, the kinematic boundary condition is that particles may not leave the surface. In the linearized approach, this is given by

$$v = \frac{\partial \eta}{\partial t} \quad \text{at} \quad z = 0.$$

At the bottom, the kinematic boundary condition is that particles may not penetrate the bottom

$$v = 0 \quad \text{at} \quad z = -h.$$

The dynamic condition states that the atmospheric pressure at the water surface is zero since the wave is only subject to gravity

$$P = 0 \quad \text{at} \quad z = \eta.$$

Taking the linearized Bernoulli equation at the surface $z = \eta$ with $P = 0$ gives

$$\frac{\partial \phi}{\partial t} + g\eta = 0 \quad \text{at} \quad z = \eta.$$

In the linear approximation, the term $\dfrac{\partial \phi}{\partial t}$ can be evaluated at $z = 0$ rather than $z = \eta$ so that

$$\frac{\partial \phi}{\partial t} = -g\eta \quad \text{at} \quad z = 0.$$

2.2 Solution of the problem

One of the analytical solutions of the Laplace equation with the kinematic boundary condition is a harmonic wave with wavenumber k and frequency ω propagating in the positive x-direction

$$\eta(x,t) = a\cos(kx - \omega t), \tag{2.1}$$

with the following velocity potential function

$$\phi = \frac{a\omega}{k}\frac{\cosh k(z+h)}{\sinh kh}\sin(kx-\omega t),$$

from which the velocity components are found as

$$\begin{aligned} u &= a\omega\frac{\cosh k(z+h)}{\sinh kh}\cos(kx-\omega t), \\ v &= a\omega\frac{\sinh k(z+h)}{\sinh kh}\sin(kx-\omega t). \end{aligned} \tag{2.2}$$

The analytical expression for the pressure is readily obtained, by substituting the velocity potential expression into the Bernoulli equation, as

$$P = \underbrace{-\rho g z}_{P_h} + \underbrace{\rho g z\frac{\cosh k(z+h)}{\cos kh}\cos(kx-\omega t)}_{P_{wave}}. \tag{2.3}$$

The first term on the right-hand side is the hydrostatic pressure, denoted by P_h, and the second term is due to the wave and is called the wave-induced pressure, denoted by P_{wave}.

To find a relation between k and ω the dynamic free surface condition is applied. Substitution of the free surface equation and velocity potential function into the dynamic surface condition gives

$$\omega = \sqrt{gk\tanh kh}, \tag{2.4}$$

which is called a dispersion relation. The phase velocity is simply derived by substituting the dispersion relation into $c = \dfrac{\omega}{k}$ which is

$$c = \sqrt{\frac{g}{k}\tanh kh} \quad \text{at arbitrary depth.}$$

In deep water, where $kh \to \infty$, this expression becomes

$$c_0 = \sqrt{\frac{g}{k_0}} \quad \text{or} \quad c_0 = \frac{g}{\omega},$$

and in shallow water, where $kh \to 0$, is

$$c = \sqrt{gh},$$

which shows the waves are non-dispersive under shallow water conditions.

Consider the superposition of two harmonic waves of equal amplitude but slightly different frequencies. Then, the combination propagates at a speed of

$$c_g = \frac{d\omega}{dk},$$

which is called the group velocity. For surface gravity waves whose dispersion relation is (2.4), the group velocity is

$$c_g = \frac{c}{2}\left[1 + \frac{2kh}{\sinh 2kh}\right].$$

In deep water, the group velocity is half of the phase speed and in very shallow water the group velocity is equal to the phase speed.

2.3 Some features of the linear waves

Particle paths

The path of a water particle is generally obtained by integrating the velocity of the particle in time. Consider $(x_0 + \xi(t), z_0 + \zeta(t))$ as the coordinates of a particle whose rest position is (x_0, z_0). For the harmonic surface wave in equation (2.1), the integration in time of (2.2) yields

$$\xi = -a\frac{\cosh k(z_0+d)}{\sinh kd}\sin(kx_0 - \omega t),$$

$$\zeta = a\frac{\sinh k(z_0+d)}{\sinh kd}\cos(kx_0 - \omega t).$$

Elimination of $(kx_0 - \omega t)$ shows that each particle goes through an ellipse

$$\frac{\xi^2}{\left[a\dfrac{\cosh k(z_0+d)}{\sinh kd}\right]^2} + \frac{\zeta^2}{\left[a\dfrac{\sinh k(z_0+d)}{\sinh kd}\right]^2} = 1.$$

In deep water, as $kd \to \infty$, the particles move through circles $r = ae^{kz}$ and in very shallow water, as $kd \to 0$, the particles move in ellipse growing flatter towards the bottom.

However, a numerical computation of a particle path shows that the pathline for one period is not a closed loop.

Stokes drift

By following a specific fluid particle during the time interval we may obtain the Stokes drift which is the difference in end positions. The Stokes drift velocity or mass transport velocity is the average velocity when following a specific particle as it travels with the fluid flow. For arbitrary water depth, it is given by

$$\overline{u}_L = a^2 \omega k \frac{\cosh 2k(z_0+d)}{2\sinh^2(kd)}.$$

Wave energy

The change of position of water particles from their rest state to some other position requires work done against gravitation which is known as potential energy, E_p. Moreover, the wave particles motion represents kinetic energy, E_k. Therefore the total energy in a wave is

$$E = \underbrace{\frac{\rho}{2l}\int_0^l \int_{-h}^0 (u^2+v^2)\,dzdx}_{E_k} + \underbrace{\frac{\rho g}{l}\int_0^l \int_0^\eta z\,dzdx}_{E_p},$$

where l is the wavelength. For a harmonic wave with amplitude a, the total energy is given by

$$E = \frac{1}{2}\rho g a^2, \tag{2.5}$$

which is a second-order property of the wave. The energy transport or energy flux per unit time and per unit crest length is

$$F = Ec_g,$$

which implies that c_g is the speed of energy propagation.

Wave shoaling

As waves travel from deep water into shallower water, the speed of wave propagation decreases. Therefore, kinetic energy which is the energy of motion will decrease. According to the linear wave theory, the total amount of energy in a wave is equally partitioned between kinetic energy and potential energy. Since the total energy is conserved, the decrease in kinetic energy causes an increase in potential energy which is directly proportional to the waveheight. Therefore, the waveheight is increased. This process is called wave shoaling. The change in the waveheight can be calculated by assuming that the energy flux remains constant during wave propagation. Consider two different locations denoted by A and B,

so $(Ec_g)_B = (Ec_g)_A$. Substituting the expression for E in (2.5) where $a = \frac{1}{2}H$ in this equation, the result will be

$$H_B = \left(\frac{c_{g_A}}{c_{g_B}}\right)^{\frac{1}{2}} H_A. \tag{2.6}$$

If we compute the waveheight , H, in shallow water from the waveheight, H_0, in deep water, the equation (2.6) can be simplified to

$$H = \left(\frac{c_0}{2c}\right)^{\frac{1}{2}} H_0.$$

Radiation Stress

The radiation stress is defined as the excess momentum flux due to the presence of the waves. To estimate the total amount of momentum beneath a wave per unit horizontal area, consider a long-crested wave propagating in the positive x-direction and a column of water beneath that wave, from the bottom to the sea surface. The amount of x-momentum per unit surface area and wave period is

$$Q_x = \overline{\int_{-h}^{\eta} \rho u \, dz},$$

where the over-bar denotes averaging over one wave period. Substituting the expression for u in (2.2), the result of the above integration is

$$Q_x = \frac{\rho a^2}{2 \tanh kh} \omega.$$

For this wave, the wave-induced y-momentum which is directed along the crest is zero, because the orbital velocity in the y-direction is zero.

The transport of wave-induced momentum is equivalent to a stress and it is called radiation stress. Firstly, we consider the horizontal transport of x-momentum in the wave direction. The transport S_{xx} through the entire vertical plane, per unit width and averaged over time becomes

$$S_{xx} = \overline{\int_{-h}^{\eta} (\rho u^2 + P_{wave}) \, dz}.$$

Using the data from the linear wave theory yields

$$S_{xx} = \frac{\rho g a^2 kh}{\sinh 2kh} + \frac{1}{4}\rho g a^2 = (2n - \frac{1}{2})E,$$

where $n = \frac{1}{2}(1 + \frac{2kh}{\sinh 2kh})$.

The transport of y-momentum in the y-direction S_{yy} can be expressed as

$$S_{yy} = -\int_{-h}^{0} \rho \overline{u_z^2}\, dz + \frac{1}{4}\rho g a^2 = E\left(\frac{kh}{\sinh 2kh}\right) = (n - \frac{1}{2})E.$$

In addition to S_{xx} and S_{yy}, there are also a transport of x-momentum in the y-direction, S_{xy}, and y-momentum in the x-direction, S_{yx}. The particle motion in the y-direction is zero, thus

$$S_{xy} = 0 = S_{yx}.$$

In deep water, when $kh \to \infty$, the ratio $\dfrac{2kh}{\sinh 2kh}$ tends to zero and so

$$S_{xx} = \frac{1}{2}E, \quad S_{yy} = 0.$$

In shallow water, when $kh \to 0$, the ratio $\dfrac{2kh}{\sinh 2kh}$ tends to 1, therefore,

$$S_{xx} = \frac{3}{2}E, \quad S_{yy} = \frac{1}{2}E.$$

Wave set-down

Wave set-down is the change in mean water level which occurs when water waves encounter a sloping beach. Consider now the balance of momentum between two fixed vertical planes $x = x_0$ and $x = x_0 + dx$. The flux of momentum across these planes are

$$S = S_{xx} + \int_{-h}^{\bar{\eta}} \rho g(\bar{\eta} - z)\, dz = S_{xx} + \frac{1}{2}\rho g(\bar{\eta} + h)^2 \quad \text{and} \quad S + \frac{\partial S}{\partial x}dx,$$

respectively. There is an additional force due to the bottom pressure, since the bottom is not horizontal, $P_h dl$, where dl is the distance between the two planes, measured along the bottom. The horizontal component of this force is

$$P_h \frac{dh}{dl} dl = P_h \frac{dh}{dx} dx.$$

By integrating the equation of vertical motion

$$-\frac{1}{\rho}\frac{\partial P}{\partial z} = g + \frac{\partial v}{\partial t} + (u\frac{\partial v}{\partial x} + v\frac{\partial v}{\partial z}),$$

over the range $-h < z < \eta$, we have

$$P_h = \rho g(h + \bar{\eta}),$$

of the second order approximation [39]. Therefore, the momentum balance gives

$$\frac{dS_{xx}}{dx} + \rho g(\bar{\eta} + h)\frac{d\bar{\eta}}{dx} = 0.$$

Since $\bar{\eta} \ll h$

$$\frac{d\bar{\eta}}{dx} = -\frac{1}{\rho g h}\frac{dS_{xx}}{dx}. \tag{2.7}$$

This shows the gradient of the surface level $\bar{\eta}$ when a constant, small horizontal force $-\dfrac{dS_{xx}}{dx}$ is applied. To find the exact integral of equation (2.7), we assume that no energy is lost by wave breaking and bottom friction and the reflexion of energy is negligible. Then, the wave amplitude may be determined by consideration that the flux of energy F towards the shore is a constant , $F = Ec_g = \text{const.}$. As the depth h changes, c_g changes and so E and S_{xx} will also change. For the linear theory

$$\bar{\eta} = \frac{-a^2 k}{2\sinh 2kh}.$$

This implies that the mean water level $\bar{\eta}$ depends on the local parameters: water depth h, wave number k and wave amplitude a. The minus sign in this expression shows that a set-down occurs. In shallow water, $kh \ll 1$, the mean surface level is given by $\bar{\eta} = \dfrac{-a^2}{4h}$.

It is also possible to express $\bar{\eta}$ as a function of the constant wave number k_0 and wave amplitude a_0 together with the local depth h. Using the assumptions that the energy flux towards the shore is a constant and that the radial frequency is conserved, give

$$\bar{\eta} = -a_0^2 k \frac{\coth^2 kh}{2(2kh + \sinh 2kh)}. \tag{2.8}$$

In shallow water, $kh \ll 1$, the mean surface level is given by

$$\bar{\eta} = \frac{-a_0^2 k_0}{8}(k_0 h)^{-3/2} = \frac{-a_0^2 g^{1/2}}{8\omega h^{3/2}}.$$

The above formulas apply so long as the linear theory is valid and there is no appreciable lose of energy.

Detailed descriptions of the basic equations for the linear wave theory are available in [19, 29, 35, 56].

Although the linear wave theory is only valid for waves which are infinitesimally small and their motion is small, it provides some insight for finite-amplitude periodic waves which are called nonlinear waves.

Chapter 3

Nonlinear Waves

When waves become too steep or propagate towards shore into shallow water, the linear wave theory is no longer valid. Therefore, high-order wave theories are required to describe the wave phenomena. There are a number of theories that can be applied to approximately predict the properties of nonlinear waves. Perhaps the theory of Gerstner [24] is the earliest of these theories and is referred to as the trochoidal theory. The flow field associated with this wave is rotational. In 1847, Stokes [49] introduced an irrotational expansion theory based on the assumption that the wave properties can be presented by perturbation series and it has a large validity range, extending to the breaking wave limit in deep water. When waves approach the shallower water, the particle motions become more and more horizontally oriented and finally, in the very shallow water all vertical acceleration might be ignored and therefore, the wave can be described by the shallow water equations. These equations are derived from the continuity equation and the Euler equations under the assumption that the pressure is hydrostatic and do not incorporate any dispersive effects. The shallow water equations are often written as

$$\begin{aligned} \eta_t + \big((\eta + h_0)u\big)_x &= 0\,, \\ u_t + g\eta_x + uu_x &= 0, \end{aligned} \tag{3.1}$$

where h_0 is the undisturbed water depth.

However, before this stage, the wave motion is not horizontal and so the shallow water system is not valid; also the linear theory does not apply. To describe the wave motion in the transition region, between deep water and very shallow water, the theory of Boussinesq are employed. This theory is an approximation valid for weakly nonlinear and fairly long waves. The main idea in the Boussinesq approximation is that the vertical coordinate is omitted from the flow equations. This idea was first employed by Joseph Boussinesq in 1871 [13] in response to John Scott Russell's observation of the solitary wave in 1834 [45]. Boussinesq derived a system for a one-dimensional situation with an even bottom. Later in 1967,

Peregrine extended the system to two-dimensional propagation over an uneven bottom by using depth-averaged velocity as a dependent variable [43]. Madsen and Sørensen in 1992 extended the applicability of the Boussinesq equations to deep water [40]. There are various types of the Boussinesq equations and the difference between them is due to different possibilities in the choice of the velocity variable. In most cases one chooses either the velocity at an arbitrary water level or the depth-averaged velocity vector.

For a horizontal bottom, the Boussinesq systems in general form [10] are given by

$$\begin{aligned} \eta_t + h_0 u^\theta_x + (\eta u^\theta)_x + \frac{h_0^3}{2}\lambda\Big(\theta^2 - \frac{1}{3}\Big)u^\theta_{xxx} - \frac{h_0^2}{2}(1-\lambda)\Big(\theta^2 - \frac{1}{3}\Big)\eta_{xxt} = 0\,, \\ u^\theta_t + g\eta_x + u^\theta u^\theta_x + \frac{h_0^2}{2}(1-\theta^2)\mu g\eta_{xxx} - \frac{h_0^2}{2}\big(1-\theta^2\big)(1-\mu)u^\theta_{xxt} = 0, \end{aligned} \tag{3.2}$$

where $u^\theta(x,t)$ represents the horizontal fluid velocity at a height $0 < \theta h_0 < h_0$ and $\eta(x,t)$ describes the surface displacement from the rest position.

The Korteweg-de Vries (KdV) equation can be derived in the case of unidirectional waves from Euler equations and is a classic nonlinear model for small amplitude and fairly long waves in shallow water [34]. The stability of all KdV cnoidal waves regardless of either their amplitude or steepness was proved by Bottman and Deconinck [12] and Benjamin [6] found that the solitary wave solution of the KdV equation is stable irrespective of amplitude.

Since the Boussines equations are derived under the assumption of small amplitude, the Boussinesq equations may have some restrictions if applied to real world wave propagation problems. Therefore, in the following, we will study a fully nonlinear system.

3.1 The Serre-Green-Naghdi system

Serre in 1953 [47, 48] made a breakthrough in the theory of nonlinearity as he derived a one-dimensional fully nonlinear weakly dispersive system for a horizontal bottom. Several years later, Su and Gardner rederived the same system [51]. In 1976, a two-dimensional fully nonlinear and weakly dispersive system for an uneven bottom was derived by Green and Naghdi [25]. The full nonlinearity makes the Serre-Green-Naghdi system an appropriate model to describe nonlinear shallow water wave propagation and wave oscillations at the shoreline. This system admits a three-parameter family of cnoidal wave solutions. Carter and Cienfuegos [15] found that in describing the kinematics of strongly nonlinear waves propagating, the solitary and cnoidal solutions of the Serre-Green-Naghdi equations perform much better than the solutions of the KdV equation. They also

established that these solutions are stable for waves of small amplitude but not for sufficiently large amplitude.

However, the SGN system is no more valid in deeper water and a fully dispersive model must be used [37].

3.1.1 Derivation and solution

The derivation of the SGN equations as a model for surface waves is recalled here since details from this derivation are used in papers A, B and C. We consider an inviscid and incompressible fluid, and assume that the fluid flow is irrotational and two-dimensional. Supposing that l represents a dominant wavelength, a_0 denotes a typical wave amplitude, b_0 a typical water depth and $c_0 = \sqrt{gb_0}$ is the limiting long-wave speed, the non-dimensional variables are defined by

$$\begin{gathered} \tilde{x} = \frac{x}{l}, \quad \tilde{z} = \frac{z}{b_0}, \quad \tilde{t} = \frac{c_0 t}{l}, \quad \tilde{\eta} = \frac{\eta}{a_0}, \quad \tilde{b} = -\frac{b}{b_0}, \\ \tilde{u} = \frac{u}{\alpha c_0}, \quad \tilde{v} = \frac{v}{\sqrt{\beta}\alpha c_0}, \quad \tilde{p} = \frac{p}{\rho g b_0}, \end{gathered} \tag{3.3}$$

where $\alpha = \frac{a_0}{b_0}$ and $\beta = \frac{b_0^2}{l^2}$. In non-dimensional variables, the free-surface problem is written as follows [56]:
The momentum equations are

$$\alpha\tilde{u}_{\tilde{t}} + \alpha^2(\tilde{u}^2)_{\tilde{x}} + \alpha^2(\tilde{u}\tilde{v})_{\tilde{z}} = -\tilde{p}_{\tilde{x}} \,, \tag{3.4a}$$

$$\alpha\beta\tilde{v}_{\tilde{t}} + \alpha^2\beta\tilde{u}\tilde{v}_{\tilde{x}} + \alpha^2\beta\tilde{v}\tilde{v}_{\tilde{z}} = -\tilde{p}_{\tilde{z}} - 1 \,. \tag{3.4b}$$

The equation of continuity and the irrotationality are expressed by

$$\tilde{u}_{\tilde{x}} + \tilde{v}_{\tilde{z}} = 0 \,, \tag{3.5a}$$

$$\tilde{u}_{\tilde{z}} - \beta\tilde{v}_{\tilde{x}} = 0 \,. \tag{3.5b}$$

The boundary conditions at the free surface and at the bottom are given by

$$\tilde{v} = \tilde{\eta}_{\tilde{t}} + \alpha\tilde{u}\tilde{\eta}_{\tilde{x}}, \qquad \text{at} \quad \tilde{z} = \alpha\tilde{\eta}(\tilde{x}) \,, \tag{3.6a}$$

$$\tilde{p} = 0, \qquad \text{at} \quad \tilde{z} = \alpha\tilde{\eta}(\tilde{x}) \,, \tag{3.6b}$$

$$\tilde{v} = \tilde{b}_{\tilde{x}}\tilde{u}, \qquad \text{at} \quad \tilde{z} = \tilde{b}(\tilde{x}) \,. \tag{3.6c}$$

Integrating the continuity equation over depth gives

$$\tilde{\eta}_{\tilde{t}} + [\tilde{h}\bar{\tilde{u}}]_{\tilde{x}} = 0, \tag{3.7}$$

where

$$\bar{\tilde{u}} = \frac{1}{\tilde{h}} \int_{\tilde{b}}^{\alpha\tilde{\eta}} \tilde{u}\, d\tilde{z},$$

is the depth-averaged horizontal velocity. Using the boundary conditions (3.6a)-(3.6c), the continuity equation (3.7) and the depth-averaged momentum equation (3.4a) yield

$$\alpha\tilde{h}\bar{\tilde{u}}_{\tilde{t}} + \alpha^2\tilde{h}\bar{\tilde{u}}\bar{\tilde{u}}_{\tilde{x}} + \alpha^2\frac{\partial}{\partial\tilde{x}}\int_{\tilde{b}}^{\alpha\tilde{\eta}}\left(\tilde{u}^2 - (\bar{\tilde{u}})^2\right)d\tilde{z} = -\int_{\tilde{b}}^{\alpha\tilde{\eta}}\tilde{p}_{\tilde{x}}\,d\tilde{z}\,. \tag{3.8}$$

Applying the Leibniz rule to the right-hand side of equation (3.8) leads to

$$\begin{aligned}\int_{\tilde{b}}^{\alpha\tilde{\eta}}\tilde{p}_{\tilde{x}}\,d\tilde{z} &= \frac{\partial}{\partial\tilde{x}}\left(\tilde{h}\bar{\tilde{p}}\right) - \alpha\eta_{\tilde{x}}\tilde{p}|_{\tilde{z}=\alpha\tilde{\eta}} + \tilde{b}_{\tilde{x}}\tilde{p}|_{\tilde{z}=\tilde{b}} \\ &= \frac{\partial}{\partial\tilde{x}}\left(\tilde{h}\bar{\tilde{p}}\right) + \tilde{b}_{\tilde{x}}\tilde{p}|_{\tilde{z}=\tilde{b}}\,.\end{aligned}$$

The momentum equation (3.4b) is rewritten as

$$\alpha\beta\Gamma(\tilde{x},\tilde{z},\tilde{t}) = -1 - \tilde{p}_{\tilde{z}}\,, \tag{3.9}$$

where

$$\Gamma(\tilde{x},\tilde{z},\tilde{t}) = \tilde{v}_{\tilde{t}} + \alpha\tilde{u}\tilde{v}_{\tilde{x}} + \alpha\tilde{v}\tilde{v}_{\tilde{z}}\,.$$

Integrating equation (3.9) from $\tilde{z}$ to $\alpha\tilde{\eta}$ yields

$$\tilde{p}(\tilde{x},\tilde{z},\tilde{t}) = (\alpha\tilde{\eta} - \tilde{z}) + \alpha\beta\int_{\tilde{z}}^{\alpha\tilde{\eta}}\Gamma(\tilde{x},\zeta,\tilde{t})\,d\zeta\,, \tag{3.10}$$

and taking the mean value gives

$$\tilde{h}\bar{\tilde{p}} = \frac{1}{2}\tilde{h}^2 + \alpha\beta\int_{\tilde{b}}^{\alpha\tilde{\eta}}\int_{\tilde{z}}^{\alpha\tilde{\eta}}\Gamma(\tilde{x},\zeta,\tilde{t})\,d\zeta\,d\tilde{z}\,.$$

Therefore, equation (3.8) can be written as

$$\begin{aligned}\bar{\tilde{u}}_{\tilde{t}} + \alpha\bar{\tilde{u}}\bar{\tilde{u}}_{\tilde{x}} + \tilde{\eta}_{\tilde{x}} + \frac{\beta}{\tilde{h}}\frac{\partial}{\partial\tilde{x}}\int_{\tilde{b}}^{\alpha\tilde{\eta}}(\tilde{z}-\tilde{b})\Gamma(\tilde{x},\tilde{z},\tilde{t})\,d\tilde{z} \\ + \frac{\beta}{\tilde{h}}\tilde{b}_{\tilde{x}}\int_{\tilde{b}}^{\alpha\tilde{\eta}}\Gamma(\tilde{x},\tilde{z},\tilde{t})\,d\tilde{z} = \frac{-\alpha}{\tilde{h}}\frac{\partial}{\partial\tilde{x}}\int_{\tilde{b}}^{\alpha\tilde{\eta}}\left(\tilde{u}^2 - (\bar{\tilde{u}})^2\right)d\tilde{z}\,.\end{aligned}$$

The non-dimensional velocity components are given (cf. [18]) to first order by

$$\tilde{u}(\tilde{x},\tilde{z},\tilde{t}) = \bar{\tilde{u}}(\tilde{x},\tilde{t}) + O(\beta)\,,$$

and

$$\tilde{v}(\tilde{x},\tilde{z},\tilde{t}) = -\left(\tilde{z} - \tilde{b}(\tilde{x})\right)\frac{\partial\bar{\tilde{u}}}{\partial\tilde{x}} + \bar{\tilde{u}}\frac{\partial\tilde{b}}{\partial\tilde{x}} + O(\beta)\,.$$

As it was shown in [18], we can expand the velocity components using Taylor series in the vertical coordinate around the bottom. Denoting by $\tilde{u}^b$ and $\tilde{v}^b$, respectively, the horizontal and vertical velocities at the bottom, the bottom kinematic condition (3.6c) is $\tilde{v}^b = \tilde{b}_{\tilde{x}}\tilde{u}^b$. In order to determine which terms should be kept to obtain an approximation for the velocity field, the incompressibility condition (3.5a) must hold to the same order in β as the evolution equations. If the non-dimensional velocity components are given by

$$\tilde{u}(\tilde{x},\tilde{z},\tilde{t}) = \tilde{u}^b(\tilde{x},\tilde{t}) + \beta(\tilde{z}-\tilde{b})\left(\tilde{b}_{\tilde{x}}\tilde{u}^b_{\tilde{x}} + (\tilde{b}_{\tilde{x}}\tilde{u}^b)_{\tilde{x}}\right) - \frac{\beta}{2}(\tilde{z}-\tilde{b})^2\tilde{u}^b_{\tilde{x}\tilde{x}} + O(\beta^2)\,, \quad (3.11)$$

$$\tilde{v}(\tilde{x},\tilde{z},\tilde{t}) = \tilde{b}_{\tilde{x}}\tilde{u}^b + (\tilde{z}-\tilde{b})\left(-\tilde{u}^b_{\tilde{x}} + \beta(\tilde{b}_{\tilde{x}}(\tilde{u}^b\tilde{b}_{\tilde{x}})_{\tilde{x}} + \tilde{u}^b_{\tilde{x}}\tilde{b}^2_{\tilde{x}})\right) - \frac{\beta}{2}(\tilde{z}-\tilde{b})^2\left(\tilde{b}_{\tilde{x}}\tilde{u}^b_{\tilde{x}\tilde{x}} + (\tilde{b}_{\tilde{x}}\tilde{u}^b_{\tilde{x}} + (\tilde{b}_{\tilde{x}}\tilde{u}^b)_{\tilde{x}})_{\tilde{x}}\right) + \frac{\beta}{3!}(\tilde{z}-\tilde{b})^3\tilde{u}^b_{\tilde{x}\tilde{x}\tilde{x}} + O(\beta^2)\,,$$

then the incompressibility condition (3.5a) holds to $O(\beta^2)$. Depth averaging (3.11) gives

$$\tilde{u}^b = \bar{\tilde{u}} - \frac{\beta}{2}\tilde{h}\left(\tilde{b}_{\tilde{x}}\bar{\tilde{u}}_{\tilde{x}} + (\tilde{b}_{\tilde{x}}\bar{\tilde{u}})_{\tilde{x}}\right) + \frac{\beta}{6}\tilde{h}^2\bar{\tilde{u}}_{\tilde{x}\tilde{x}} + O(\beta^2,\alpha\beta^2)\,.$$

Thus, the horizontal velocity is

$$\tilde{u}(\tilde{x},\tilde{z},\tilde{t}) = \bar{\tilde{u}} - \beta\left(\tilde{b}_{\tilde{x}}\bar{\tilde{u}}_{\tilde{x}} + (\tilde{b}_{\tilde{x}}\bar{\tilde{u}})_{\tilde{x}}\right)\left(\frac{\tilde{h}}{2} - (\tilde{z}-\tilde{b})\right) + \beta\left(\frac{\tilde{h}^2}{6} - \frac{1}{2}(\tilde{z}-\tilde{b})^2\right)\bar{\tilde{u}}_{\tilde{x}\tilde{x}} + O(\beta^2,\alpha\beta^2)\,. \quad (3.12)$$

Taking squares of equation (3.12)

$$\tilde{u}^2(\tilde{x},\tilde{z},\tilde{t}) = \bar{\tilde{u}}^2 - \beta\left(\tilde{b}_{\tilde{x}}\bar{\tilde{u}}_{\tilde{x}}\bar{\tilde{u}} + (\tilde{b}_{\tilde{x}}\bar{\tilde{u}})_{\tilde{x}}\bar{\tilde{u}}\right)\left(\tilde{h} - 2(\tilde{z}-\tilde{b})\right) + \beta\left(\frac{\tilde{h}^2}{2} - (\tilde{z}-\tilde{b})^2\right)\bar{\tilde{u}}\bar{\tilde{u}}_{\tilde{x}\tilde{x}} + O(\beta^2,\alpha\beta^2)\,. \quad (3.13)$$

Integrating equation (3.13) from $\tilde{b}$ to $\alpha\tilde{\eta}$, and after some simplifications, it follows that

$$\int_{\tilde{b}}^{\alpha\tilde{\eta}}\left(\tilde{u}^2 - (\bar{\tilde{u}})^2\right)d\tilde{z} = O(\beta^2,\alpha\beta^2)\,,$$

and that

$$\Gamma(\tilde{x},\tilde{z},\tilde{t}) = (\tilde{z}-\tilde{b})\left[\alpha\bar{\tilde{u}}_{\tilde{x}}^2 - \bar{\tilde{u}}_{\tilde{x}\tilde{t}} - \alpha\bar{\tilde{u}}\bar{\tilde{u}}_{\tilde{x}\tilde{x}}\right] + \\ + \tilde{b}_{\tilde{x}}(\bar{\tilde{u}}_{\tilde{t}} + \alpha\bar{\tilde{u}}\bar{\tilde{u}}_{\tilde{x}}) + \alpha\tilde{b}_{\tilde{x}\tilde{x}}\bar{\tilde{u}}^2 + O(\beta,\alpha\beta)\ . \quad (3.14)$$

Evaluating the integrals $\int_{\tilde{b}}^{\alpha\tilde{\eta}}\Gamma d\tilde{z}$ and $\int_{\tilde{b}}^{\alpha\tilde{\eta}}(\tilde{z}-\tilde{b})\Gamma d\tilde{z}$ yields

$$\int_{\tilde{b}}^{\alpha\tilde{\eta}}\Gamma d\tilde{z} = \frac{1}{2}\tilde{h}\tilde{\mathcal{P}} + \tilde{h}\tilde{\mathcal{Q}}\,,$$

and

$$\int_{\tilde{b}}^{\alpha\tilde{\eta}}(\tilde{z}-\tilde{b})\Gamma d\tilde{z} = \frac{1}{3}\tilde{h}^2\tilde{\mathcal{P}} + \frac{1}{2}\tilde{h}^2\tilde{\mathcal{Q}}\,,$$

where

$$\tilde{\mathcal{P}} = \tilde{h}\left[\alpha\bar{\tilde{u}}_{\tilde{x}}^2 - \bar{\tilde{u}}_{\tilde{x}\tilde{t}} - \alpha\bar{\tilde{u}}\bar{\tilde{u}}_{\tilde{x}\tilde{x}}\right]\ ,$$

and

$$\tilde{\mathcal{Q}} = \tilde{b}_{\tilde{x}}(\bar{\tilde{u}}_{\tilde{t}} + \alpha\bar{\tilde{u}}\bar{\tilde{u}}_{\tilde{x}}) + \tilde{b}_{\tilde{x}\tilde{x}}\bar{\tilde{u}}^2\ .$$

Finally we find the second equation of the system as

$$\bar{\tilde{u}}_{\tilde{t}} + \alpha\bar{\tilde{u}}\bar{\tilde{u}}_{\tilde{x}} + \tilde{\eta}_{\tilde{x}} + \frac{\beta}{\tilde{h}}\frac{\partial}{\partial\tilde{x}}\left\{\left(\tfrac{1}{3}\tilde{\mathcal{P}} + \tfrac{1}{2}\tilde{\mathcal{Q}}\right)\tilde{h}^2\right\} + \beta\tilde{b}_{\tilde{x}}\left(\tfrac{1}{2}\tilde{\mathcal{P}} + \tilde{\mathcal{Q}}\right) = O(\alpha\beta^2)\ . \quad (3.15)$$

In the case of horizontal bottom, the system becomes

$$\tilde{\eta}_{\tilde{t}} + [h\bar{\tilde{u}}]_{\tilde{x}} = 0\ , \quad (3.16a)$$

$$\bar{\tilde{u}}_{\tilde{t}} + \alpha\bar{\tilde{u}}\bar{\tilde{u}}_{\tilde{x}} + \tilde{\eta}_{\tilde{x}} - \frac{\beta}{3h}\frac{\partial}{\partial\tilde{x}}\left(h^3(\bar{\tilde{u}}_{\tilde{x}\tilde{t}} + \alpha\bar{\tilde{u}}\bar{\tilde{u}}_{\tilde{x}\tilde{x}} - \alpha(\bar{\tilde{u}}_{\tilde{x}})^2)\right) = O(\beta^2,\alpha\beta^2)\ . \quad (3.16b)$$

By setting the right-hand side of (3.15) equal to zero, and writing the variables in dimensional form the SGN system with uneven bottom reads

$$\eta_t + [h\bar{u}]_x = 0\ , \quad (3.17a)$$

$$\bar{u}_t + \bar{u}\bar{u}_x + g\eta_x + \frac{1}{h}\left[h^2\left(\tfrac{1}{3}\mathcal{P} + \tfrac{1}{2}Q\right)\right]_x - b_x\left(\tfrac{1}{2}\mathcal{P} + Q\right) = 0\,, \quad (3.17b)$$

where $\mathcal{P} = h\left[\bar{u}_x^2 - \bar{u}_{xt} - \bar{u}\bar{u}_{xx}\right]$ and $Q = -b_x(\bar{u}_t + \bar{u}\bar{u}_x) - b_{xx}\bar{u}^2$.

The dimensional form of the water particle velocities at any location (x,z) in the vertical plane becomes

$$u = \bar{u} + \left(\frac{h^2}{6} - \frac{z^2}{2}\right)\bar{u}_{xx}\ , \quad (3.18a)$$

$$v = -z\bar{u}_x\ . \quad (3.18b)$$

An asymptotic expression for the pressure $\tilde{p}(\tilde{x},\tilde{z},\tilde{t})$ can be obtained by substituting formula (3.14) into (3.10). Such a formula was derived in [42] in the form

$$\begin{aligned}\tilde{p}(\tilde{x},\tilde{z},\tilde{t}) = \alpha\tilde{\eta} - \tilde{z} + + \frac{\alpha\beta}{2}\left[-\bar{\tilde{u}}_{\tilde{x}\tilde{t}} - \alpha\bar{\tilde{u}}\bar{\tilde{u}}_{\tilde{x}\tilde{x}} + \alpha\bar{\tilde{u}}_{\tilde{x}}^2\right]\left(\tilde{h}^2 - (\tilde{z}-\tilde{b})^2\right) \\ + \alpha\beta\left(\alpha\tilde{b}_{\tilde{x}\tilde{x}}\bar{\tilde{u}}^2 + \alpha\tilde{b}_{\tilde{x}}\bar{\tilde{u}}\bar{\tilde{u}}_{\tilde{x}} + \tilde{b}_{\tilde{x}}\bar{\tilde{u}}_{\tilde{t}}\right)(\alpha\tilde{\eta} - \tilde{z}) + O(\alpha\beta^2)\,. \quad (3.19)\end{aligned}$$

The SGN system with a horizontal bottom

The SGN system (3.16) has the following dimensional form

$$\begin{aligned}&\eta_t + [h\bar{u}]_x = 0,\\ &\bar{u}_t + \bar{u}\bar{u}_x + gh_x - \frac{1}{3h}\frac{\partial}{\partial x}\left(h^3(\bar{u}_{xt} + \bar{u}\bar{u}_{xx} - (\bar{u}_x)^2)\right) = 0\,.\end{aligned} \quad (3.20)$$

The shallow water system

System (3.16) reduces to the shallow water system when $\beta \to 0$,

$$\begin{aligned}\tilde{\eta}_{\tilde{t}} + [(1+\alpha\tilde{\eta})\bar{\tilde{u}}]_{\tilde{x}} = 0\,,\\ \bar{\tilde{u}}_{\tilde{t}} + \alpha\bar{\tilde{u}}\bar{\tilde{u}}_{\tilde{x}} + \tilde{\eta}_{\tilde{x}} = O(\alpha^2)\,,\end{aligned}$$

and in dimensional variables is given by (3.1).

The classical Boussinesq system

Considering long waves of small amplitude, $\beta \sim \alpha$, the SGN system could be simplified as

$$\tilde{\eta}_{\tilde{t}} + [(1+\alpha\tilde{\eta})\bar{\tilde{u}}]_{\tilde{x}} = 0\,, \quad (3.21a)$$

$$\bar{\tilde{u}}_{\tilde{t}} + \alpha\bar{\tilde{u}}\bar{\tilde{u}}_{\tilde{x}} + \tilde{\eta}_{\tilde{x}} - \frac{\beta}{3}\bar{u}_{\tilde{x}\tilde{x}\tilde{t}} = O(\alpha\beta,\beta^2)\,, \quad (3.21b)$$

and in dimensional form, we have

$$\begin{aligned}\eta_t + [h\bar{u}]_x = 0\,,\\ \bar{u} + g\eta_x + \bar{u}\bar{u}_x - \frac{1}{3}\bar{u}_{xxt} = 0\,,\end{aligned}$$

where $h = h_0 + \eta$. This is the classical Boussinesq system. If a horizontal velocity u^θ is used instead of the average velocity $\bar{u}$, then this system may be generalized to

$$\begin{aligned}\eta_t + (\eta u^\theta)_x - \tfrac{h_0^2}{2}(\theta^2 - \tfrac{1}{3})\eta_{xxt} = 0\,,\\ u_t^\theta + g\eta_x + u^\theta u_x^\theta - \tfrac{h_0^2}{2}(1-\theta^2)u_{xxt}^\theta = 0\,.\end{aligned}$$

Actually, this system is a restriction of (3.2) to the case where $\lambda = 0$ and $\mu = 0$. It is interesting to note that the original Boussinesq system is equivalent to the above system if $\theta^2 = \frac{1}{3}$, and this is also the case when the dispersion relation is the closest approximation of the full dispersion relation

$$\omega^2 = gk\tanh(kh_0)\,.$$

However as noted in [8], from a numerical point of view, the values $\frac{1}{3} < \theta^2 < 1$ are most convenient since both equations in the system are then of the same type, boundary conditions may be imposed in a straightforward way, and the resulting system can be integrated numerically with great efficiency. For example, a spectral scheme has been employed in [9].

3.1.2 Particle trajectories

In this section, we consider the SGN system (3.20). Following [20], the SGN system admits the following family of solutions

$$\begin{aligned}
&h(x,t) = a_0 + a_1\mathrm{dn}^2(\theta,m),\\
&\bar{u} = c\Big(1 - \frac{h_0}{h(x,t)}\Big),\\
&\kappa = \sqrt{\frac{3a_1}{4a_0(a_0+a_1)(a_0+(1-m^2)a_1)}},\\
&c = \frac{1}{h_0}\sqrt{ga_0(a_0+a_1)(a_0+(1-m^2)a_1)}\,,
\end{aligned} \tag{3.22}$$

where $\theta = \kappa(x-ct)$, a_1 and a_2 are real positive parameters, and $d(.,m)$ is a Jacobi elliptic function with elliptic modulus $m \in (0,1)$. Also the mean water depth is $h_0 = a_0 + a_1\dfrac{E(m)}{K(m)}$ in which $K(m)$ and $E(m)$ are the complete elliptic integrals of the first and the second kinds, respectively. As $m \to 1^-$, these solutions limit to the solitary wave solutions

$$\begin{aligned}
&h(x,t) = a_0 + a_1\mathrm{sech}^2(\theta),\\
&\bar{u} = c\Big(1 - \frac{a_0}{h(x,t)}\Big),\\
&\kappa = \sqrt{\frac{3a_1}{4a_0(a_0+a_1)}},\\
&c = \sqrt{g(a_0+a_1)}\,.
\end{aligned} \tag{3.23}$$

In paper A, the focus is on numerical simulation of particle trajectories associated with the periodic solutions of the SGN system. The velocity field (3.18) has been used to simulate particle paths. Let $(\xi(t),\zeta(t))$ be the location of a particle whose rest position is (ξ_0,ζ_0). Then the particle motion is described by the differential equations

$$\begin{aligned}\frac{\partial\xi(t)}{\partial t} &= u(\xi(t),\zeta(t),t),\\ \frac{\partial\zeta(t)}{\partial t} &= v(\xi(t),\zeta(t),t)\,.\end{aligned} \tag{3.24}$$

To find the particle trajectories, the system (3.24) is solved numerically using a fourth-order Runge-Kutta method. For the solitary wave solution (3.23), the

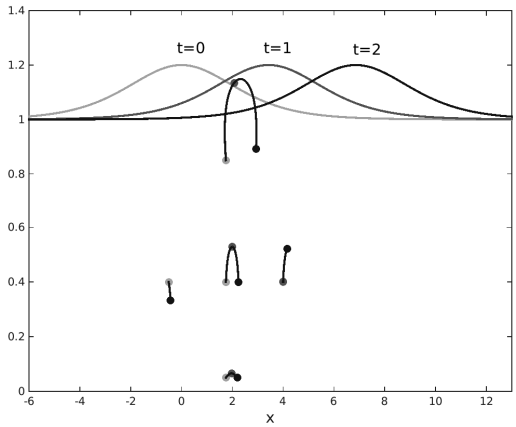

Figure 3.1: The solitary wave profile with amplitude $a_1 = 0.2$ is shown at $t = 0$ (light-gray), $t = 1$ (dark-gray) and $t = 2$ (black). The wave crest initially located at $x = 0$. The paths of particles initially located at $(-0.5, 0.4)$, $(1.75, 0.4)$, $(4, 0.4)$, $(1.75, 0.05)$ and $(1.75, 0.85)$. The light-gray dot indicates the particle location at time $t = 0$. The dark-gray dot indicates the particle location at time $t = 1$ and the black dot indicates the particle location at time $t = 2$. The particles located on the left of the crest move to the right and downwards and the particles located on the right of the crest move to the right and upwards. The vertical excursion is less than its horizontal displacement and diminishes rapidly with the depth of the path beneath the free surface.

velocity field at a time t, at an arbitrary point (x,z) in the fluid is given by

$$u = \bar{u} + \Big(\frac{-2a_1a_0c\kappa^2}{h^2}\Big)\Big(\frac{h^2}{6} - \frac{z^2}{2}\Big)\big[-2\mathrm{sech}^2(\theta)\tanh^2(\theta) + \mathrm{sech}^4(\theta)\big],$$
$$v = \Big(\frac{2a_0a_1cz\kappa}{h^2}\Big)\mathrm{sech}^2(\theta)\tanh(\theta).$$

The surface profile and the particle paths beneath the solitary waves are shown in Figure (3.1). The particle motion due to the propagation of the periodic solution (3.22) at the surface is described by the system (3.24) where the velocity field is given by

$$u = \bar{u} + \Big(\frac{-2a_1h_0cm^2\kappa^2}{h^2}\Big)\Big(\frac{h^2}{6} - \frac{z^2}{2}\Big)\big[\mathrm{dn}^2(\theta)(-3\mathrm{sn}^2(\theta)+2) + \mathrm{sn}^2(\theta) - 1\big],$$
$$v = \Big(\frac{2h_0a_1czm^2\kappa}{h^2}\Big)\mathrm{cn}(\theta)\mathrm{sn}(\theta)\mathrm{dn}(\theta).$$

The surface profile and the particle trajectories below a periodic dnoidal wave with $a_0 = 0.3$, $a_1 = 0.1$ and $m = 0.99$ are shown in Figure (3.2). In paper A, we have shown that the particles display a forward drift due to the passage of the solitary waves, however, for the dnoidal waves the particle paths are nearly elliptic but not completely closed. In fact, the particles experience a forward drift near the surface but, as the depth decreases the drift becomes negative. This can be explained by

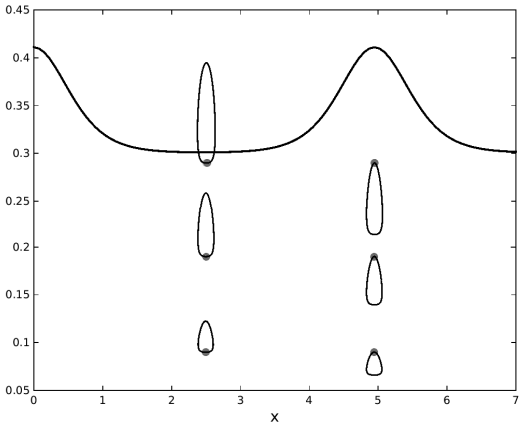

Figure 3.2: The surface profile with wavelength 4.945 is shown. The crest of the wave is centered at $x = 0$ and the particles are initially located beneath the trough and the crest.

the fact that the mean velocity, $\int_0^T \bar{u}\,dt$, over one wave period is negative which causes a negative horizontal displacement for particles. More details can be found in [32].

3.1.3 Mechanical balance laws

The modeling of surface gravity waves relies heavily on the concept of conservation of mass, momentum and energy, the main focus of this section is on deriving the mechanical balance for the SGN system. Smooth solutions of system (3.20) satisfy the following conservation laws:

$$(h)_t + (h\bar{u})_x = 0, \tag{3.25}$$

$$(h\bar{u})_t + \left(\frac{1}{2}gh^2 + h\bar{u}^2 - \frac{1}{3}h^3\bar{u}_{xt} + \frac{1}{3}h^3\bar{u}_x^2 - \frac{1}{3}h^3\bar{u}\bar{u}_{xx}\right)_x = 0, \tag{3.26}$$

$$\left(\frac{1}{2}h\left(gh + \bar{u}^2 + \tfrac{1}{3}h^2\bar{u}_x^2\right)\right)_t + \left(h\bar{u}\left(gh + \tfrac{1}{2}\bar{u}^2 + \tfrac{1}{2}h^2\bar{u}_x^2 - \tfrac{1}{3}h^2(\bar{u}_{xt} + \bar{u}\bar{u}_{xx})\right)\right)_x = 0, \tag{3.27}$$

$$\left(\bar{u} - hh_x\bar{u}_x - \frac{1}{3}h^2\bar{u}_{xx}\right)_t + \left(gh + \frac{1}{2}\bar{u}^2 - hh_x\bar{u}\bar{u}_x - \tfrac{1}{2}h^2\bar{u}_x^2 - \tfrac{1}{3}h^2\bar{u}\bar{u}_{xx}\right)_x = 0. \tag{3.28}$$

We will show that the conservation law (3.25) describes the mass conservation and (3.26) illustrates the momentum conservation and (3.27) represents the energy conservation in the SGN approximation. In paper B, the focus is on deriving the mass, momentum and energy densities and fluxes associated with the SGN system (3.17) and the procedure of finding these quantities follows a similar scheme as the derivations in [4] for a class of Boussinesq system and [5] for the KdV equation. In paper C, the focus is on giving a precise physical meaning to the quantities appearing in the equation (3.28). All the balance laws consist of terms of the same asymptotic order as in the SGN system.

Mass balance

In this section we consider the SGN system (3.17). The total mass of the fluid contained in a control volume (Figure 3.3) of unit width, bounded by the lateral sides of the interval $[x_1, x_2]$, and by the free surface and the bottom is given by

$$\mathcal{M} = \int_{x_1}^{x_2}\int_{-b}^{\eta} \rho\,dz\,dx.$$

According to the principle of mass conservation, the rate of change in the total mass is equal to the mass net flux, and the fact that there is no mass flux through

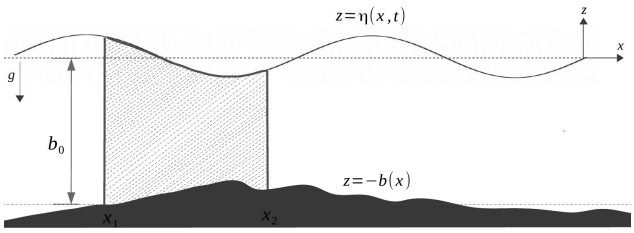

Figure 3.3: Schematic picture describing control volume.

the bottom or the free surface, the mass conservation can be formulated as

$$\frac{d}{dt}\int_{x_1}^{x_2}\int_{-b}^{\eta}\rho\,dz\,dx=\left[\int_{-b}^{\eta}\rho u(x,z,t)\,dz\right]_{x_2}^{x_1}.$$

In non-dimensional form, this equation becomes

$$\frac{d}{d\tilde{t}}\int_{\tilde{x}_1}^{\tilde{x}_2}\int_{\tilde{b}}^{\alpha\tilde{\eta}}d\tilde{z}\,d\tilde{x}=\alpha\left[\int_{\tilde{b}}^{\alpha\tilde{\eta}}\tilde{u}(\tilde{x},\tilde{z},\tilde{t})\,d\tilde{z}\right]_{\tilde{x}_2}^{\tilde{x}_1}.$$

Let us substitute the expression (3.12) for $\tilde{u}$ and integrate the equation with respect to $\tilde{z}$. Then using the Leibnitz rule and differentiating with respect to $\tilde{x}$ we obtain the mass balance equation

$$(\alpha\tilde{\eta}-\tilde{b})_{\tilde{t}}+(\alpha\bar{\tilde{u}}(\alpha\tilde{\eta}-\tilde{b}))_{\tilde{x}}=O(\alpha\beta)\,.$$

Denoting the non-dimensional mass density by $\tilde{M}=\alpha\tilde{\eta}-\tilde{b}$ and the non-dimensional mass flux by $\tilde{q}_M=\alpha\bar{\tilde{u}}(\alpha\tilde{\eta}-\tilde{b})$, the mass balance is

$$\frac{\partial\tilde{M}}{\partial\tilde{t}}+\frac{\partial\tilde{q}_M}{\partial\tilde{x}}=O(\alpha\beta)\,.$$

Using the scalings $M=\rho h_0\tilde{M}$ and $q_M=\rho h_0 c_0\tilde{q}_M$, the dimensional forms of mass density and mass flux are

$$M=\rho(\eta-b)\,,$$

and

$$q_M=\rho\bar{u}(\eta-b)\,,$$

respectively. The relation

$$\frac{\partial M}{\partial t}+\frac{\partial q_M}{\partial x}=0\,,$$

is exactly the first equation in the SGN system (3.17). In the case of horizontal bottom $b = -h_0$, the mass density and flux become

$$\mathcal{M} = \rho(\eta + h_0)\,,$$
$$q_{\mathcal{M}} = \rho\bar{u}(\eta + h_0)\,,$$

respectively. Denoting $h = \eta + h_0$, we obtain the relation (3.25).

Momentum balance

The total horizontal momentum of a fluid of constant density ρ contained in the control volume is given by

$$I = \int_{x_1}^{x_2}\int_{-b}^{\eta} \rho u\, dz\, dx\,.$$

According to the principle of momentum balance, the rate of change of I is equal to the net influx of momentum through the boundaries plus the net work done on the boundary of the control volume, the momentum conservation can be expressed as

$$\frac{d}{dt}\int_{x_1}^{x_2}\int_{-b}^{\eta} \rho u\, dz\, dx = \left[\int_{-b}^{\eta} \rho u^2(x,z)\, dz + \int_{-b}^{\eta} p dz\right]_{x_2}^{x_1} - \int_{x_1}^{x_2} p b_x\, dx\,.$$

Non-dimensionalization of this expression leads to

$$\alpha\frac{d}{d\tilde{t}}\int_{\tilde{x}_1}^{\tilde{x}_2}\int_{\tilde{b}}^{\alpha\tilde{\eta}} \tilde{u}\, d\tilde{z}\, d\tilde{x} = \left[\alpha^2\int_{\tilde{b}}^{\alpha\tilde{\eta}} \tilde{u}^2\, d\tilde{z} + \int_{\tilde{b}}^{\alpha\tilde{\eta}} \tilde{p}\, d\tilde{z}\right]_{\tilde{x}_2}^{\tilde{x}_1} - \int_{\tilde{x}_1}^{\tilde{x}_2} \tilde{P}_b \tilde{b}_{\tilde{x}}\, dx\,.$$

We substitute the values for $\tilde{u}$ and $\tilde{p}$ in equations (3.12) and (3.19) in the latter equation and integrate the resulting equation with respect to $\tilde{z}$. Then we differentiate the result with respect to $\tilde{x}$ to obtain the balance equation:

$$\begin{aligned}
&\left(\alpha\bar{\tilde{u}}(\alpha\tilde{\eta} - \tilde{b})\right)_{\tilde{t}} + \\
&\left(\alpha^2\bar{\tilde{u}}^2(\alpha\tilde{\eta} - \tilde{b}) + \frac{(\alpha\tilde{\eta} - \tilde{b})^2}{2} - \frac{\alpha\beta}{3}(\alpha\tilde{\eta} - \tilde{b})^3(\bar{\tilde{u}}_{\tilde{x}\tilde{t}} + \alpha\bar{\tilde{u}}\bar{\tilde{u}}_{\tilde{x}\tilde{x}} - \alpha(\bar{\tilde{u}}_{\tilde{x}})^2)\right)_{\tilde{x}} + \\
&\left(\frac{\alpha\beta}{2}(\alpha\tilde{b}_{\tilde{x}\tilde{x}}\bar{\tilde{u}}^2 + \tilde{b}_{\tilde{x}}\left(\alpha\bar{\tilde{u}}\bar{\tilde{u}}_{\tilde{x}} + \bar{\tilde{u}}_{\tilde{t}}\right))(\alpha\tilde{\eta} - \tilde{b})^2\right)_{\tilde{x}} = -\tilde{P}_b\tilde{b}_{\tilde{x}} + O(\alpha\beta^2)\,.
\end{aligned}$$

The non-dimensional momentum density is defined as

$$\tilde{I} = \alpha\bar{\tilde{u}}(\alpha\tilde{\eta} - \tilde{b})\,,$$

whiles the momentum flux is

$$\tilde{q}_I = \alpha^2\tilde{\bar{u}}^2(\alpha\tilde{\eta}-\tilde{b}) + \frac{(\alpha\tilde{\eta}-\tilde{b})^2}{2} - \frac{\alpha\beta}{3}(\alpha\tilde{\eta}-\tilde{b})^3\big(\tilde{\bar{u}}_{\tilde{x}\tilde{t}} + \alpha\tilde{\bar{u}}\tilde{\bar{u}}_{\tilde{x}\tilde{x}} - \alpha(\tilde{\bar{u}}_{\tilde{x}})^2\big) + \frac{\alpha\beta}{2}\big(\alpha\tilde{b}_{\tilde{x}\tilde{x}}\tilde{\bar{u}}^2 + \tilde{b}_{\tilde{x}}(\alpha\tilde{\bar{u}}\tilde{\bar{u}}_{\tilde{x}} + \tilde{\bar{u}}_{\tilde{t}})\big)(\alpha\tilde{\eta}-\tilde{b})^2 \,.$$

Using the scalings $I = \rho c_0 h_0 \tilde{I}$ and $q_I = \rho c_0^2 h_0 \tilde{q}_I$, the dimensional forms of the momentum density and momentum flux per unit span are given by

$$I = \rho\bar{u}(\eta - b) \,,$$

and

$$q_I = \rho\bar{u}^2(\eta-b) + \frac{\rho g}{2}(\eta-b)^2 - \frac{\rho}{3}(\bar{u}_{xt} + \bar{u}\bar{u}_{xx} - \bar{u}_x^2)(\eta-b)^3 - \frac{\rho}{2}(b_{xx}\bar{u}^2 + b_x(\bar{u}\bar{u}_x + \bar{u}_t))(\eta-b)^2 \,,$$

respectively. It appears that momentum conservation is also exactly satisfied and can be written in the form

$$\frac{\partial I}{\partial t} + \frac{\partial q_I}{\partial x} = b_x p \,.$$

For a horizontal bottom $b = h_0$, the dimensional forms of the momentum density and momentum flux per unit span are given by

$$I = \rho\bar{u}(h_0 + \eta) \,,$$

and

$$q_I = \rho\bar{u}^2(h_0+\eta) + \frac{\rho g}{2}(h_0+\eta)^2 - \frac{\rho}{3}(h_0+\eta)^3(\bar{u}_{xt} + \bar{u}\bar{u}_{xx} - \bar{u}_x^2) \,,$$

respectively, and by denoting $h = \eta + h_0$, the momentum balance equation can be written as:

$$\frac{\partial}{\partial t}(\bar{u}h) + \frac{\partial}{\partial x}\big(\bar{u}^2 h + \frac{g}{2}h^2 - \frac{1}{3}h^3(\bar{u}_{xt} + \bar{u}\bar{u}_{xx} - \bar{u}_x^2)\big) = 0 \,,$$

which is the same as equation (3.26).

Energy balance

The total mechanical energy inside a control volume can be written as

$$\mathcal{E} = \int_{x_1}^{x_2}\int_{-b}^{\eta}\Big\{\frac{\rho}{2}(u^2+v^2) + \rho g z\Big\}\,dz\,dx \,.$$

Then, the conservation of total mechanical energy can be expressed as

$$\frac{d}{dt}\int_{x_1}^{x_2}\int_{-b}^{\eta}\left\{\frac{\rho}{2}(u^2+v^2)+\rho gz\right\}dz\,dx=\left[\int_{-b}^{\eta}\left\{\left(\frac{\rho}{2}(u^2+v^2)+\rho gz\right)u+uP\right\}dz\right]_{x_2}^{x_1},$$

and in non-dimensional variables as:

$$\frac{d}{d\tilde{t}}\int_{\tilde{x}_1}^{\tilde{x}_2}\int_{\tilde{b}}^{\alpha\tilde{\eta}}\left\{\frac{\alpha^2}{2}(\tilde{u}^2+\beta\tilde{v}^2)+\tilde{z}\right\}d\tilde{z}\,d\tilde{x}=$$
$$\alpha\left[\int_{\tilde{b}}^{\alpha\tilde{\eta}}\left\{\frac{\alpha^2}{2}(\tilde{u}^3+\beta\tilde{v}^2\tilde{u})+\tilde{z}\tilde{u}+\tilde{p}\tilde{u}\right\}d\tilde{z}\right]_{\tilde{x}_2}^{\tilde{x}_1}.$$

By substituting the expressions for $\tilde{u}$, $\tilde{v}$ and $\tilde{p}$, the differential form of the energy balance equation is given by

$$\left(\frac{\alpha^2}{2}(\bar{\tilde{u}}^2+\beta\tilde{b}_{\tilde{x}}^2\bar{\tilde{u}}^2)\tilde{h}-\frac{\alpha^2\beta}{2}\tilde{b}_{\tilde{x}}\tilde{h}^2\bar{\tilde{u}}\bar{\tilde{u}}_{\tilde{x}}+\frac{\alpha^2\beta}{6}\tilde{h}^3\bar{\tilde{u}}_{\tilde{x}}^2+\frac{\tilde{h}^2}{2}+\tilde{b}\tilde{h}\right)_{\tilde{t}}+$$
$$\left(\frac{\alpha^3}{2}\bar{\tilde{u}}^3\tilde{h}+\alpha\bar{\tilde{u}}\tilde{h}^2-\frac{\alpha^2\beta}{3}\tilde{h}^3\bar{\tilde{u}}(\bar{\tilde{u}}_{\tilde{x}\tilde{t}}+\alpha\bar{\tilde{u}}\bar{\tilde{u}}_{\tilde{x}\tilde{x}}-\frac{3}{2}\alpha\bar{\tilde{u}}_{\tilde{x}}^2)-\frac{\alpha^3\beta}{2}\tilde{b}_{\tilde{x}}\bar{\tilde{u}}_{\tilde{x}}\bar{\tilde{u}}^2\tilde{h}^2\right)_{\tilde{x}}$$
$$-\left(\frac{\alpha^2\beta}{2}\left(\alpha\tilde{b}_{\tilde{x}\tilde{x}}\bar{\tilde{u}}^2+\alpha\tilde{b}_{\tilde{x}}(\bar{\tilde{u}}\bar{\tilde{u}}_{\tilde{x}}+\bar{\tilde{u}}_{\tilde{t}})\right)\tilde{h}^2\right)_{\tilde{x}}=O(\alpha\beta^2)\,.$$

We find that the non-dimensional energy density is

$$\tilde{E}=\frac{\alpha^2}{2}(\bar{\tilde{u}}^2+\beta\tilde{b}_{\tilde{x}}^2\bar{\tilde{u}}^2)\tilde{h}-\frac{\alpha^2\beta}{2}\tilde{b}_{\tilde{x}}\tilde{h}^2\bar{\tilde{u}}\bar{\tilde{u}}_{\tilde{x}}+\frac{\alpha^2\beta}{6}\tilde{h}^3\bar{\tilde{u}}_{\tilde{x}}^2+\frac{\tilde{h}^2}{2}+\tilde{b}\tilde{h}\,,$$

whiles the non-dimensional energy flux is written as

$$\tilde{q}_E=\frac{\alpha^3}{2}\bar{\tilde{u}}^3\tilde{h}+\alpha\bar{\tilde{u}}\tilde{h}^2+\frac{\alpha^3\beta}{2}\tilde{b}_{\tilde{x}}^2\bar{\tilde{u}}^3+\alpha\bar{\tilde{u}}\tilde{b}\tilde{h}-\frac{\alpha^2\beta}{3}\tilde{h}^3\bar{\tilde{u}}(\bar{\tilde{u}}_{\tilde{x}\tilde{t}}+\alpha\bar{\tilde{u}}\bar{\tilde{u}}_{\tilde{x}\tilde{x}}-$$
$$\frac{3}{2}\alpha\bar{\tilde{u}}_{\tilde{x}}^2)-\frac{\alpha^3\beta}{2}\tilde{b}_{\tilde{x}}\bar{\tilde{u}}_{\tilde{x}}\bar{\tilde{u}}^2\tilde{h}^2-\frac{\alpha^2\beta}{2}\left(\alpha\tilde{b}_{\tilde{x}\tilde{x}}\bar{\tilde{u}}^2+\tilde{b}_{\tilde{x}}(\alpha\bar{\tilde{u}}\bar{\tilde{u}}_{\tilde{x}}+\bar{\tilde{u}}_{\tilde{t}})\right)\bar{\tilde{u}}\tilde{h}^2.$$

Therefore, the energy balance is

$$\frac{\partial\tilde{E}}{\partial\tilde{t}}+\frac{\partial\tilde{q}_E}{\partial\tilde{x}}=O(\alpha\beta^2)\,.$$

Using the scaling $E=\rho c_0^2h_0\tilde{E}$ and $q_E=\rho c_0^3h_0\tilde{q}_E$, the dimensional form of energy density is given as the sum of the kinetic energy and the potential energy by

$$E=\underbrace{\frac{\rho}{2}\bar{u}^2(1+b_x^2)h+\frac{\rho}{2}\bar{u}\bar{u}_xb_xh^2+\frac{\rho}{6}\bar{u}_x^2h^3}_{E_k}+\underbrace{\frac{\rho g}{2}h^2-\rho gbh}_{E_p},$$

and the dimensional form of energy flux per unit span is given by

$$q_E = \rho g\bar{u}(h^2 - bh) + \frac{\rho}{2}\bar{u}^3 h(1+b_x) - \frac{\rho}{3}h^3\bar{u}(\bar{u}_{xt} + \bar{u}\bar{u}_{xx} - \frac{3}{2}\bar{u}_x^2) + \frac{\rho}{2}\bar{u}^2\bar{u}_x b_x h^2 + \frac{\rho}{2}\bar{u}h^2\big(b_{xx}\bar{u}^2 + b_x(\bar{u}\bar{u}_x + \bar{u}_t)\big) .$$

The energy balance is also valid to the same asymptotic order as the SGN system. For a horizontal bottom the dimensional form of energy density and energy flux per unit span are given by

$$E = \frac{\rho g}{2}(2h_0\eta + \eta^2) + \frac{\rho}{2}(h_0+\eta)\bar{u}^2 + \frac{\rho}{6}(h_0+\eta)^3\bar{u}_x^2 ,$$

and

$$q_E = \rho g\bar{u}(h_0+\eta)^2 + \frac{\rho}{2}\bar{u}^3(h_0+\eta) - \frac{\rho}{3}(h_0+\eta)^3\bar{u}(\bar{u}_{xt} + \bar{u}\bar{u}_{xx} - \frac{3}{2}\bar{u}_x^2) , \quad (3.29)$$

respectively. Assuming $h = \eta + h_0$, the equation (3.27) can be obtained.

A kinematic balance law

Let us consider the tangent velocity K along the free surface given by

$$K = u + wh_x, \quad z = h(t,x) .$$

Using the non-dimensional variables (3.3) for the case of horizontal bottom, the quantity K in non-dimensional form is written as

$$\tilde{K} = \tilde{u} + \beta\tilde{w}\tilde{h}\tilde{h}_{\tilde{x}} . \quad (3.30)$$

Substituting $\tilde{u}$ and $\tilde{w}$ in the following equations

$$\tilde{u} = \tilde{\bar{u}} + \beta\Big(\frac{\tilde{h}^2}{6} - \frac{\tilde{z}^2}{2}\Big)\tilde{\bar{u}}_{\tilde{x}\tilde{x}} + O(\beta^2) ,$$
$$\tilde{w} = -\tilde{z}\tilde{\bar{u}}_{\tilde{x}} + \beta ,$$

into (3.30) and evaluating at the free surface yields

$$\tilde{K} = \tilde{\bar{u}} - \frac{\beta}{3}\tilde{h}^2\tilde{\bar{u}}_{\tilde{x}\tilde{x}} - \beta\tilde{h}\tilde{h}_{\tilde{x}}\tilde{\bar{u}}_{\tilde{x}} .$$

The conservation law (1.5) turns into

$$\Big(\tilde{\bar{u}} - \frac{\beta}{3}\tilde{h}^2\tilde{\bar{u}}_{\tilde{x}\tilde{x}} - \beta\tilde{h}\tilde{h}_{\tilde{x}}\tilde{\bar{u}}_{\tilde{x}}\Big)_{\tilde{t}} + \Big(\frac{1}{2}\tilde{\bar{u}}^2 - \frac{\beta}{3}\tilde{h}^2\tilde{\bar{u}}\tilde{\bar{u}}_{\tilde{x}\tilde{x}} - \beta\tilde{h}\tilde{h}_{\tilde{x}}\tilde{\bar{u}}\tilde{\bar{u}}_{\tilde{x}} + \tilde{h} - \frac{\beta}{2}\tilde{h}^2\tilde{\bar{u}}_{\tilde{x}}^2\Big)_{\tilde{x}} = O(\beta^2) .$$

We define the non-dimensional quantities $\tilde{\mathcal{K}}$ and $\tilde{q}_{\mathcal{K}}$ by

$$\tilde{\mathcal{K}} = \tilde{\bar{u}} - \frac{\beta}{3}\tilde{h}^2\tilde{\bar{u}}_{\tilde{x}\tilde{x}} - \beta\tilde{h}\tilde{h}_{\tilde{x}}\tilde{\bar{u}}_{\tilde{x}} ,$$

and

$$\tilde{q}_{\mathcal{K}} = \frac{1}{2}\tilde{\bar{u}}^2 - \frac{\beta}{3}\tilde{h}^2\tilde{\bar{u}}\tilde{\bar{u}}_{\tilde{x}\tilde{x}} - \beta\tilde{h}\tilde{h}_{\tilde{x}}\tilde{\bar{u}}\tilde{\bar{u}}_{\tilde{x}} + \tilde{h} - \frac{\beta}{2}\tilde{h}^2\tilde{\bar{u}}_{\tilde{x}}^2 .$$

Converting to the dimensional form by using the scalings $\mathcal{K} = c_0\tilde{\mathcal{K}}$ and $q_{\mathcal{K}} = c_0^2\tilde{q}_{\mathcal{K}}$, we obtain

$$\mathcal{K} = \bar{u} - \frac{1}{3}h^2\bar{u}_{xx} - hh_x\bar{u}_x ,$$

$$q_{\mathcal{K}} = gh + \frac{1}{2}\bar{u}^2 - \frac{1}{3}h^2\bar{u}\bar{u}_{xx} - hh_x\bar{u}\bar{u}_x - \frac{1}{2}h^2\bar{u}_x^2 ,$$

and therefore,

$$\frac{\partial\mathcal{K}}{\partial t} + \frac{\partial q_{\mathcal{K}}}{\partial x} = 0 ,$$

which is the same as equation (3.28). This equation is an exact balance law for solutions of the SGN system (3.20). The details for the derivation of the same conservation law for the three-dimensional SGN system has been given in [23].

3.1.4 Energy conservation in undular bores

When a long wave propagates into shallow water in some cases, it steepens and forms a bore. More generally, a bore is a transition between two uniform free-surface flows with different flow depths. For sufficiently large transitions, the front of the bores are often turbulent however, transitions of moderate amplitude are accompanied by wave trains without breaking and are called undular bores [6]. The bore shape and characteristics evolve rapidly with time in response to change in bathymetry. Well-known examples are the bores on the River Severen in England and the River Dordogne in France. The classical bore theory, Lamb [36], applied a well developed bore advancing at constant velocity and calculated the fluxes of mass, momentum and energy across the bore in a frame of reference moving with the bore velocity. It is shown that if the mass and momentum are conserved, energy must be necessarily lost. Benjamin and Lighthill [7] employed this approach within the approximation of the KdV equation and showed that if mass, momentum and energy are conserved the wave is a solitary wave and if energy is lost the wave is a cnoidal wave. Experimental measurements by Favre [22] show that undular bores form when the ratio of the change in level to the initial depth of water, α which is called the strength of the bore, is less than 0.28. If $(0.28 < \alpha < 0.78)$, then there are still undulation but one or a few waves behind the

bore front are starting to break. For ($0.78 < \alpha$), bore front breaks and a so-called turbulent occurs. The wave Froude number $Fr = \sqrt{[(2h_1/h_0+1)^2-1]/8}$ can also determine the bore strength. Specifically, when $Fr \gtrsim 1.4$, the bore consists of a steep front while undulations are growing at the bore front in the near-critical state $Fr \approx 1$ [16].

In paper B, the energy loss in the undular bore provided by the SGN system have been studied. Byatt-Smith [14] claimed that viscous action absorbs some of the energy at the bore which is not accounted for by the classical theory of the bore. However, using a dispersive model to study the energy loss in the undular bore shows that the energy loss is absorbed by the increasing number of oscillations following the bore front [2].

In our numerical analysis of the energy balance of undular bores, we have used

$$h(x,0) = h_0 + \frac{1}{2}(h_1 - h_0)\tanh(\frac{x}{2}),$$

as an initial surface condition that operates the generation of the undular bore. We have also considered an initial flow given by the following velocity profile

$$u(x,0) = \frac{\delta}{h_1}\sqrt{\frac{g}{2h_0}\left(2h_0^2 + 3(\delta h)h_0 + (\delta h)^2\right)}\left(1 - \tanh(\frac{x}{2})\right),$$

where $\delta h = h_1 - h_0$. A Galerkin method with cubic spline has been applied for solving the initial boundary value problem consist of the SGN system (3.17) subjec to reflective boundary conditions [31]. Taking $h_0 = 1$ and $\frac{h_1}{h_0} = 1.1, 1.2, .., 1.7$, we monitored the energy flux and work rate due to the pressure force, given by $q_E(x_1) - q_E(x_2)$ as defined in (3.29). We also monitored the gain in energy in the control interval which is given by $\mathcal{E}(t) = \int_{x_1}^{x_2} E\,dx$. Results are shown in Table 3.1 which shows that the energy balance laws is satisfied with accuracy 10^{-8} and confirms our previous finding that the energy is exactly conserved in the SGN model.

Table 3.1: Rate of change in energy for $T = 30$.

h_1/h_0	Fr	$q_E(x_1) - q_E(x_2)$	$\frac{d\mathcal{E}}{dt}$
1.1	1.07	3.6481059	3.6481059
1.2	1.15	8.6017456	8.6017456
1.3	1.22	15.100378	15.100378
1.4	1.30	23.394470	23.394470
1.5	1.37	33.746103	33.746103
1.6	1.44	46.429376	46.429376
1.7	1.51	61.730669	61.730669

Thus the energy lost in the shallow-water model is fed into oscillations behind the bore front.

3.2 The KDV equation

The SGN system describes the two-way propagation of water waves and it is used to model highly nonlinear weakly dispersive waves propagating at the surface of a shallow water. However, the KdV equation describes water waves traveling in one direction and it can model weakly nonlinear and dispersive waves at the surface of a shallow water. The KdV equation along with its cnoidal solution has been used to examine the waveheight change in surface waves with a sufficiently slow variation in depth in paper D.

3.2.1 Derivation and solution

From the equations (3.21a) and (3.21b) we have $\tilde{\eta}_{\tilde{t}} + \tilde{\bar{u}}_{\tilde{x}} = O(\alpha)$ and $\tilde{\bar{u}}_{\tilde{t}} + \tilde{\eta}_{\tilde{x}} = O(\alpha, \beta)$ respectively. Therefore, the wave equation follows as $\tilde{\eta}_{\tilde{t}\tilde{t}} + \tilde{\eta}_{\tilde{x}\tilde{x}} = O(\alpha, \beta^2)$. Consider a solution of the wave equation which satisfies $\tilde{\eta}_{\tilde{t}} + \tilde{\eta}_{\tilde{x}} = O(\alpha, \beta)$. Then the wave travels to the right and we choose

$$\tilde{\bar{u}} = \tilde{\eta} + \alpha A + \beta B + O(\alpha^2, \beta^2), \tag{3.31}$$

where A and B are functions of $\tilde{\eta}$ and its derivatives with respect to $\tilde{x}$ and can be found by substituting the expression (3.31) for $\tilde{\bar{u}}$ into system (3.21) and using the low order approximations $A_{\tilde{t}} + A_{\tilde{x}} = O(\alpha, \beta)$ and $B_{\tilde{t}} + B_{\tilde{x}} = O(\alpha, \beta)$. So we obtain $A = -\frac{1}{4}\tilde{\eta}^2$ and $B = \frac{1}{6}\tilde{\eta}_{\tilde{x}\tilde{x}}$. Therefore, $\tilde{\bar{u}} = \tilde{\eta} - \frac{\alpha}{4}\tilde{\eta}^2 + \frac{\beta}{6}\tilde{\eta}_{\tilde{x}\tilde{x}} + O(\alpha^2, \beta^2)$. By substituting the expression (3.31) for $\tilde{\bar{u}}$ into equation (3.21a), the non-dimensional KdV equation is

$$\tilde{\eta}_{\tilde{t}} + \tilde{\eta}_{\tilde{x}} + \frac{3}{2}\alpha\tilde{\eta}\tilde{\eta}_{\tilde{x}} + \frac{1}{6}\beta\tilde{\eta}_{\tilde{x}\tilde{x}\tilde{x}} = O(\alpha^2, \beta^2). \tag{3.32}$$

By neglecting terms of second order in α and β, the dimensional form of the KdV equation can be obtained as

$$\eta_t + c_0\eta_x + \frac{3c_0}{2h_0}\eta\eta_x + \frac{c_0 h_0^2}{6}\eta_{xxx} = 0\ , \tag{3.33}$$

and the velocity becomes

$$u = \frac{c_0}{h_0}\eta - \frac{c_0}{4h_0^2}\eta^2 + \frac{c_0 h_0}{6}\eta_{xx}.$$

The linearized form of this equation gives the dispersion relation

$$\omega = c_0 k - \frac{1}{6} c_0 h_0^2 k^3 \,,$$

which shows the KdV equation incorporates dispersive effects in the shallow water theory.

Cnoidal wave solution

Equation (3.33) has stationary solution in the form of

$$\eta = f_2 + (f_1 - f_2)\mathrm{cn}^2\Big(\sqrt{\frac{3(f_1-f_3)}{4h_0^3}}(x - Ct); m\Big), \tag{3.34}$$

where cn is the Jacobian elliptic function with modulus $m = \dfrac{f_1 - f_2}{f_1 - f_3}$ such that $0 < m < 1$. These solutions show the long flat troughs and narrow crests characteristics of waves in shallow water. The wave speed is

$$C = c_0\Big(1 + \frac{f_1 + f_2 + f_3}{2h_0}\Big) \,, \tag{3.35}$$

and the wavelength is defined by

$$L = K(m)\sqrt{\frac{16h_0^3}{3(f_1 - f_3)}} \,, \tag{3.36}$$

where $K(m) = \int_0^{\frac{\pi}{2}} \frac{1}{\sqrt{1 - m\sin^2\theta}}\, d\theta$ is the complete elliptic integral of the first kind. These solutions depend on three parameters f_1, f_2 and f_3 which can be taken in the form $f_1 > f_2 > f_3$. The parameters f_1 and f_2 denote the wave crest and trough, respectively, while f_3 is a parameter that only affects the shape of the wave. Any cnoidal wave is completely determined as long as these three parameters are fixed. Let us consider

$$f(\zeta) = f_2 + (f_1 - f_2)\mathrm{cn}^2\big(\frac{\zeta}{\sigma}; m\big) \,,$$

such that $f(\zeta_1) = f_1$ and $f(\zeta_2) = f_2$. Then the mean value of the surface displacement over one wavelength must be equal to

$$\begin{aligned} \bar{\eta} &= \frac{2}{L}\int_{\zeta_1}^{\zeta_2} f(\zeta)\, d\zeta \\ &= \frac{2\sigma}{L}\big((f_1 - f_3)E(m) + f_3 K(m)\big) \,, \end{aligned}$$

where $\sigma = \sqrt{\frac{4}{3(f_1-f_3)}}$ and $E(m) = \int_0^{\frac{\pi}{2}} \sqrt{1-m\sin^2\theta}\, d\theta$ is the complete elliptic integral of the second kind. Therefore, the expressions for f_1, f_2 and f_3 in terms of waveheight, $H = f_1 - f_2$, and modulus m may be written as

$$\begin{aligned} f_1 &= f_3 + \frac{H}{m}, \\ f_2 &= f_1 - H, \\ f_3 &= \frac{\sqrt{3mH}L\tilde{\eta} - 4HE(m)}{4mK(m)}. \end{aligned} \tag{3.37}$$

In the limit as $m \to 1^-$, the solutions correspond to the infinitely long solitary waves. In the limit when $m \to 0^+$, the cnoidal theory generates a linear wave.

3.2.2 Mechanical balance laws

In paper D, we have examined the evolution of a cnoidal wave solution of the KdV equation by using conservation of momentum and energy in the context of the KdV equation. A brief review of the derivation of balance law is given in the following sections. More details about derivation of conservation laws for the KdV equation will be found in [5].

Mass balance

Mass conservation can be written as

$$\frac{d}{dt}\int_{x_1}^{x_2}\int_{-h_0}^{\eta} dz\,dx = \Big[\int_{-h_0}^{\eta} \phi_x(x,z,t)\,dz\Big]_{x_2}^{x_1}.$$

In non-dimensional form this relation becomes

$$\frac{d}{d\tilde{t}}\int_{\tilde{x}_1}^{\tilde{x}_2}\int_0^{1+\alpha\tilde{\eta}} d\tilde{z}d\tilde{x} = \alpha\Big[\int_0^{1+\alpha\tilde{\eta}} \tilde{\phi}_{\tilde{x}}(\tilde{x},\tilde{z},\tilde{t})\; d\tilde{z}\Big]_{\tilde{x}_2}^{\tilde{x}_1}.$$

Substituting the expression for $\tilde{\phi}_{\tilde{x}}$,in terms of $\tilde{\eta}$, given by

$$\tilde{\phi}_{\tilde{x}} = \tilde{\eta} + \frac{1}{4}\alpha\tilde{\eta}^2 + \beta(\frac{1}{3} - \frac{\tilde{z}^2}{2})\tilde{\eta}_{\tilde{x}\tilde{x}} + O(\alpha^2, \alpha\beta, \beta^2)\,, \tag{3.38}$$

and integrating with respect to $\tilde{z}$ leads to the approximation

$$\frac{d}{d\tilde{t}}\int_{\tilde{x}_1}^{\tilde{x}_2}(1+\alpha\tilde{\eta})\,d\tilde{x} = \alpha\Big[\tilde{\eta} + \frac{3}{4}\alpha\tilde{\eta}^2 + \frac{1}{6}\beta\tilde{\eta}_{\tilde{x}\tilde{x}} + O(\alpha\beta, \beta^2)\Big]_{\tilde{x}_2}^{\tilde{x}_1}.$$

One may divide by the length of the interval and taking the limit as $\tilde{x}_2 \to \tilde{x}_1$ to find

$$\tilde{\eta}_{\tilde{t}} + \tilde{\eta}_{\tilde{x}} + \frac{3}{2}\alpha\tilde{\eta}\tilde{\eta}_{\tilde{x}} + \frac{1}{6}\beta\tilde{\eta}_{\tilde{x}\tilde{x}\tilde{x}} = O(\alpha\beta, \beta^2) \,. \tag{3.39}$$

Therefore, if we denote the non-dimensional mass density by

$$\tilde{M} = 1 + \alpha\tilde{\eta} \,,$$

and the non-dimensional mass flux by

$$\tilde{q_M} = \alpha\tilde{\eta} + \frac{3}{4}\alpha^2\tilde{\eta}^2 + \frac{1}{6}\alpha\beta\tilde{\eta}_{\tilde{x}\tilde{x}} \,,$$

the non-dimensional mass balance is

$$\frac{\partial}{\partial\tilde{t}}\tilde{M} + \frac{\partial}{\partial\tilde{x}}\tilde{q}_M = O(\alpha\beta, \beta^2) \,.$$

Using the scalings $M = h_0\tilde{M}$ and $q_M = h_0 c_0 \tilde{q}_M$, give the dimensional forms of the balance equation

$$\frac{\partial}{\partial x}M + \frac{\partial}{\partial t}q_M = 0 \,,$$

where

$$M = h_0 + \eta \,,$$

and

$$q_M = c_0\Big(\eta + \frac{3}{4h_0}\eta^2 + \frac{h_0^2}{6}\eta_{xx}\Big) \,.$$

One can see from equation (3.39) that the KdV equation is a mass balance equation.

Momentum balance

A relation for momentum conservation can be expressed by

$$\frac{d}{dt}\int_{x_1}^{x_2}\int_{-h_0}^{\eta}\phi_x\,dz\,dx = \Big[\int_{-h_0}^{\eta}(\phi_x^2 + P)\,dz\Big]_{x_2}^{x_1} \,.$$

In non-dimensional variables, it is of the form

$$\alpha\frac{d}{d\tilde{t}}\int_{\tilde{x}_1}^{\tilde{x}_2}\int_0^{1+\alpha\tilde{\eta}}\tilde{\phi}_{\tilde{x}}\,d\tilde{z}\,d\tilde{x} = \Big[\int_0^{1+\alpha\tilde{\eta}}\big(\alpha^2\tilde{\phi}_{\tilde{x}}^2 + \alpha\tilde{P'} - (\tilde{z}-1)\big)\,d\tilde{z}\Big]_{\tilde{x}_2}^{\tilde{x}_1} \,.$$

Substituting the expression (3.38) for $\tilde{\phi}_{\tilde{x}}$ and using the relation

$$\tilde{P'} = \tilde{\eta} - \frac{1}{2}\beta(\tilde{z}^2 - 1)\tilde{\eta}_{\tilde{x}\tilde{x}} + O(\alpha\beta, \beta^2) \,,$$

yield

$$\alpha\frac{d}{d\tilde{t}}\int_{\tilde{x}_1}^{\tilde{x}_2}\Big\{\tilde{\eta}+\frac{3}{4}\alpha\tilde{\eta}^2+\frac{1}{6}\beta\tilde{\eta}_{\tilde{x}\tilde{x}}\Big\}d\tilde{x}= \Big[\alpha^2\tilde{\eta}^2+\frac{(1+\alpha\tilde{\eta})^2}{2}+\frac{\alpha\beta}{3}\tilde{\eta}_{\tilde{x}\tilde{x}}\Big]_{\tilde{x}_2}^{\tilde{x}_1}+O(\alpha^3,\alpha^2\beta,\alpha\beta^2)\ .$$

Differentiating with respect to $\tilde{x}$ gives the balance equation

$$\Big(\tilde{\eta}+\frac{3}{4}\alpha\tilde{\eta}^2+\frac{1}{6}\beta\tilde{\eta}_{\tilde{x}\tilde{x}}\Big)_{\tilde{t}}+\Big(\tilde{\eta}+\frac{3}{2}\alpha\tilde{\eta}^2+\frac{1}{3}\beta\tilde{\eta}_{\tilde{x}\tilde{x}}\Big)_{\tilde{x}}=O(\alpha^2,\alpha\beta,\beta^2)\ .$$

By considering the non-dimensional momentum density as

$$\tilde{I}=\alpha\tilde{\eta}+\frac{3}{4}\alpha^2\tilde{\eta}^2+\frac{1}{6}\alpha\beta\tilde{\eta}_{\tilde{x}\tilde{x}}\ ,$$

and the non-dimensional momentum flux as

$$\tilde{q_I}=\frac{1}{2}+\alpha\tilde{\eta}+\frac{3}{2}\alpha^2\tilde{\eta}^2+\frac{1}{3}\alpha\beta\tilde{\eta}_{\tilde{x}\tilde{x}}\ ,$$

the momentum balance may be written in the following form

$$\frac{\partial}{\partial\tilde{t}}\tilde{I}+\frac{\partial}{\partial\tilde{x}}\tilde{q}_I=O(\alpha^2,\alpha\beta,\beta^2)\ .$$

Using the scalings $I=c_0h_0\tilde{I}$ and $q_I=c_0^2h_0\tilde{q}_I$, the dimensional of the momentum density and momentum flux are given by

$$I=c_0(\eta+\frac{3}{4h_0}\eta^2+\frac{h_0^2}{6}\eta_{xx})\ ,$$

and

$$q_I=c_0^2(\frac{h_0}{2}+\eta+\frac{3}{2h_0}\eta^2+\frac{h_0^2}{3}\eta_{xx})\ . \tag{3.40}$$

Energy balance

Conservation of the total mechanical energy can be written as

$$\frac{\partial}{\partial t}\int_{x_1}^{x_2}\int_{-h_0}^{\eta}\{\frac{1}{2}|\nabla\phi|^2+gz\}\,dz\,dx=\Big[\int_{-h_0}^{\eta}\{\frac{1}{2}|\nabla\phi|^2+gz\}\phi_x\,dz+\int_{-h_0}^{\eta}\phi_xP\,dz\Big]_{x_2}^{x_1}\ .$$

Converting to non-dimensional variables gives

$$\frac{\partial}{\partial\tilde{t}}\int_{\tilde{x}_1}^{\tilde{x}_2}\int_0^{1+\alpha\tilde{\eta}}\Big\{\frac{\alpha^2}{2}\big(\tilde{\phi}_{\tilde{x}}^2+\frac{1}{\beta}\tilde{\phi}_{\tilde{z}}^2\big)+(\tilde{z}-1)\Big\}\,d\tilde{z}d\tilde{x}$$
$$=\alpha\Big[\int_0^{1+\alpha\tilde{\eta}}\Big\{\frac{\alpha^2}{2}\big(\tilde{\phi}_{\tilde{x}}^3+\frac{1}{\beta}\tilde{\phi}_{\tilde{x}}^2\tilde{\phi}_{\tilde{x}}\big)+(\tilde{z}-1)\tilde{\phi}_{\tilde{x}}\Big\}\,d\tilde{z}$$
$$+\alpha\int_0^{1+\alpha\tilde{\eta}}\tilde{P}'\tilde{\phi}_{\tilde{x}}d\tilde{z}+\int_0^{1+\alpha\tilde{\eta}}(1-\tilde{z})\tilde{\phi}_{\tilde{x}}d\tilde{z}\Big]_{\tilde{x}_2}^{\tilde{x}_1}.$$

Substituting (3.38) for $\tilde{\phi}_{\tilde{x}}$ and $\tilde{\phi}_{\tilde{z}}=\beta\tilde{z}\tilde{\eta}_{\tilde{x}}+O(\alpha\beta,\beta^2)$ and integrating with respect to $\tilde{z}$ will give

$$\frac{d}{d\tilde{t}}\int_{\tilde{x}_1}^{\tilde{x}_2}\Big\{\alpha^2\tilde{\eta}^2+\frac{\alpha^3}{4}\tilde{\eta}^3+\frac{\alpha^2\beta}{6}\tilde{\eta}\tilde{\eta}_{\tilde{x}\tilde{x}}+\frac{\alpha^2\beta}{6}\tilde{\eta}_{\tilde{x}}^2\Big\}\,d\tilde{x}=$$
$$\Big[\alpha^2\tilde{\eta}^2+\frac{5}{4}\alpha^3\tilde{\eta}^3+\frac{\alpha^2\beta}{2}\tilde{\eta}\tilde{\eta}_{\tilde{x}\tilde{x}}\Big]_{\tilde{x}_2}^{\tilde{x}_1}+O(\alpha^4,\alpha^3\beta,\alpha^2\beta^2)\,.$$

Therefore, the differential form of the energy balance equation can be written as

$$\Big(\tilde{\eta}^2+\frac{\alpha}{4}\tilde{\eta}^3+\frac{\beta}{6}\tilde{\eta}\tilde{\eta}_{\tilde{x}\tilde{x}}+\frac{\beta}{6}\tilde{\eta}_{\tilde{x}}^2\Big)_{\tilde{t}}+\Big(\tilde{\eta}^2+\frac{5}{4}\alpha\tilde{\eta}^3+\frac{1}{2}\beta\tilde{\eta}\tilde{\eta}_{\tilde{x}\tilde{x}}\Big)_{\tilde{x}}=O(\alpha^2,\alpha\beta,\beta^2)\,.$$

Thus the non-dimensional energy density is

$$\tilde{E}=\alpha^2\tilde{\eta}^2+\frac{\alpha^3}{4}\tilde{\eta}^3+\frac{\alpha^2\beta}{6}\tilde{\eta}\tilde{\eta}_{\tilde{x}\tilde{x}}+\frac{\alpha^2\beta}{6}\tilde{\eta}_{\tilde{x}}^2\,,$$

and the energy flux is given by

$$\tilde{q_E}=\alpha^2\tilde{\eta}^2+\frac{5}{4}\alpha^3\tilde{\eta}^3+\frac{1}{2}\alpha^2\beta\tilde{\eta}\tilde{\eta}_{\tilde{x}\tilde{x}}\,.$$

Using the scalings $E=c_0^2h_0\tilde{E}$ and $q_E=c_0^3h_0\tilde{q}_E$ the dimensional form of energy density and energy flux are given by

$$E=c_0^2\Big(\frac{1}{h_0}\eta^2+\frac{1}{4h_0^2}\eta^3+\frac{h_0}{6}\eta\eta_{xx}+\frac{h_0}{6}\eta_x^2\Big)\,,$$

and

$$q_E=c_0^3\Big(\frac{1}{h_0}\eta^2+\frac{5}{4h_0^2}\eta^3+\frac{h_0}{2}\eta\eta_{xx}\Big)\,. \tag{3.41}$$

3.2.3 Wave shoaling

The waves propagation from deep water to shallow water is affected by the reducing depth $h(x)$, due to the sloping bottom. The depth reduction causes significant changes in the wave shape, height H, length L, and phase velocity c, while the wave period T remains constant. The momentous function of engineers is to predict these changes before the waves become unstable and break. These changes in water wave which is known as wave shoaling have been studied significantly in both theoretical and experimental areas and the existing literature is extensive. Many interesting results can be found in [26, 28, 30, 33, 41, 46]. Green's law, a classical linear theory, describes the evolution of the wave height of periodic waves on plane beaches. It predicts that the maximum height of the wave is proportional to $h^{\frac{-1}{4}}$, where h is the local undisturbed water depth. The Boussinesq's law incorporates both dispersion and nonlinearity and states that the waveheight of a shoaling solitary wave can be predicted by h^{-1}. The different zones of evolution of solitary waves are discussed by Synolakis and Skjelbreia [55]. The linear shoaling theory applies to predict the waveheight of a periodic wave of arbitrary wavelength with small wave steepness and it is based on conservation of the wave frequency and the energy flux. In this theory, the waveheight can be described by $\frac{H}{H_0} = \sqrt{\frac{C_{g,0}}{C_g}}$, where H_0 is the waveheight in deep water, $C_{g,0}$ is the deep-water group velocity, H is the waveheight in the local depth and C_g is the local group velocity. A number of studies [41, 46, 52, 53, 54] employed a time-periodic solution of the KdV equation to represent the behavior of the periodic long waves due to sloping bottom. Paper D is concerned with the slow transformation of a long wave over a gently sloping bottom slope in the context of the KdV equation (3.32). In [46, 52, 53] the conservation of energy flux was based on the formula originating from linear water wave theory. In paper D, we present a new study in which the energy flux is evaluated strictly in the framework of the KdV approximation. The expression (3.41) for energy flux has been used in our study. The variation of the height of shoaling can now be computed in a straightforward manner by imposing constant time period and conservation of mass in addition to conservation of energy. Assuming incident periodic waves of wavelength L^A at water depth h^A, we can find the waveheight at water depth h by using the following equations:

$$\begin{aligned} \frac{c^A}{L^A} &= \frac{c}{L}\,, \\ \int_0^T q_E^A\, dt &= \int_0^T q_E dt\,, \\ \int_0^L \eta^A dx &= \int_0^L \eta dx\,. \end{aligned}$$

Using the exact solution of the KdV equation (3.34) with wave speed (3.35) and wavelength (3.36) and the expression (3.41) for energy flux q_E, these three equations can be converted into a system of three nonlinear equations for the parameters f_1, f_2 and f_3. This system of equations can be solved numerically and the parameters for a wave at water depth h will be obtained. In order to study the shoaling of solitary waves, the parameters for the incident waves are chosen such that the wave is very long and its trough is situated at the undisturbed depth h^A.

Comparing with previous work, note that the authors of [52] represented the variation of the cnoidal wave height to deep water data by matching the energy flux at a cut-off point $\frac{h}{L_0} = 0.10$, while the authors of [53] imposed continuity in wave height at the matching point but in this case, energy was not conserved. These two methods of treating the cut-off points give rather difference results. It can be shown that the use of the expression q_E eliminates the difference between the two methods. Figure (3.4) illustrates a comparison between the result of paper D and the result of Svendsen and Brink-kjær [52] for a specific wave profile.

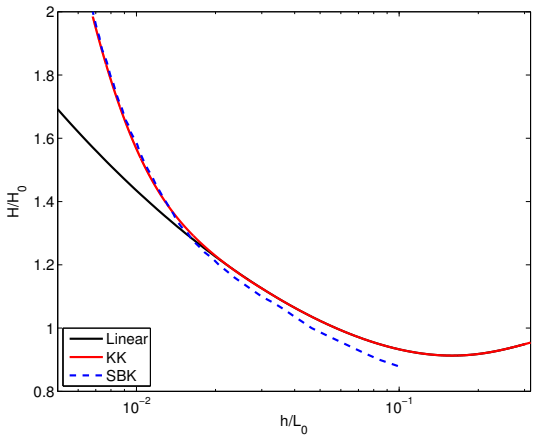

Figure 3.4: The shoaling curves for a periodic wave profile with $\frac{H_0}{L_0} = 0.001$ and $\frac{L_0}{h_0} = 13.8$. The red curve, KK, is the shoaling curve based on the paper D. The blue dashed curve, SBK, is the shoaling curve after Svendsen and Brink-Kjær. The curve SBK, which was obtained by matching the calculated energy flux values of the cnoidal theory and the linear theory at $\frac{h}{L_0} = 0.1$, has a discontinuity in waveheight. The curve KK, which was obtained by using the nonlinear energy flux in the context of the KdV equation, eliminates the discontinuity in the wave height.

Also, the method is applied to the shoaling of solitary waves, and the shoaling

curves of the paper D are compared with the numerical results of [27]. In this work, the authors used an advanced two-dimensional fully nonlinear numerical wave model based on potential flow theory to compute solitary wave variation over plane slopes. The results of the comparison are displayed in the paper D.

3.2.4 Further work

Attempts should be made to modify our result by using the effects of the radiation stress. As it was mentioned before, the principal component, S_{xx}, of the radiation stress is

$$S_{xx} = \int_{-h}^{\eta} (P + \rho u^2)\, dz - \int_{-h}^{0} \rho g z\, dz,$$

where the first integral on the right-hand side is the mean value of the flux of horizontal momentum across a plane x = constant. Following [5], an expression for the momentum flux in the context of KdV equation is (3.40). Therefore, an expression for the x-component of the radiation stress in the KdV model can be obtained in the following form

$$\begin{aligned} S_{xx} = q_I - \int_{-h_0}^{0} \rho g z\, dz &= \rho g h_0 \Big(\frac{(h_0+\eta)^2}{2h_0} + \frac{h_0^2}{3}\eta_{xx} + \frac{\eta^2}{h_0} \Big) - \frac{1}{2}\rho g h_0^2 \\ &= \rho g \Big(h_0\eta + \frac{3}{2}\eta^2 + \frac{h_0^3}{3}\eta_{xx} \Big). \end{aligned}$$

Let us consider the momentum balance equation which is given by

$$\frac{dS_{xx}}{dx} + \rho g(\bar{\eta} + h)\frac{d\bar{\eta}}{dx} = 0. \tag{3.42}$$

Now we integrate the equation (3.42) over the interval $[X, X+dX]$

$$\int_X^{X+dX} \frac{dS_{xx}}{dx}\, dx + \int_X^{X+dX} \rho g \bar{\eta} \frac{d\bar{\eta}}{dx}\, dx + \int_X^{X+dX} \rho g h \frac{d\bar{\eta}}{dx}\, dx = 0.$$

Let us denote $F|_{(x=X)} = F^A$ and $F|_{(x=X+dX)} = F^B$, we obtain

$$S_{xx}^B - S_{xx}^A = \frac{\rho g}{2}\big((\bar{\eta}^A)^2 - (\bar{\eta}^B)^2\big) + \rho g(h^A\bar{\eta}^A - h^B\bar{\eta}^B) + \frac{\rho g}{2} dX (h_x^B\bar{\eta}^B + h_x^A\bar{\eta}^A),$$

where $h_x^B = h_x^A = \frac{h^B - h^A}{dX}$, thus

$$\begin{aligned} S_{xx}^B - S_{xx}^A &= \frac{\rho g}{2}\big((\bar{\eta}^A)^2 - (\bar{\eta}^B)^2\big) + \frac{\rho g}{2}(h^A + h^B)(\bar{\eta}^A - \bar{\eta}^B) \\ &= \frac{\rho g}{2}(\bar{\eta}^A - \bar{\eta}^B)(\bar{\eta}^A + h^A + \bar{\eta}^B + h^B). \end{aligned} \tag{3.43}$$

As the shoaling phenomenon lowers the mean surface level, in this study, we include set-down (2.8) in our calculation at the transition point, transition between the linear theory and the cnoidal theory, and replace the equation

$$\int_0^L \eta^A dx = \int_0^L \eta dx$$

by equation (3.43).

By assuming that the motion at a certain water depth h^A is given, the motion at a new water depth is determined by solving numerically the following system and using (3.37) to get the initial values for parameters f_1, f_2 and f_3 hence,

$$\begin{aligned}
\frac{c^A}{L^A} &= \frac{c}{L}, \\
\int_0^T q_E^A dt &= \int_0^T q_E \, dt, \\
\int_0^T S_{xx}^A dt &= \int_0^T \left(S_{xx} + \frac{\rho g}{2} (h^A + \bar{\eta}^A + h + \bar{\eta})(\bar{\eta} - \bar{\eta}^A) \right) dt \ .
\end{aligned}$$

We have done some preliminary work on the numerical solution but no definite results have been obtained yet.

Bibliography

[1] G. B. Airy. Tides and waves. *Encyclopedia Metropolitana*, 192:241–396, 1845.

[2] A. Ali and H. Kalisch. Energy balance for undular bores. *C. R. Mecanique*, 338:67–70, 2010.

[3] A. Ali and H. Kalisch. A dispersive model for undular bores. *Anal. Math. Phys.*, 2:347–366, 2012.

[4] A. Ali and H. Kalisch. Mechanical balance laws for Boussinesq models of surface water waves. *J. Nonlinear Sci.*, 22:371–398, 2012.

[5] A. Ali and H. Kalisch. On the formulation of mass, momentum and energy conservation in the KdV equation. *Acta Appl. Math.*, 133:113–131, 2014.

[6] T.B. Benjamin. The solitary wave with surface tension. *Quarterly of Applied Mathematics*, pages 231–234, July 1982.

[7] T.B. Benjamin and M. J. Lighthill. On cnoidal waves and bores. *Proc. Roy. Soc. London*, A 224:448–460, 1954.

[8] M. Bjørkavåg and H. Kalisch. Wave breaking in Boussinesq models for undular bores. *Physics Letters A*, 375:1570–1578, 2011.

[9] M. Bjørkavåg, H. Kalisch, Z. Khorsand, and D. Mitsotakis. Legendre pseudospectral approximation of boussinesq systems and applications to wave breaking. *J. Math. Stud.*, 49(3):221–238, 2016.

[10] J.L. Bona, M. Chen, and J.-C. Saut. Boussinesq equations and other systems for small-amplitude long waves in nonlinear dispersive media. I: Derivation and linear theory. *J. Nonlinear Sci.*, 12:283–318, 2002.

[11] H. Borluk and H. Kalisch. Particle dynamics in the KdV approximation. *Wave Motion*, 49:691–709, 2012.

[12] N. Bottman and B. Deconinck. KdV cnoidal waves are linearly stable. *Discrete Contin. Dyn. Syst.*, A 25:1163–1180, 2009.

[13] J. Boussinesq. Théorie de líntumescence liquide appele onde solitaire ou de translation se propageant dans un canal rectangulaire. *Comptes Rendus Acad. Sci (Paris)*, 72:755–759, 1871.

[14] J. G. B. Byatt-Smith. The effect of laminar viscosity on the solution of the undular bore. *J. Fluid Mech.*, 48:33–40, 1971.

[15] D. Carter and R. Cienfuegos. The kinematics and stability of solitary and cnoidal wave solutions of the Serre equations. *European Journal of Mechanics B/Fluids*, 30:259–268, 2011.

[16] H. Chanson. Current knowledge in hydraulic jumps and related phenomena. A survey of experimental results. *European journal of Mechanics B/Fluids*, 28:191–210, 2009.

[17] D. Christodoulou. The Euler equations of compressible fluid flow. *Bulletin of the American Mathematical Society*, 44(4):581602, 2007.

[18] R. Cienfuegos, E. Barthelemy, and P. Bonneton. A fourth-order compact finite volume scheme for fully nonlinear and weakly dispersive Boussinesq-type equations. Part I: Model development and analysis. *Int. J. Numer. Meth. Fluids*, 51:1217–1253, 2006.

[19] R. G. Dean and R. A. Dalrymple. *Water wave mechanics for engineers and scientists*. World Scientific Publishing Co. Pte. Ltd., 1991. ISBN-9810204205.

[20] G. A. El, R. H. J. Grimshaw, and N. F. Smyth. Unsteady undular bores in fully nonlinear shallow-water theory. *Phys. Fluids*, 18(027104), 2006.

[21] L. Euler. Principes generaux du mouvement des fluides. *Mémoires de lAcademie des Sciences de Berlin*, 11:274–315, 1757.

[22] H. Favre. *Ondes de Translation*. Dunod, Paris, 1935.

[23] S. Gavrilyuk, H. Kalisch, and Z. Khorsand. A kinematic conservation law in free surface flow. *Nonlinearity*, 28:1805–1821, 2015.

[24] F.J. Gerstner. Theorie der wellen. *Abhandlunger der Kniglichen Bhmischen Geselschaft der Wissenschaften, Prague*, 1802.

[25] A. Green and P. Naghdi. A derivation of equations for wave propagation in water of variable depth. *J. Fluid Mech.*, 78:237–246, 1976.

[26] S.T. Grilli, R. Subramanya, I.A. Svendsen, and J. Veeramony. Shoaling of solitary waves on plane beaches. *J. Wtrwy. Port, Coast., and Engrg.*, 120:609–628, 1994.

[27] S.T. Grilli, I.A. Svendsen, and R. Subramanya. Breaking criterion and characteristics for solitary waves on slopes. *J. Wtrwy., Port, Coast., and Oc. Engrg.*, 123:102–112, 1997.

[28] R. Grimshaw. The solitary wave in water of variable depth, part 2. *J. Fluid Mech*, 46:611–622, 1971.

[29] L. H. Holthuijsen. *Waves in oceanic and coastal waters*. Cambridge University Press, 2007. ISBN 978-0-521-86028-4.

[30] A.T. Ippen and G. Kulin. The shoaling and breaking of the solitary wave. *Pro. 5th Conf. On Coast. Eng. Grenoble*, pages 27–47, 1954.

[31] H. Kalisch, Z. Khorsand, and D. Mitsotakis. Mechanical balance laws for fully nonlinear and weakly dispersive water waves. *Physica D*, 333:243–253, 2016.

[32] Z. Khorsand. Particle trajectories in the serre equations. *Applied Mathematics and Computations*, 230:35–42, 2014.

[33] Z. Khorsand and H. Kalisch. On the shoaling of soiltary waves in the KdV equation. *Proc. 34th Conf. Coastal Engng, Seoul*, pages 1–10, 2014. DOI: https://doi.org/10.9753/icce.v34.waves.44.

[34] D.J. Korteweg and G. de Vries. On the change of form of long waves advancing in a rectangular channel and on a new type of long stationary wave. *Philos. Mag*, 39(5):422–443, 1895.

[35] P.K. Kundu and I.M. Cohen. *Fluid Mechanics*. Elsevier Academic Press, 2004. ISBN-0-12-178253-0.

[36] H. Lamb. *Hydrodaynamics*. Cambridge University Press, 1932. Sixth edition.

[37] D. Lannes and P. Bonneton. Derivation of asymptotic two-dimensional time-dependent equations for surface water wave propagation. *Physics of Fluids*, 21:016601, 2009.

[38] R. Lemoine. Sur les ondes positives de translation dans les canaux et sur le ressaut ondule de faible amplitude. *Jl. La Houille Blanche*, pages 183–185, 1948.

[39] M.S. Longuet-Higgins and R.W. Stewart. Radiation stress and mass transport in gravity waves, with application to "surf beats". *J. Fluid Mech.*, 13:481–504, 1962.

[40] P. A. Madsen and O. R. Sørensen. A new form of the boussinesq equations with improved linear dispersion characteristics. part 2. A slowly-varying bathymetry. *Coastal Engineering*, 18:183–204, 1992.

[41] L.A. Ostrovskiy and E.N. Pelinovskiy. Wave transformation on the surface of a fluid on variable depth. *Atmos. Ocean. Phys.*, 6:552–555, 1970.

[42] E. N. Pelinovsky and H. S. Choi. A mathematical model for non-linear waves due to moving disturbances in a basin of variable depth. *J. Korean Soc. Coastal Ocean Eng.*, 5:191–197, 1993.

[43] D. H. Peregrine. Calculations of the development of an undular bore. *J. Fluid Mech.*, 25:321–330, 1966.

[44] Lord Rayleigh. On the Theory of Long Waves and Bores. *Proc. R. Soc. Lond.*, A 90:324–328, 1914.

[45] J. S. Russell. Report on waves. *Fourteenth meeting of the British Association for the Advancement of Science*, 1844.

[46] T. Sakai and J. Battjes. Wave shoaling calculated from cokelet's theory. *Coastal Engineering*, 4:65–84, 1980.

[47] F. Serre. *Houille Blanche*, 8:374–388, 1953.

[48] F. Serre. *Houille Blanche*, 8:830–872, 1953.

[49] G. G. Stokes. On the theory of oscillatory waves. *Trans. Camp. Phil. Soc.*, 8:441–455, 1847.

[50] B. Sturtevant. Implications of experiments on the weak undular bore. *Phys. Fluids*, 6:1052–1055, 1965.

[51] C.H. Su and C.S. Gardner. Korteweg-de Vries equation and generalizations. iii. Derivation of the Korteweg-de Vries equation and Burgers equation. *J. Math. Phys.*, 10:536–539, 1969.

[52] I.A. Svendsen and O. Brink-Kjær. Shoaling of cnoidal waves. *Proc. 13th Conf. Coastal Engng, Vancouver*, pages 365–383, 1972.

[53] I.A. Svendsen and J. Buhr Hansen. The wave height variation for regular waves in shoaling water. *Coastal Engineering*, 1:261–284, 1977.

[54] I.A. Svendsen and J. Buhr Hansen. On the deformation of periodic long waves over a gently sloping bottom. *J. Fluid Mech.*, 87:433–448, 1978.

[55] C.E. Synolakis and J.E. Skjelbreia. Evolution of maximum amplitude of solitary waves on plane beaches. *J. Wtrwy., Port, Coast., and Oc. Engrg., ASCE*, 119:323–342, 1993.

[56] G. Whitham. *Linear and Nonlinear Waves*. New York: Wiley, 1974. ISBN-0-471-94090-9.

Part II

Papers and Reports

A

Paper A

Particle trajectories in the Serre equations *

* *Published in Applied Mathematics and Computation 230, 2014.*

Applied Mathematics and Computation 230 (2014) 35–42

Contents lists available at ScienceDirect

Applied Mathematics and Computation

journal homepage: www.elsevier.com/locate/amc

Particle trajectories in the Serre equations

Zahra Khorsand

Department of Mathematics, University of Bergen, 5020 Bergen, Norway

ARTICLE INFO

Keywords:
Surface waves
Serre equations
Particle trajectories
Solitary waves
Periodic waves

ABSTRACT

We present a numerical study of particle paths in an irrotational free surface flow over a flat bottom where the Serre equations are considered as the governing equations. For solitary surface waves, we obtain that the particle paths are parabolic with a large forward drift. Periodic solutions of the Serre equations feature nearly closed particle trajectories with a slight backward drift depending on the initial depth of the particles. This backward drift appears to be due to negative mean horizontal velocity in the periodic solutions.

© 2013 Elsevier Inc. All rights reserved.

1. Introduction

The evolution of gravity waves on the surface of a body of fluid is widely studied. The fundamental model for inviscid fluid motion are the Euler equations. When coupled with free surface boundary conditions these are very difficult to study both numerically and theoretically. For many applications, there are a variety of approximate model equations. The Korteweg–de Vries (KdV) equation is a model equation describing long waves with small amplitude. A great deal of research has been invested in the study of the analytical and numerical solutions for different types of the KdV equation [1–4]. The Serre equations are obtained by depth-averaging the Euler system and can model highly nonlinear waves with finite amplitude. These equations are named after François Serre, who derived this model for the first time in 1953 [5]. Several years later, these equations were independently rediscovered by Su and Gardner [6], and Green, Laws and Naghdi [7] with different methods. The extension of Serre equations for general uneven bathymetries was derived by Seabra-Santos et al. [8]. For some generalizations and to find an extended set of the Serre equations we refer to studies by Dias and Milewski [9], Barthélemy [10], and Carter and Cienfuegos [12]. It is also possible to find exact solutions of these equations describing solitary and periodic water waves. The relevance of the Serre solitary and cnoidal solutions were investigated by Carter and Cienfuegos [12]. A variety of numerical methods have been applied to the Serre equations [11,13,14]. Comparison of numerical simulations with physical experiments indicates the accuracy of the Serre equations in describing strongly nonlinear shallow water waves.

In the present study, the focus is on numerical simulation of particle trajectories associated with certain wave patterns at the surface of the fluid. Let us briefly introduce the model system to be used here. We consider a two-dimensional irrotational flow of an inviscid incompressible fluid. Let a_0 be a typical wave amplitude, l the wavelength and h_0 the mean water depth. There are two important parameters associated with long waves. One is the relative amplitude of the waves, $\alpha = a_0/h_0$, and the other one is the ratio of undisturbed depth square to typical wave length square, $\beta = h_0^2/l^2$. In non-dimensional variables, the Serre system takes the form

$$\tilde{\eta}_{\tilde{t}} + [\tilde{h}\tilde{u}]_{\tilde{x}} = 0,$$

E-mail address: Zahra.Khorsand@math.uib.no

0096-3003/$ - see front matter © 2013 Elsevier Inc. All rights reserved.
http://dx.doi.org/10.1016/j.amc.2013.12.018

$$\tilde{\bar{u}}_{\tilde{t}} + \alpha\tilde{\bar{u}}\tilde{\bar{u}}_{\tilde{x}} + \tilde{\eta}_{\tilde{x}} - \frac{\beta}{3h}\frac{\partial}{\partial\tilde{x}}(h^3(\tilde{\bar{u}}_{\tilde{x}\tilde{t}} + \alpha\tilde{\bar{u}}\tilde{\bar{u}}_{\tilde{x}\tilde{x}} - \alpha(\tilde{\bar{u}}_{\tilde{x}})^2)) = \mathcal{O}(\beta^2, \alpha\beta^2).$$

Here $\tilde{\eta}$ is the non-dimensional excursion of the free surface, and $\tilde{\bar{u}}$ represents the non-dimensional depth-averaged horizontal velocity. Keeping all terms implies that the amplitude of the waves may not be small, thus $\alpha \sim \mathcal{O}(1)$. We refer the reader to Barthélemy [10] for details. Following the method introduced by Ali and Kalisch [25], in order to determine which terms should be kept to obtain an approximation for the velocity field, the incompressibility $\tilde{u}_{\tilde{x}} + \tilde{v}_{\tilde{z}} = 0$ must hold to the same order in β as the evolution equations. Therefore the non-dimensional velocity components are given by:

$$\tilde{u}(\tilde{x}, \tilde{z}, \tilde{t}) = \tilde{\bar{u}} + \frac{1}{6}\beta h^2\frac{\partial^2\tilde{\bar{u}}}{\partial\tilde{x}^2} - \frac{1}{2}\beta\tilde{z}^2\frac{\partial^2\tilde{\bar{u}}}{\partial\tilde{x}^2} + \mathcal{O}(\beta^2, \alpha\beta^2),$$

$$\tilde{v}(\tilde{x}, \tilde{z}, \tilde{t}) = -\tilde{z}\frac{\partial\tilde{\bar{u}}}{\partial\tilde{x}} + \mathcal{O}(\beta).$$

By ignoring the quadratic terms, in dimensional form the system reads

$$\eta_t + [h\bar{u}]_x = 0,$$

$$\bar{u}_t + \bar{u}\bar{u}_x + g\eta_x - \frac{1}{3h}\frac{\partial}{\partial x}\left(h^3(\bar{u}_{xt} + \bar{u}\bar{u}_{xx} - (\bar{u}_x)^2)\right) = 0,$$

where $\bar{u}$ is the depth averaged horizontal velocity of the fluid, h is the total water depth, and g is the acceleration due to gravity. The dimensional form of the velocity field at any location (x, z) in the vertical plane becomes

$$u = \bar{u} + \left(\frac{h^2}{6} - \frac{z^2}{2}\right)\bar{u}_{xx},$$

$$v = -z\bar{u}_x.$$

We will use the velocity field in the fluid associated with a periodic traveling solution of the Serre equations to simulate particle paths.

Since dispersion can be important in shallow water, it is worthwhile to examine the linear dispersion relation for the Serre equations. Considering long waves of small amplitude, we obtain the classical Boussinesq system [15]:

$$\eta_t + h_0\bar{u}_x = 0,$$

$$\bar{u}_t + g h_x - \frac{1}{3}h_0^2\bar{u}_{xxt} = 0.$$

Thus according to the work of Bjørkavåg and Kalisch [16] the linear dispersion relation for the Serre system is

$$\omega^2 = \frac{3gh_0k^2}{3 + k^2h_0^2}$$

and it is much closer than the linear dispersion relation for the KdV equation to the dispersion relation for the full water-wave problem.

The classical description of the water particle motion in the fluid is obtained by using the linear water wave theory and the water particles are predicted in closed orbits [17,18]. However, it is well known that no particle trajectory is actually closed [19,20], and this result is known as the Stokes drift. Particle paths associated with solitary wave solutions of the water wave problem were analyzed by Constantin and Escher [21]. They used maximum principles for elliptic operators to prove qualitative results about the particle trajectories and velocities. Ionescu–Kruse [22] investigated the particle trajectories in an irrotational shallow water flow over a flat bottom as periodic waves propagate on the water's free surface. Using the linear theory they showed these trajectories are not closed. Hsu et al. [23] provided experiments in a wave tank to investigate the particle trajectories beneath a solitary water wave and obtained the particle orbits do not comprise any backward motions. In [24], Borluk and Kalisch investigated numerically particle paths associated with exact solutions of the KdV equation. They considered solitary waves, periodic traveling waves and the two-soliton solutions, and found that the approximate particle paths are nearly closed for periodic traveling waves.

The current work is structured as follows: In Section 2, we study particle paths associated with surface solitary waves. Section 3 features a study of particle paths associated with the propagation of a periodic wave. We close with some concluding remarks in Section 4.

2. Particle paths in solitary waves

In this section, our goal is to describe the particle paths in the fluid due to the passage of a solitary wave at the surface. The Serre equations have a solitary wave solution [26], given by

$$h(x,t) = a_0 + a_1 \mathrm{sech}^2(\vartheta), \tag{1}$$

$$\bar{u} = c\left(1 - \frac{a_0}{h(x,t)}\right), \tag{2}$$

where

$$\kappa = \sqrt{\frac{3a_1}{4a_0^2(a_0+a_1)}} \tag{3}$$

and

$$c = \sqrt{g(a_0+a_1)} \tag{4}$$

is the phase velocity. Here the argument is $\vartheta = \kappa(x - ct)$, and a_0 and a_1 are positive real parameters. For the solitary wave solution of the Serre equations, the velocity components at a time t and at an arbitrary point (x,z) in the fluid are given by

$$u = \bar{u} + \frac{-2a_1a_0c\kappa^2}{h^2}\left(\frac{h^2}{6} - \frac{z^2}{2}\right)[-2\mathrm{sech}^2(\vartheta)\tanh^2(\vartheta) + \mathrm{sech}^4(\vartheta)],$$

$$v = \frac{2a_1a_0c\kappa z}{h^2}\mathrm{sech}^2(\vartheta)\tanh(\vartheta).$$

Taking $(\xi(t),\zeta(t))$ to describe a particle's location as a function of time which originally located at the point (ξ_0,ζ_0), the particle motion is described by the differential equations

$$\frac{\partial\xi}{\partial t} = u(\xi(t),\zeta(t),t), \qquad \frac{\partial\zeta}{\partial t} = w(\xi(t),\zeta(t),t). \tag{5}$$

These equations can be solved numerically. Discretization of these equations can be efficiently effected by using a high-order time-stepping methods, such as a fourth-order Runge–Kutta method.

The surface profile and the particle motions beneath the solitary waves are shown in Figs. 1–3. In these Figures, sample particle paths are shown during the propagation of a solitary wave with amplitude $a_1 = 0.2$. In Figs. 1 and 2 the wave profile is shown at $t = 0$ (light-gray), $t = 1$ (dark-gray) and $t = 2$ (black). The particle location at the three instances where the wave profile is shown, are color coded: the light-gray dot indicates the particle position at time $t = 0$, the dark-gray dot indicates the particle position at time $t = 1$ and the black dot indicates the particle position at time $t = 2$. Fig. 1 presents the trajectory for a surface particle located to the right of the crest. It can be seen that the particle moves to the right and upwards. In Fig. 2, fluid particles move to the right and upwards if they are located to the right of the crest. Particles located on the left of the

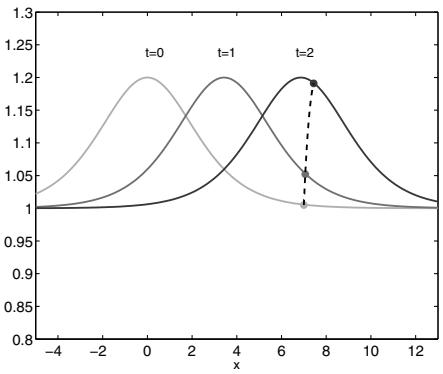

Fig. 1. The wave profile is shown at $t = 0$ (light-gray), $t = 1$ (dark-gray) and $t = 2$ (black). The wave crest is initially located at $x = 0$. The path of particle initially located in the surface at $(7, 1.005)$ is shown by dashed curve.

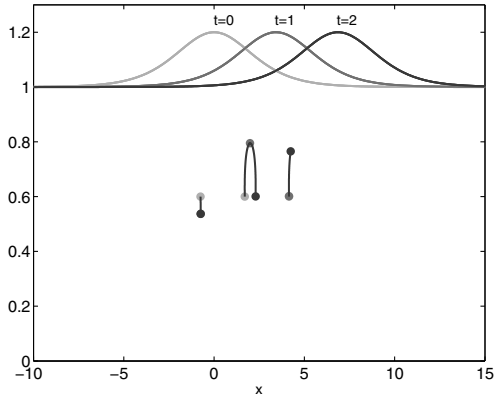

Fig. 2. The wave profile is shown at $t = 0$ (light-gray), $t = 1$ (dark-gray) and $t = 2$ (black). The wave crest is initially located at $x = 0$. The paths of fluid particles initially located at $(-0.75, 0.6)$, $(1.7, 0.6)$, and $(4.15, 0.6)$. The light-gray dot indicates the particle position at time $t = 0$, the dark-gray dot indicates the particle position at time $t = 1$ and the black dot indicates the particle position at time $t = 2$. The particles located on the left of the crest move to the right and downwards and the particles located on the right of the crest move to the right and upwards.

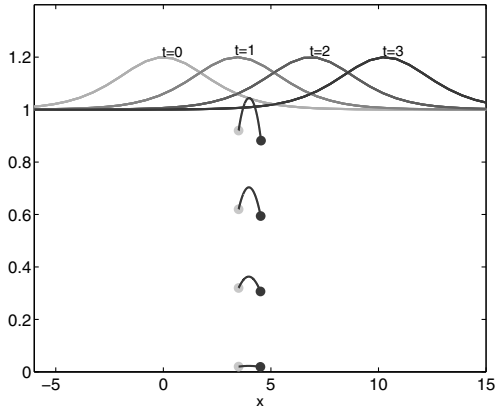

Fig. 3. The wave profile is shown at $t = 0$, $t = 1$, $t = 2$, and $t = 3$. The paths of fluid particles are initially located at $(4, 0.02)$, $(4, 0.32)$, $(4, 0.62)$, and $(4, 0.92)$ are shown. The paths resemble the particle paths taken during the full passage of a solitary wave. The vertical excursion is less than its horizontal displacement and diminishes rapidly with the depth of the trajectory below the free surface. At the bottom, the trajectory becomes a straight line and only a horizontal displacement exits. The net forward horizontal displacement during one complete wave cycle is largest at the free surface and decreases at deeper levels.

crest move to the right and downwards. Fig. 3 illustrates the particle paths during one complete wave cycle. We can see the vertical excursion is less than its horizontal displacement and decreases rapidly with the depth of the trajectory below the free surface. Therefore, the particles closer to the bottom have smaller amplitude and at the bottom, the trajectory becomes a straight line because the vertical movement of the particle is zero, and only a horizontal displacement exists. Our results are in agreement with the findings of Borluk and Kalisch [24].

3. Particle paths in periodic waves

Attention will now be turned to particle paths in the fluid flow due to the propagation of periodic traveling waves at the surface. The Serre equations admit the following solution [27]:

$$h(x,t) = a_0 + a_1 \mathrm{dn}^2(\vartheta, m), \tag{6}$$

$$\bar{u} = c\left(1 - \frac{h_0}{h(x,t)}\right), \tag{7}$$

$$\kappa = \sqrt{\frac{3a_1}{4a_0(a_0+a_1)(a_0+(1-m^2)a_1)}}, \tag{8}$$

$$c = \frac{1}{h_0}\sqrt{g a_0(a_0+a_1)(a_0+(1-m^2)a_1)}, \tag{9}$$

where the argument is $\vartheta = \kappa(x - ct)$, a_0 and a_1 are real positive parameters, and $\mathrm{dn}(\cdot, m)$ is a Jacobi elliptic function with elliptic modulus $m \in (0,1)$. The mean water depth h_0 is computed by averaging the water depth over one wavelength $\lambda = 2K(m)/\kappa$, resulting in

$$h_0 = \frac{1}{\lambda}\int_0^{\lambda} h(x,t)dx = a_0 + a_1\frac{E(m)}{K(m)},$$

where $K(m)$ and $E(m)$ are the complete elliptic integrals of the first and second kind, respectively.

The particle motion is described by the differential Eqs. (5). The velocity field may be written in terms of the Jacobian elliptic functions cn, sn and dn as follows:

$$u = \bar{u} + \left(\frac{h^2}{6} - \frac{z^2}{2}\right)\left(\frac{-2a_1h_0cm^2\kappa^2}{h^2}\right) \times [\mathrm{dn}^2(\vartheta)(-3\mathrm{sn}^2(\vartheta)+2) + \mathrm{sn}^2(\vartheta) - 1],$$

$$v = \left(\frac{2a_1h_0cm^2\kappa}{h^2}\right)z\mathrm{cn}(\vartheta)\mathrm{sn}(\vartheta)\mathrm{dn}(\vartheta).$$

A solution of the Serre equations can be specified by fixing the values for the parameters a_0, a_1 and m. Fig. 4 presents some particle paths below a periodic dnoidal wave with $a_0 = 0.3$, $a_1 = 0.1$ and $m = 0.99$. The crest of the wave is centered at $x = 0$, and the particles are initially located below the trough and the crest. Fig. 5 illustrates a close-up of particle paths and we can see that they are nearly elliptic but not completely closed. Indeed, there is a forward drift of particles near the surface during one period. Then, as depth increases the drift becomes negative and backward. While this finding might be interpreted to be in conflict with the Stokes drift which is approximately valid for small amplitude waves, it can be explained by the fact that the periodic solution, (6)–(9), incorporates a mean negative horizontal velocity in the flow underneath the surface. To explain this in more detail, recall that in the linear theory, fluid particles move in closed orbits but if a second-order approximation is used, then is found that the particles experience a forward drift, i.e., a drift in the same direction as the wave

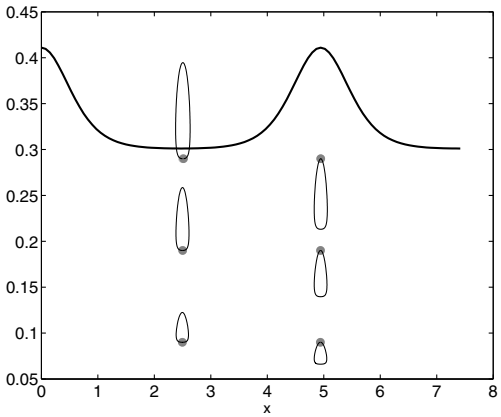

Fig. 4. The wave with wavelength 4.945 is shown. The paths of fluid particles are located at (x,z) where initial x-coordinates are $x = 2.5$ and $x = 4.945$ and initial z-coordinates are $z = 0.09$, $z = 0.19$, and $z = 0.29$.

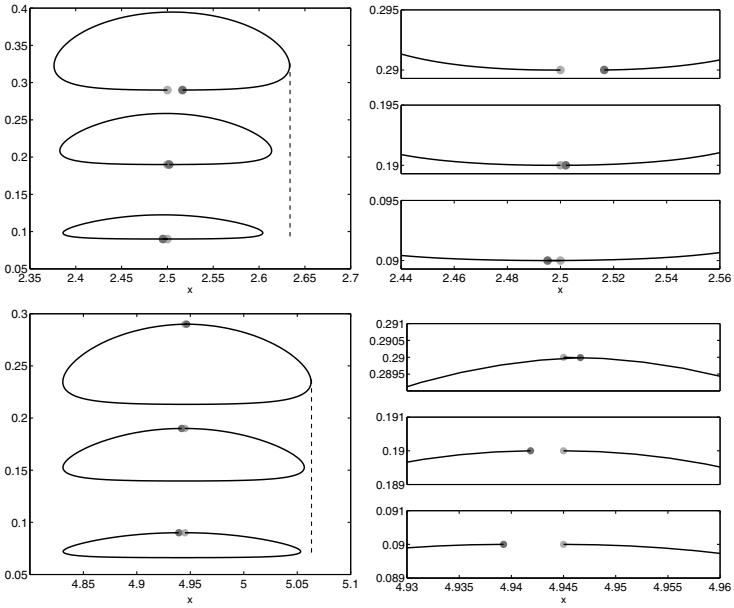

Fig. 5. A close up of particle path starting below the trough of the surface wave is shown in the upper panel and a close up of particle path starting below the crest is shown in the lower panel.

motion. This forward drift is known as the Stokes drift, and the drift velocity can be estimated using a Taylor expansion to be

$$u_s = a^2\omega k \frac{\cosh(2kz)}{2\sinh^2(kh_0)},$$

where k and ω are wavenumber and circular frequency, respectively.

One might expect that the forward particle drift due to the dnoidal solution, (6)–(9), is similar to the Stokes drift if the wave amplitude is small. However, as can be shown, the mean horizontal velocity over one wave period, $\int_0^T \bar{u}dt$, is negative. Therefore, on average the forward particle drift is canceled by the negative mean velocity. Indeed, it can be shown that the sum of the Stokes drift and the negative mean velocity is nearly equal to the particle drift computed in the dnoidal solution of the Serre equations.

Let $\mathcal{L}_{\text{Serre}}(z)$ be the horizontal displacement of a particle originally located at a height z in the fluid column predicted by the dnoidal solutions of the Serre system. In Table 1, the Stokes displacement Tu_s is tabulated, along with the mean countercurrent $\int_0^T \bar{u}dt$ for a number of amplitudes and wavelengths. The results are averaged over the depth. Then in the fifth column, the sum

$$S = \frac{1}{h}\int_0^h Tu_s dz + \int_0^T \bar{u}dt \tag{10}$$

Table 1
The first column of this table shows the amplitude and the second column shows the wavelength of a dnoidal wave and a linear wave. The third column shows the Stokes displacement of the particle path due to the passage of the linear wave and the fourth column shows the mean countercurrent by using $\int_0^T \bar{u}dt$. The fifth column presents the sum, S, and the sixth column shows the Serre displacement of the particle path due to the propagation of the dnoidal wave.

Amplitude a	Wavelength λ	Stokes disp. $\frac{1}{h}\int_0^h Tu_s dz$	Countercurrent $\int_0^T \bar{u}dt$	Sum S	Serre disp. $\frac{1}{h}\int_0^h \mathcal{L}_{\text{Serre}}(z)dz$
0.009	3.33	1.03×10^{-3}	-1.15×10^{-3}	-1.18×10^{-4}	-5.32×10^{-4}
0.017	2.69	2.18×10^{-3}	-2.69×10^{-3}	-5.09×10^{-4}	-9.20×10^{-4}
0.026	2.41	3.32×10^{-3}	-4.60×10^{-3}	-1.28×10^{-3}	-1.87×10^{-3}
0.035	2.29	4.19×10^{-3}	-6.51×10^{-3}	-2.32×10^{-3}	-2.96×10^{-3}

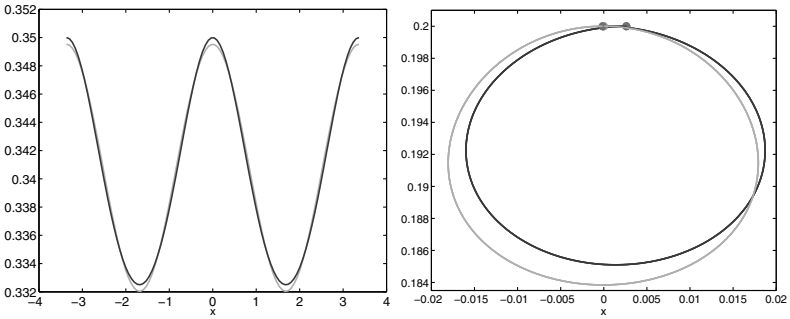

Fig. 6. The left panel shows a dnoidal wave profile (light-gray) and a linear wave profile (black) of the same wavelength 3.33 and amplitude 0.009. The right panel shows the paths of a particle initially located below the crest at $(0, 0.2)$ associated with both wave profiles with similar color-coding used in the left panel.

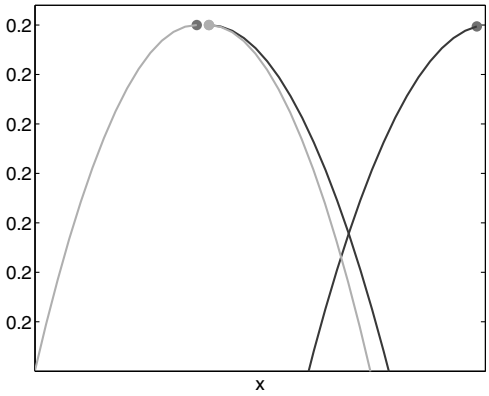

Fig. 7. A close up of particle paths starting at $(0, 0.2)$ is shown. The particle path shown by the light-gray curve is due to the propagation of a dnoidal wave and the particle trajectory shown by the black curve is associated with the passage of a linear wave over one period. The light-gray dot indicates the particle position at time $t = 0$ and the dark-gray dots indicate the particle position at $t =$ wave period.

is tabulated and compared to the average of $\mathcal{L}_{\text{Serre}}(z)$ which is tabulated in the sixth column. As can be seen, the sum is of the same order as the Serre displacement, which confirms that the countercurrent inherent in the dnoidal solution of the Serre system is responsible for reducing the forward drift experienced by the particle paths during one wave cycle.

A graphical comparison is in Fig. 6. In the left panel of Fig. 6, we see a dnoidal wave profile and a linear wave profile of the same wavelength and amplitude. We note that the wave profiles are very similar. The right panel of Fig. 6 illustrates a particle initially located below the crest at $(0, 0.2)$. The path of the particle during the propagation of the dnoidal wave over one period presented in the left panel is shown by light-gray curve and the particle path due to the passage of the linear wave is shown by black curve. Comparison of two particle paths shows a forward drift due to the linear wave and a short negative drift associated with the dnoidal wave (see Fig. 7).

4. Conclusion

In this study, the Serre equations have been used to describe the motion of particles in the fluid column below the surface wave. The particle motion is described by two coupled ordinary differential equations which are found in terms of the velocity field associated with a surface wave. These differential equations have been solved numerically by using a fourth-order Runge–Kutta method. The evolution of particles in the fluid was investigated due to the passage of a solitary wave and a periodic traveling wave at the surface. For solitary waves the particles display a forward drift, however, for dnoidal waves the fact that the mean velocity is negative implies a negative horizontal displacement for particles.

References

[1] D.D. Bhatta, M.I. Bhatti, Numerical solution of KdV equation using modified Bernstein polynomials, Appl. Math. Comput. 174 (2006) 1255–1268.
[2] A.M. Wazwaz, Exact specific solutions with solitary patterns for the nonlinear dispersive KdV equations, Chaos Solitons Fract. 13 (1) (2001) 161–170.
[3] A.M. Wazwaz, Solitons and periodic solutions for the fifth-order KdV equation, Appl. Math. Lett. 19 (2006) 1162–1167.
[4] M. Kazeminia, S. Soleimani-Amiri, S.A. Zahedi, Exact and numerical solutions for nonlinear higher order modified KdV equations by using variational iteration method, Adv. Studies Theor. Phys. 4 (9) (2010) 437–447.
[5] F. Serre, Contribution à l'étude des écoulements permanents et variables dans les canaux, Houille Blanche 8 (1953) 374–388.
[6] C.H. Su, C.S. Gardner, Korteweg–de Vries equation and generalizations, III. Derivation of the Korteweg–de Vries equation and Burgers equation, J. Math. Phys. 10 (1969) 536–539.
[7] A.E. Green, N. Laws, P.M. Naghdi, On the theory of water waves, Proc. R. Soc. Lond. A 338 (1974) 43–55.
[8] F.J. Seabra-Santos, D.P. Renouard, A.M. Temperville, Numerical and experimental study of the transformation of a solitary wave over a shelf or isolated obstacle, J. Fluid Mech. 176 (1987) 117–134.
[9] F. Dias, P. Milewski, On the fully-nonlinear shallow-water generalized Serre equations, Phys. Lett. A 374 (2010) 1049–1053.
[10] E. Barthélemy, Nonlinear shallow water theories for coastal waves, Surv. Geophys. 25 (2004) 315–337.
[11] O. Le Métayer, S. Gavrilyuk, S. Hank, A numerical scheme for the Green–Naghdi model, J. Comput. Phys. 229 (2010) 2034–2045.
[12] J.D. Carter, R. Cienfuegos, The kinematics and stability of solitary and cnoidal wave solutions of the Serre equations, Eur. J. Mech. B/Fluids 30 (2011) 259–268.
[13] D. Dutykh, D. Clamond, P. Milewski, D. Mitsotakis, Finite volume and pseudo-spectral schemes for the fully nonlinear 1D Serre equations. arXiv:1104.4456v4[Physics.flu-dyn], 13 February 2013.
[14] R. Cienfuegos, E. Barthélemy, P. Bonneton, A fourth-order compact finite volume scheme for fully nonlinear and weakly dispersive Boussinesq-type equations, Part I: model development and analysis, Int. J. Numer. Methods Fluids 51 (2006) 1217–1253.
[15] D.H. Peregrine, Long waves on beaches, Fluid Dyn. Trans. 10 (1980) 77–111.
[16] M. Bjrkavåg, H. Kalisch, Wave breaking in Boussinesq models for undular bores, Phys. Lett. A 375 (2011) 1570–1578.
[17] L. Debnath, Nonlinear Water Waves, Academic Press Inc., Boston, MA, 1994.
[18] J. Lighthill, Waves in Fluids, Cambridge University Press, 2001.
[19] A. Constantin, G. Villari, Particle trajectories in linear water waves, J. Math. Fluid Mech. 10 (2008) 1–18.
[20] A.-V. Matioc, On particle trajectories in linear water waves, Nonlinear Anal.: Real World Appl. 11 (2010) 4275–4284.
[21] A. Constantin, J. Escher, Particle trajectories in solitary water waves, Bull. Am. Math. Soc. 44 (2007) 423–431.
[22] D. Ionescu-Kruse, Particle trajectories in linearized irrotational shallow water flows, J. Nonlinear Math. Phys. 15 (2008) 13–27.
[23] H.-C. Hsu, Y.-Y. Chen, C.-Y. Lin, C.-Y. Cheng, Experimental study of the velocity field in solitary waves, J. Nonlinear Math. Phys 19 (1) (2012) 1240003. pp. 11.
[24] H. Borluk, H. Kalisch, Particle dynamics in the KdV approximation, Wave Motion 49 (2012) 691–709.
[25] A. Ali, H. Kalisch, Mechanical balance laws for Boussinesq models of surface water waves, J. Nonlinear Sci. 22 (2012) 371–398.
[26] E. Barthélemy, Nonlinear shallow water theories for coastal waves, Surv. Geophys. 25 (3–4) (2004) 315–337.
[27] G.A. El, R.H.J. Grimshaw, N.F. Smyth, Unsteady undular bores in fully nonlinear shallow-water theory, Phys. Fluids 18 (2006) 027104.

View publication stats

Paper B

Mechanical balance laws for fully nonlinear and weakly dispersive water waves *

B

* *Published in Physica D 333, 2016*

Physica D 333 (2016) 243–253

Contents lists available at ScienceDirect

Physica D

journal homepage: www.elsevier.com/locate/physd

Mechanical balance laws for fully nonlinear and weakly dispersive water waves

Henrik Kalisch [a], Zahra Khorsand [a], Dimitrios Mitsotakis [b,*]

[a] Department of Mathematics, University of Bergen, Norway
[b] School of Mathematics, Statistics and Op. Research, Victoria University of Wellington, New Zealand

HIGHLIGHTS

- Systematic derivation of balance laws for the Serre–Green–Naghdi (SGN) equations.
- Numerical solution of the SGN system using a high-order finite element method.
- Study of the energy balance in undular bores.
- Numerical simulation of shoaling solitary waves.

ARTICLE INFO

Article history:
Received 27 July 2015
Received in revised form
1 February 2016
Accepted 1 March 2016
Available online 18 March 2016

This article is dedicated to the memory of Professor Gerald B. Whitham. Professor Whitham's work on dispersive shock waves, modulation theory and the Whitham equation has had a profound impact on the work of the authors, and his encyclopedic book "Linear and Nonlinear Waves" continues to be an important source of inspiration. Much of the authors work on nonlocal dispersive equations, wave breaking and peaking, undular bores and conservation laws has been influenced in some form or another by Professor Whitham's writings

Keywords:
Conservation laws
Serre system
Dispersive shock waves
Solitary waves

ABSTRACT

The Serre–Green–Naghdi system is a coupled, fully nonlinear system of dispersive evolution equations which approximates the full water wave problem. The system is known to describe accurately the wave motion at the surface of an incompressible inviscid fluid in the case when the fluid flow is irrotational and two-dimensional. The system is an extension of the well known shallow-water system to the situation where the waves are long, but not so long that dispersive effects can be neglected. In the current work, the focus is on deriving mass, momentum and energy densities and fluxes associated with the Serre–Green–Naghdi system. These quantities arise from imposing balance equations of the same asymptotic order as the evolution equations. In the case of an even bed, the conservation equations are satisfied exactly by the solutions of the Serre–Green–Naghdi system. The case of variable bathymetry is more complicated, with mass and momentum conservation satisfied exactly, and energy conservation satisfied only in a global sense. In all cases, the quantities found here reduce correctly to the corresponding counterparts in both the Boussinesq and the shallow-water scaling. One consequence of the present analysis is that the energy loss appearing in the shallow-water theory of undular bores is fully compensated by the emergence of oscillations behind the bore front. The situation is analyzed numerically by approximating solutions of the Serre–Green–Naghdi equations using a finite-element discretization coupled with an adaptive Runge–Kutta time integration scheme, and it is found that the energy is indeed conserved nearly to machine precision. As a second application, the shoaling of solitary waves on a plane beach is analyzed. It appears that the Serre–Green–Naghdi equations are capable of predicting both the shape of the free surface and the evolution of kinetic and potential energy with good accuracy in the early stages of shoaling.

© 2016 Elsevier B.V. All rights reserved.

1. Introduction

In this paper we study mechanical balance laws for fully nonlinear and dispersive shallow-water waves. In particular, the Serre–Green–Naghdi (SGN) system of equations with variable bathymetry is considered. This system was originally derived for one-dimensional waves over a horizontal bottom in 1953 by F. Serre [1,2]. Several years later, the same system was rederived by Su and Gardner [3]. In 1976, Green and Naghdi [4] derived a two-dimensional fully nonlinear and weakly dispersive system for an uneven bottom which was integrated in one spatial dimension by Seabra-Santos et al. [5] and El et al. [6]. Lannes and Bonneton derived several other systems including the SGN equations using

* Corresponding author. Tel.: +64 44636739; fax: +64 44635045.
E-mail address: dimitrios.mitsotakis@vuw.ac.nz (D. Mitsotakis).
URL: https://sites.google.com/site/dmitsot/ (D. Mitsotakis).

http://dx.doi.org/10.1016/j.physd.2016.03.001
0167-2789/© 2016 Elsevier B.V. All rights reserved.

a new formulation of the water wave problem, [7]. For more information and generalizations of the SGN equations we refer to Lannes [8] and the references therein, while we refer to the paper by Barthélemy [9] for an extensive review.

The Serre–Green–Naghdi (SGN) system and several variants of it are extensively used in coastal modeling [10–12,8]. In the present contribution, the focus is on the derivation and use of associated mechanical balance equations, and in particular a differential energy balance equation. While it is known that the equations admit local conservation equations corresponding to mass, momentum and energy conservation if the bed is even [13], it appears that the connection to the mechanical balance laws of the original Euler equations has not been firmly established so far. One possible method for establishing the link between the conservation laws and the requisite physical quantities is outlined in the work of Miles and Salmon [14]. In this work, the Serre–Green–Naghdi (SGN) equations are shown to follow from Hamilton's principle of least action in the same way as the full free-surface water wave problem does if it is assumed that the fluid moves in vertical columns, or in other words that the horizontal displacement of fluid particles is uniform throughout the fluid column. This approximation preserves several of the symmetries of the full water-wave problem [15], and in particular gives rise to corresponding conservation laws for mass, momentum and energy through the use of Noether's theorem.

We follow a different route in that we make the same approximation in both the evolution equations (Euler equations) and in the corresponding mechanical balance laws directly. Using this approach, we show that the first three conservation laws of the Serre–Green–Naghdi (SGN) equations arise as approximations of mechanical balance laws in the context of the Euler equations, both in the case of even beds, and in the case of nontrivial bathymetry. While one may have doubts about the link between the resulting approximate balance laws at a mathematical level, it can be established (see [13]) that these balance equations also arise as exact consequences of the Serre–Green–Naghdi (SGN) equations.

As it was shown in [16], the Serre–Green–Naghdi (SGN) equations also admit a fourth conservation law which may be interpreted as conservation of potential vorticity, and arises from a certain relabeling symmetry of the Lagrangian density used in [14]. This fourth conservation law can also be shown to be related to a kinematic identity similar to Kelvin's circulation theorem [17].

Let us first review some modeling issues regarding the Serre–Green–Naghdi (SGN) system. Suppose a denotes a typical amplitude, and l a typical wavelength of a wavefield under study. Suppose also that b_0 represents the average water depth. In order to be a valid description of such a situation, the SGN equations require the shallow water condition, $\beta \doteq b_0^2/l^2 \ll 1$. In contrast, the range of validity of the weakly nonlinear and weakly dispersive Boussinesq equations is limited to waves with small amplitude and large wavelength, i.e. $\alpha \doteq a/b_0 \ll 1$ and $\beta \ll 1$. In this scaling regime, one also finds the weakly nonlinear, fully dispersive Whitham equation [8,18,19].

The SGN equations can be derived by depth-averaging the Euler equations and truncating the resulting set of equations at $\mathcal{O}(\beta^2)$ without making any assumptions on the order of α, other than $\alpha \leq \mathcal{O}(1)$.

In their dimensionless and scaled form the SGN equations can be written as

$$\eta_t + [h\bar{u}]_x = 0, \tag{1a}$$

$$\bar{u}_t + \bar{u}\bar{u}_x + g\eta_x + \frac{1}{h}\left[h^2\left(\frac{1}{3}\mathcal{P} + \frac{1}{2}\mathcal{Q}\right)\right]_x - b_x\left(\frac{1}{2}\mathcal{P} + \mathcal{Q}\right) = 0, \tag{1b}$$

with $\mathcal{P} = h\left[\bar{u}_x^2 - \bar{u}_{xt} - \bar{u}\bar{u}_{xx}\right]$ and $\mathcal{Q} = -b_x(\bar{u}_t + \bar{u}\bar{u}_x) - b_{xx}\bar{u}^2$, $x \in \mathbb{R}$, $t > 0$, along with the initial conditions $h(x,0) = h_0(x)$, $\bar{u}(x,0) = \bar{u}_0(x)$. Here, $\eta = \eta(x,t)$ is the free surface displacement, while

$$h \doteq \eta + b, \tag{2}$$

denotes the total fluid depth. The unknown $\bar{u} = \bar{u}(x,t)$ is the depth-averaged horizontal velocity, and η_0, $\bar{u}_0$ are given real functions, such that $\eta_0 + b > 0$ for all $x \in \mathbb{R}$. In these variables, the location of the horizontal bottom is given by $z = -b$ (cf. Fig. A.1). For a review of the derivation and the basic properties of this system we also refer to [9,20].

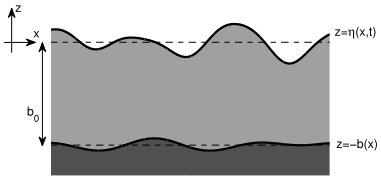

Fig. A.1. The geometry of the problem.

In the case of small-amplitude waves, i.e. if $\beta \sim \alpha$, the SGN equations reduce to Peregrine's system [21]. On the other hand, in the case of very long waves, i.e. $\beta \to 0$, the dispersive terms disappear, and the system reduces to the nondispersive shallow water equations.

The SGN system for waves over a flat bottom possesses solitary and cnoidal wave solutions given in closed form. For example, the solitary wave with speed c_s can be written as

$$h_s(\xi) \doteq h_s(x,t) = a_0 + a_1\,\mathrm{sech}^2(K_s\,\xi), \tag{3a}$$

$$u_s(\xi) \doteq u_s(x,t) = c_s\left(1 - \frac{a_0}{h_s(\xi)}\right), \tag{3b}$$

where $\xi = x - c_s t$, $K_s = \sqrt{3a_1/4a_0^2c_s^2}$, $c_s = \sqrt{a_0 + a_1}$, and $a_0 > 0$ and $a_1 > 0$. For more information about the solitary and cnoidal waves and their dynamical properties we refer to [9,22–26].

It is important to note that the SGN system has a Hamiltonian structure, even in the case of two-dimensional waves over an uneven bed cf. [24,27–29]. Specifically, any solution $(h, \bar{u})$ of (1) conserves the Hamiltonian functional

$$\mathcal{H}(t) = \frac{1}{2}\int_{-\infty}^{\infty} g\eta^2 + h\bar{u}^2 - h\left[h_x b_x + \frac{1}{2}hb_{xx} - b_x^2\right]\bar{u}^2 - \frac{1}{3}\left[h^3\bar{u}_x\right]_x\bar{u}\,dx, \tag{4}$$

in the sense that $d\mathcal{H}(t)/dt = 0$. Note however that (1a), (1b) are recovered only if a non-canonical symplectic structure matrix is used. While in many simplified models equations, the Hamiltonian functions does not represent the mechanical energy of the wave system [30], in the case of SGN, the Hamiltonian does represent the approximate total energy of the wave system. Thus the Hamiltonian can be written in the form

$$\mathcal{H}(t) = \int_{-\infty}^{\infty} E(x,t)\,dx,$$

where the integrand

$$E = \frac{1}{2}\left(g\eta^2 + h\bar{u}^2 - h\left[h_x b_x + \frac{1}{2}hb_{xx} - b_x^2\right]\bar{u}^2 - \frac{1}{3}\left[h^3\bar{u}_x\right]_x\bar{u}\right)$$

is the depth-integrated energy density. In the present paper, we also identify a local depth-integrated energy flux q_E, such that an equation of the form

$$\frac{\partial E}{\partial t} + \frac{\partial q_E}{\partial x} = 0, \tag{5}$$

is satisfied approximately. The procedure of finding the quantities E and q_E follows a similar outline as the derivations in [31] for a class of Boussinesq systems and [32] for the KdV equation. It is noted that some other estimates for energy functionals for Boussinesq systems can be found in [33].

The analytical results are put to use in the study of undular bores. It is well known that the shallow-water theory for bores predicts an energy loss [34]. In an undular bore, the energy is thought to be disseminated through an increasing number of oscillations behind the bore, and the traditional point of view is that dissipation must also have an effect here [35,36]. However, recent studies [37] have shown that if dispersion is included into the model equations, then the energy loss experienced by an undular bore can be accounted for without making appeal to dissipative mechanisms.

Indeed, it was argued in [37,38] that the energy loss in an undular bore could be explained wholly within the realm of conservative dynamics by investigating a higher-order dispersive system, and monitoring the associated energy functional. However, there was a technical problem in the analysis in these works, as the energy functional was not the same as the one required by the more in-depth analysis in [31]. On the other hand, the energy functional found in [31] did not reduce to the shallow-water theory in the correct way. In the current contribution, it is our purpose to remedy this situation by using the SGN system which reduces in the correct way to the shallow-water equations, and also features exact energy conservation in the case of a flat bed.

The numerical method to be used is a standard Galerkin/Finite Element Method (FEM) for the SGN equations with reflective boundary conditions extending the numerical method presented in [39]. For the sake of completeness we mention that there are several numerical methods applied to boundary value problems of the SGN equations. For example finite volume [40–42], finite differences [20,43,44], spectral [45,41] and Galerkin methods [39,46].

The paper is organized as follows: A review of the derivation of the SGN equations based on [9,20] is presented in Section 2. The derivation of the mass, momentum and energy balance laws in the asymptotic order of the SGN equations is presented in Section 3. Applications to undular bores and solitary waves are discussed in Section 4. The numerical method to be used in this paper is presented briefly in the Appendix.

2. The SGN equations over a variable bed

Before introducing the balance laws for the SGN equations, we briefly review the derivation of the SGN equations from the Euler equations following the work [9], but in the case of a general bathymetry. This well known derivation is included here to set the stage for the development of the approximate mechanical balance laws in the next section. We consider an inviscid and incompressible fluid, and assume that the fluid flow is irrotational and two-dimensional. Let a_0 be a typical amplitude, l a typical wavelength and b_0 a typical water depth. We perform the change of variables $\tilde{x} = x/l$, $\tilde{z} = z/b_0$, $\tilde{t} = c_0 t/l$, which yields non-dimensional independent variables identified by tildes, where x represents the horizontal and z the vertical coordinate. The limiting long-wave speed is defined by $c_0 = \sqrt{gb_0}$, and g denotes the acceleration due to gravity. The non-dimensional velocity components are defined by $\tilde{u} = u/\alpha c_0$, $\tilde{v} = v/\sqrt{\beta}\alpha c_0$, where $\alpha = a_0/b_0$ and $\beta = b_0^2/l^2$. Finally, the free surface deflection, bottom topography and pressure are non-dimensionalized by taking $\tilde{\eta} = \eta/a_0$, $\tilde{b} = -b/b_0$, and $\tilde{p} = p/\rho g b_0$.

In non-dimensional variables, the free-surface problem is written as follows [47]: The momentum equations are

$$\alpha\tilde{u}_{\tilde{t}} + \alpha^2(\tilde{u}^2)_{\tilde{x}} + \alpha^2(\tilde{u}\tilde{v})_{\tilde{z}} = -\tilde{p}_{\tilde{x}}, \tag{6a}$$

$$\alpha\beta\tilde{v}_{\tilde{t}} + \alpha^2\beta\tilde{u}\tilde{v}_{\tilde{x}} + \alpha^2\beta\tilde{v}\tilde{v}_{\tilde{z}} = -\tilde{p}_{\tilde{z}} - 1. \tag{6b}$$

The equation of continuity and the irrotationality are expressed by

$$\tilde{u}_{\tilde{x}} + \tilde{v}_{\tilde{z}} = 0, \tag{7a}$$

$$\tilde{u}_{\tilde{z}} - \beta\tilde{v}_{\tilde{x}} = 0. \tag{7b}$$

The boundary conditions at the free surface and at the bottom are given by

$$\tilde{v} = \tilde{\eta}_{\tilde{t}} + \alpha\tilde{u}\tilde{\eta}_{\tilde{x}}, \qquad \text{at } \tilde{z} = \alpha\tilde{\eta}(\tilde{x}), \tag{8a}$$

$$\tilde{p} = 0, \qquad \text{at } \tilde{z} = \alpha\tilde{\eta}(\tilde{x}), \tag{8b}$$

$$\tilde{v} = \tilde{b}_{\tilde{x}}\tilde{u}, \qquad \text{at } \tilde{z} = \tilde{b}(\tilde{x}). \tag{8c}$$

The first equation in the system (1) is obtained by integrating the equation of continuity over the total depth. The result is written in terms of the depth-averaged horizontal velocity

$$\bar{\tilde{u}} = \frac{1}{\tilde{h}}\int_{\tilde{b}}^{\alpha\tilde{\eta}} \tilde{u}\, dz, \tag{9}$$

in the form

$$\tilde{\eta}_{\tilde{t}} + [\tilde{h}\bar{\tilde{u}}]_{\tilde{x}} = 0. \tag{10}$$

Using the boundary conditions (8a)–(8c), the continuity equation (10) and the depth-averaged momentum equation (6a) yields

$$\alpha\tilde{h}\bar{\tilde{u}}_{\tilde{t}} + \alpha^2\tilde{h}\bar{\tilde{u}}\bar{\tilde{u}}_{\tilde{x}} + \alpha^2\frac{\partial}{\partial\tilde{x}}\int_{\tilde{b}}^{\alpha\tilde{\eta}}\left(\tilde{u}^2 - (\bar{\tilde{u}})^2\right) d\tilde{z} = -\int_{\tilde{b}}^{\alpha\tilde{\eta}} \tilde{p}_{\tilde{x}}\, d\tilde{z}. \tag{11}$$

Applying the Leibniz rule to the right-hand side of Eq. (11) yields

$$\begin{aligned}\int_{\tilde{b}}^{\alpha\tilde{\eta}} \tilde{p}_{\tilde{x}}\, d\tilde{z} &= \frac{\partial}{\partial\tilde{x}}\big(\tilde{h}\bar{\tilde{p}}\big) - \alpha\tilde{\eta}_{\tilde{x}}\tilde{p}|_{\tilde{z}=\alpha\tilde{\eta}} + \tilde{b}_{\tilde{x}}\tilde{p}|_{\tilde{z}=\tilde{b}} \\ &= \frac{\partial}{\partial\tilde{x}}\big(\tilde{h}\bar{\tilde{p}}\big) + \tilde{b}_{\tilde{x}}\tilde{p}|_{\tilde{z}=\tilde{b}}.\end{aligned} \tag{12}$$

The momentum equation (6b) is rewritten as

$$\alpha\beta\Gamma(\tilde{x},\tilde{z},\tilde{t}) = -1 - \tilde{p}_{\tilde{z}}, \tag{13}$$

where

$$\Gamma(\tilde{x},\tilde{z},\tilde{t}) = \tilde{v}_{\tilde{t}} + \alpha\tilde{u}\tilde{v}_{\tilde{x}} + \alpha\tilde{v}\tilde{v}_{\tilde{z}}. \tag{14}$$

Integrating Eq. (13) from $\tilde{z}$ to $\alpha\tilde{\eta}$ yields

$$\tilde{p}(\tilde{x},\tilde{z},\tilde{t}) = (\alpha\tilde{\eta} - \tilde{z}) + \alpha\beta\int_{\tilde{z}}^{\alpha\tilde{\eta}} \Gamma(\tilde{x},\zeta,\tilde{t})\, d\zeta, \tag{15}$$

and taking the mean value gives

$$\tilde{h}\bar{\tilde{p}} = \frac{1}{2}\tilde{h}^2 + \alpha\beta\int_{\tilde{b}}^{\alpha\tilde{\eta}}\int_{\tilde{z}}^{\alpha\tilde{\eta}} \Gamma(\tilde{x},\zeta,\tilde{t})\, d\zeta\, d\tilde{z}. \tag{16}$$

Therefore, Eq. (11) can be written as

$$\begin{aligned}&\bar{\tilde{u}}_{\tilde{t}} + \alpha\bar{\tilde{u}}\bar{\tilde{u}}_{\tilde{x}} + \tilde{\eta}_{\tilde{x}} + \frac{\beta}{\tilde{h}}\frac{\partial}{\partial\tilde{x}}\int_{\tilde{b}}^{\alpha\tilde{\eta}} (\tilde{z} - \tilde{b})\Gamma(\tilde{x},\tilde{z},\tilde{t})\, d\tilde{z} \\ &\quad + \frac{\beta}{\tilde{h}}\tilde{b}_{\tilde{x}}\int_{\tilde{b}}^{\alpha\tilde{\eta}} \Gamma(\tilde{x},\tilde{z},\tilde{t})\, d\tilde{z} = \frac{-\alpha}{\tilde{h}}\frac{\partial}{\partial\tilde{x}}\int_{\tilde{b}}^{\alpha\tilde{\eta}}\left(\tilde{u}^2 - (\bar{\tilde{u}})^2\right) d\tilde{z}.\end{aligned}$$

The non-dimensional velocity components are given (cf. [20]) to first order by

$$\tilde{u}(\tilde{x},\tilde{z},\tilde{t}) = \bar{\tilde{u}}(\tilde{x},\tilde{t}) + \mathcal{O}(\beta), \tag{17}$$

and

$$\tilde{v}(\tilde{x},\tilde{z},\tilde{t}) = -\big(\tilde{z}-\tilde{b}(\tilde{x})\big)\frac{\partial\bar{\tilde{u}}}{\partial\tilde{x}} + \bar{\tilde{u}}\frac{\partial\tilde{b}}{\partial\tilde{x}} + \mathcal{O}(\beta). \tag{18}$$

As it was shown in [20], we can expand the velocity components using Taylor series in the vertical coordinate around the bottom. Denoting by $\tilde{u}^b$ and $\tilde{v}^b$, respectively, the horizontal and vertical velocities at the bottom, the bottom kinematic condition (8c) imposes that $\tilde{v}^b = \tilde{b}_{\tilde{x}}\tilde{u}^b$. In order to determine which terms should be kept to obtain an approximation for the velocity field, the incompressibility condition (7a) must hold to the same order in β as the evolution equations. If the non-dimensional velocity components are given by

$$\begin{aligned}\tilde{u}(\tilde{x},\tilde{z},\tilde{t}) &= \tilde{u}^b(\tilde{x},\tilde{t}) + \beta(\tilde{z}-\tilde{b})\left(\tilde{b}_{\tilde{x}}\tilde{u}^b_{\tilde{x}} + (\tilde{b}_{\tilde{x}}\tilde{u}^b)_{\tilde{x}}\right)\\ &\quad - \frac{\beta}{2}(\tilde{z}-\tilde{b})^2\tilde{u}^b_{\tilde{x}\tilde{x}} + \mathcal{O}(\beta^2),\\ \tilde{v}(\tilde{x},\tilde{z},\tilde{t}) &= \tilde{b}_{\tilde{x}}\tilde{u}^b + (\tilde{z}-\tilde{b})\left(-\tilde{u}^b_{\tilde{x}} + \beta(\tilde{b}_{\tilde{x}}(\tilde{u}^b\tilde{b}_{\tilde{x}})_{\tilde{x}} + \tilde{u}^b_{\tilde{x}}\tilde{b}^2_{\tilde{x}})\right)\\ &\quad - \frac{\beta}{2}(\tilde{z}-\tilde{b})^2\left(\tilde{b}_{\tilde{x}}\tilde{u}^b_{\tilde{x}\tilde{x}} + (\tilde{b}_{\tilde{x}}\tilde{u}^b_{\tilde{x}} + (\tilde{b}_{\tilde{x}}\tilde{u}^b)_{\tilde{x}})_{\tilde{x}}\right)\\ &\quad + \frac{\beta}{3!}(\tilde{z}-\tilde{b})^3\tilde{u}^b_{\tilde{x}\tilde{x}\tilde{x}} + \mathcal{O}(\beta^2),\end{aligned} \tag{19}$$

then the incompressibility condition (7a) holds to $\mathcal{O}(\beta^2)$. Depth averaging (19) gives

$$\tilde{u}^b = \bar{\tilde{u}} - \frac{\beta}{2}\tilde{h}\left(\tilde{b}_{\tilde{x}}\bar{\tilde{u}}_{\tilde{x}} + (\tilde{b}_{\tilde{x}}\bar{\tilde{u}})_{\tilde{x}}\right) + \frac{\beta}{6}\tilde{h}^2\bar{\tilde{u}}_{\tilde{x}\tilde{x}} + \mathcal{O}(\beta^2,\alpha\beta^2).$$

Thus the horizontal velocity is

$$\begin{aligned}\tilde{u}(\tilde{x},\tilde{z},\tilde{t}) &= \bar{\tilde{u}} - \beta\left(\tilde{b}_{\tilde{x}}\bar{\tilde{u}}_{\tilde{x}} + (\tilde{b}_{\tilde{x}}\bar{\tilde{u}})_{\tilde{x}}\right)\left(\frac{\tilde{h}}{2} - (\tilde{z}-\tilde{b})\right)\\ &\quad + \beta\left(\frac{\tilde{h}^2}{6} - \frac{1}{2}(\tilde{z}-\tilde{b})^2\right)\bar{\tilde{u}}_{\tilde{x}\tilde{x}} + \mathcal{O}(\beta^2,\alpha\beta^2).\end{aligned} \tag{20}$$

Taking squares in Eq. (20)

$$\begin{aligned}\tilde{u}^2(\tilde{x},\tilde{z},\tilde{t}) &= \bar{\tilde{u}}^2 - \beta\left(\tilde{b}_{\tilde{x}}\bar{\tilde{u}}_{\tilde{x}}\bar{\tilde{u}} + (\tilde{b}_{\tilde{x}}\bar{\tilde{u}})_{\tilde{x}}\bar{\tilde{u}}\right)\left(\tilde{h} - 2(\tilde{z}-\tilde{b})\right)\\ &\quad + \beta\left(\frac{\tilde{h}^2}{2} - (\tilde{z}-\tilde{b})^2\right)\bar{\tilde{u}}\bar{\tilde{u}}_{\tilde{x}\tilde{x}} + \mathcal{O}(\beta^2,\alpha\beta^2).\end{aligned} \tag{21}$$

Integrating Eq. (21) from $\tilde{b}$ to $\alpha\tilde{\eta}$ and after some simplifications it follows that

$$\int_{\tilde{b}}^{\alpha\tilde{\eta}}\left(\tilde{u}^2 - (\bar{\tilde{u}})^2\right)d\tilde{z} = \mathcal{O}(\beta^2,\alpha\beta^2),$$

and that

$$\begin{aligned}\Gamma(\tilde{x},\tilde{z},\tilde{t}) &= (\tilde{z}-\tilde{b})\left[\alpha\bar{\tilde{u}}^2_{\tilde{x}} - \bar{\tilde{u}}_{\tilde{x}\tilde{t}} - \alpha\bar{\tilde{u}}\bar{\tilde{u}}_{\tilde{x}\tilde{x}}\right]\\ &\quad + + \tilde{b}_{\tilde{x}}(\bar{\tilde{u}}_{\tilde{t}} + \alpha\bar{\tilde{u}}\bar{\tilde{u}}_{\tilde{x}}) + \alpha\tilde{b}_{\tilde{x}\tilde{x}}\bar{\tilde{u}}^2 + \mathcal{O}(\beta,\alpha\beta).\end{aligned} \tag{22}$$

Evaluating the integrals $\int_{\tilde{b}}^{\alpha\tilde{\eta}}\Gamma\,d\tilde{z}$ and $\int_{\tilde{b}}^{\alpha\tilde{\eta}}(\tilde{z}-\tilde{b})\Gamma\,d\tilde{z}$ yields

$$\int_{\tilde{b}}^{\alpha\tilde{\eta}}\Gamma\,d\tilde{z} = \frac{1}{2}\tilde{h}\tilde{\mathcal{P}} + \tilde{h}\tilde{\mathcal{Q}},$$

and

$$\int_{\tilde{b}}^{\alpha\tilde{\eta}}(\tilde{z}-\tilde{b})\Gamma\,d\tilde{z} = \frac{1}{3}\tilde{h}^2\tilde{\mathcal{P}} + \frac{1}{2}\tilde{h}^2\tilde{\mathcal{Q}},$$

where

$$\tilde{\mathcal{P}} = \tilde{h}\left[\alpha\bar{\tilde{u}}^2_{\tilde{x}} - \bar{\tilde{u}}_{\tilde{x}\tilde{t}} - \alpha\bar{\tilde{u}}\bar{\tilde{u}}_{\tilde{x}\tilde{x}}\right], \tag{23}$$

and

$$\tilde{\mathcal{Q}} = \tilde{b}_{\tilde{x}}\left(\bar{\tilde{u}}_{\tilde{t}} + \alpha\bar{\tilde{u}}\bar{\tilde{u}}_{\tilde{x}}\right) + \tilde{b}_{\tilde{x}\tilde{x}}\bar{\tilde{u}}^2. \tag{24}$$

Finally we find the second equation of the system as

$$\begin{aligned}&\bar{\tilde{u}}_{\tilde{t}} + \alpha\bar{\tilde{u}}\bar{\tilde{u}}_{\tilde{x}} + \tilde{\eta}_{\tilde{x}} + \frac{\beta}{\tilde{h}}\frac{\partial}{\partial\tilde{x}}\left\{\left(\frac{1}{3}\tilde{\mathcal{P}} + \frac{1}{2}\tilde{\mathcal{Q}}\right)\tilde{h}^2\right\}\\ &\quad + + \beta\tilde{b}_{\tilde{x}}\left(\frac{1}{2}\tilde{\mathcal{P}} + \tilde{\mathcal{Q}}\right) = \mathcal{O}(\alpha\beta^2).\end{aligned}$$

By setting the right-hand side equal to zero, and writing the variables in dimensional form the system reads

$$\eta_t + [h\bar{u}]_x = 0, \tag{25a}$$

$$\bar{u}_t + \bar{u}\bar{u}_x + g\eta_x + \frac{1}{h}\left[h^2\left(\frac{1}{3}\mathcal{P} + \frac{1}{2}\mathcal{Q}\right)\right]_x - b_x\left(\frac{1}{2}\mathcal{P} + \mathcal{Q}\right) = 0, \tag{25b}$$

where $\mathcal{P} = h\left[\bar{u}^2_x - \bar{u}_{xt} - \bar{u}\bar{u}_{xx}\right]$ and $\mathcal{Q} = -b_x(\bar{u}_t + \bar{u}\bar{u}_x) - b_{xx}\bar{u}^2$.

In order to determine which terms should be kept for the velocity field at a certain order of approximation, the incompressibility condition (7a) can be used. Then, the dimensional form of the water particle velocities at any location (x, z) in the vertical plane become

$$u = \bar{u} + \left(\frac{h^2}{6} - \frac{z^2}{2}\right)\bar{u}_{xx}, \tag{26a}$$

$$v = -z\bar{u}_x. \tag{26b}$$

As it was mentioned before, system (1a) and (1b) reduces to the shallow water system when $\beta \to 0$ and to the classical Boussinesq system when $\beta \sim \alpha$.

An asymptotic expression for the pressure $\tilde{p}(\tilde{x},\tilde{z},\tilde{t})$ can be obtained by substituting formula (22) into (15). Such a formula was derived in [48] in the form

$$\begin{aligned}\tilde{p}(\tilde{x},\tilde{z},\tilde{t}) &= \alpha\tilde{\eta} - \tilde{z}\\ &\quad + \frac{\alpha\beta}{2}\left[-\bar{\tilde{u}}_{\tilde{x}\tilde{t}} - \alpha\bar{\tilde{u}}\bar{\tilde{u}}_{\tilde{x}\tilde{x}} + \alpha\bar{\tilde{u}}^2_{\tilde{x}}\right]\left(\tilde{h}^2 - (\tilde{z}-\tilde{b})^2\right)\\ &\quad + \alpha\beta\left(\alpha\tilde{b}_{\tilde{x}\tilde{x}}\bar{\tilde{u}}^2 + \alpha\tilde{b}_{\tilde{x}}\bar{\tilde{u}}\bar{\tilde{u}}_{\tilde{x}} + \tilde{b}_{\tilde{x}}\bar{\tilde{u}}_{\tilde{t}}\right)(\alpha\tilde{\eta} - \tilde{z})\\ &\quad + \mathcal{O}(\alpha\beta^2).\end{aligned} \tag{27}$$

3. Mechanical balance laws for the SGN equations

In this section, we derive the mechanical balance laws such as the mass, momentum and energy conservation for the SGN equations extending the results related to some Boussinesq systems found in [31]. The balance laws consist of terms of the same asymptotic order as in the SGN equations. We start with the conservation of mass.

3.1. Mass balance

We investigate the mass conservation properties of Eqs. (25a) and (25b). Our starting point is the total mass of the fluid contained in a control volume of unit width, bounded by the lateral sides of the interval $[x_1, x_2]$, and by the free surface and the bottom. This mass is given by

$$\mathcal{M} = \int_{x_1}^{x_2}\int_{-b}^{\eta}\rho\,dz\,dx.$$

According to the principle of mass conservation and the fact that there is no mass flux through the bottom or the free surface, mass

conservation can be considered in terms of the flow variables as follows:

$$\frac{d}{dt}\int_{x_1}^{x_2}\int_{-b}^{\eta}\rho\,dz\,dx=\left[\int_{-b}^{\eta}\rho u(x,z,t)\,dz\right]_{x_2}^{x_1}.$$

In non-dimensional form this equation becomes

$$\frac{d}{d\tilde{t}}\int_{\tilde{x}_1}^{\tilde{x}_2}\int_{\tilde{b}}^{\alpha\tilde{\eta}}d\tilde{z}\,d\tilde{x}=\alpha\left[\int_{\tilde{b}}^{\alpha\tilde{\eta}}\tilde{u}(\tilde{x},\tilde{z},\tilde{t})\,d\tilde{z}\right]_{\tilde{x}_2}^{\tilde{x}_1}.$$

Substituting the expression (20) for $\tilde{u}$ and integrating with respect to $\tilde{z}$ yields

$$\frac{d}{d\tilde{t}}\int_{\tilde{x}_1}^{\tilde{x}_2}\tilde{h}d\tilde{x}=\alpha\left[\bar{\tilde{u}}\tilde{h}\right]_{\tilde{x}_2}^{\tilde{x}_1}+\mathcal{O}(\alpha\beta^2),\tag{28}$$

where $\tilde{h}=\alpha\tilde{\eta}-\tilde{b}$ denotes the nondimensional total depth. Dividing (28) by $\tilde{x}_2-\tilde{x}_1$ and taking $\tilde{x}_2-\tilde{x}_1\to 0$ then the mass balance equation is written as

$$\tilde{h}_{\tilde{t}}+(\alpha\bar{\tilde{u}}\tilde{h})_{\tilde{x}}=\mathcal{O}(\alpha\beta^2).\tag{29}$$

Denoting the non-dimensional mass density by $\tilde{M}=\tilde{h}$ and the non-dimensional mass flux by $\tilde{q}_M=\alpha\bar{\tilde{u}}\tilde{h}$, then the mass balance is

$$\frac{\partial\tilde{M}}{\partial\tilde{t}}+\frac{\partial\tilde{q}_M}{\partial\tilde{x}}=\mathcal{O}(\alpha\beta^2).$$

Using the scaling $M=\rho b_0\tilde{M}$ and $q_M=\rho b_0 c_0\tilde{q}_M$ the dimensional forms of mass density and mass flux are $M=\rho h$ and $q_M=\rho\bar{u}h$ respectively. Then the dimensional form of the mass balance is obtained by discarding the right-hand side of the scaled mass balance equation and using the unscaled quantities:

$$\frac{\partial M}{\partial t}+\frac{\partial q_M}{\partial x}=0.\tag{30}$$

It is noted that the mass balance is satisfied exactly by the solutions of the SGN system, in fact (30) is the same equation as (25a).

The expressions for mass density and the mass flux do not depend on the shape of the bottom topography, and in particular, they have the same form for both even and uneven beds. The dimensional form of (29) coincides with analogous formulas of the shallow-water wave system and the classical Boussinesq system [31]. While this may be expected, it should be pointed out that in the case of other asymptotically equivalent systems, mass conservation may be satisfied only to the same order as the order of the equations, [31].

3.2. Momentum balance

The total horizontal momentum of a fluid of constant density ρ contained in a control volume of the same type as in the previous section is

$$\mathcal{I}=\int_{x_1}^{x_2}\int_{-b}^{\eta}\rho u\,dz\,dx.$$

Conservation of momentum implies that the rate of change of $\mathcal{I}$ is equal to the net influx of momentum through the boundaries plus the net force at the boundary of the control volume. Therefore, the conservation of momentum is written

$$\frac{d}{dt}\int_{x_1}^{x_2}\int_{-b}^{\eta}\rho u\,dz\,dx=\int_{x_1}^{x_2}pb_x\,dx+\left[\int_{-b}^{\eta}\rho u^2(x,z)\,dz+\int_{-b}^{\eta}pdz\right]_{x_2}^{x_1}.$$

Non-dimensionalization of this expression leads to

$$\alpha\frac{d}{d\tilde{t}}\int_{\tilde{x}_1}^{\tilde{x}_2}\int_{\tilde{b}}^{\alpha\tilde{\eta}}\tilde{u}\,d\tilde{z}\,d\tilde{x}=-\int_{\tilde{x}_1}^{\tilde{x}_2}\tilde{P}_b\tilde{b}_{\tilde{x}}\,d\tilde{x}+\left[\alpha^2\int_{\tilde{b}}^{\alpha\tilde{\eta}}\tilde{u}^2\,d\tilde{z}+\int_{\tilde{b}}^{\alpha\tilde{\eta}}\tilde{p}\,d\tilde{z}\right]_{\tilde{x}_2}^{\tilde{x}_1},$$

where $\tilde{P}_b$ denotes the pressure at the bottom $\tilde{P}_b=\tilde{h}+\frac{\alpha\beta}{2}[-\bar{\tilde{u}}_{\tilde{x}\tilde{t}}-\alpha\bar{\tilde{u}}\bar{\tilde{u}}_{\tilde{x}\tilde{x}}+\alpha\bar{\tilde{u}}_{\tilde{x}}^2]\tilde{h}^2+\alpha\beta(\alpha\tilde{b}_{\tilde{x}\tilde{x}}\bar{\tilde{u}}^2+\alpha\tilde{b}_{\tilde{x}}\bar{\tilde{u}}\bar{\tilde{u}}_{\tilde{x}}+\tilde{b}_{\tilde{x}}\bar{\tilde{u}}_{\tilde{t}})\tilde{h}$. Substituting the values of $\tilde{u}$ and $\tilde{p}$ from Eqs. (20) and (15) and integrating with respect to $\tilde{z}$ yields

$$\alpha\frac{d}{d\tilde{t}}\int_{\tilde{x}_1}^{\tilde{x}_2}\bar{\tilde{u}}\tilde{h}d\tilde{x}=-\int_{\tilde{x}_1}^{\tilde{x}_2}\tilde{P}_b\tilde{b}_{\tilde{x}}\,d\tilde{x}+\left[\alpha^2\bar{\tilde{u}}^2\tilde{h}+\frac{\tilde{h}^2}{2}-\frac{\alpha\beta}{3}\tilde{h}^3\left(\bar{\tilde{u}}_{\tilde{x}\tilde{t}}+\alpha\bar{\tilde{u}}\bar{\tilde{u}}_{\tilde{x}\tilde{x}}-\alpha(\bar{\tilde{u}}_{\tilde{x}})^2\right)\right]_{\tilde{x}_2}^{\tilde{x}_1}+\left[\frac{\alpha\beta}{2}\tilde{h}^2\left(\alpha\tilde{b}_{\tilde{x}\tilde{x}}\bar{\tilde{u}}^2+\tilde{b}_{\tilde{x}}(\alpha\bar{\tilde{u}}\bar{\tilde{u}}_{\tilde{x}}+\bar{\tilde{u}}_{\tilde{t}})\right)\right]_{\tilde{x}_2}^{\tilde{x}_1}+\mathcal{O}(\alpha\beta^2).$$

Applying similar techniques used for the derivation of the mass balance equation we obtain the momentum balance equation in the form

$$\left(\alpha\bar{\tilde{u}}\tilde{h}\right)_{\tilde{t}}+\left(\alpha^2\bar{\tilde{u}}^2\tilde{h}+\frac{\tilde{h}^2}{2}-\frac{\alpha\beta}{3}\tilde{h}^3\left(\bar{\tilde{u}}_{\tilde{x}\tilde{t}}+\alpha\bar{\tilde{u}}\bar{\tilde{u}}_{\tilde{x}\tilde{x}}-\alpha(\bar{\tilde{u}}_{\tilde{x}})^2\right)\right)_{\tilde{x}}+\left(\frac{\alpha\beta}{2}\tilde{h}^2\left(\alpha\tilde{b}_{\tilde{x}\tilde{x}}\bar{\tilde{u}}^2+\tilde{b}_{\tilde{x}}(\alpha\bar{\tilde{u}}\bar{\tilde{u}}_{\tilde{x}}+\bar{\tilde{u}}_{\tilde{t}})\right)\right)_{\tilde{x}}=-\tilde{P}_b\tilde{b}_{\tilde{x}}+\mathcal{O}(\alpha\beta^2).\tag{31}$$

If the non-dimensional momentum density is defined by

$$\tilde{I}=\alpha\bar{\tilde{u}}\tilde{h}$$

and the momentum flux plus pressure force is defined by

$$\tilde{q}_I=\alpha^2\bar{\tilde{u}}^2\tilde{h}+\frac{\tilde{h}^2}{2}-\frac{\alpha\beta}{3}\tilde{h}^3(\bar{\tilde{u}}_{\tilde{x}\tilde{t}}+\alpha\bar{\tilde{u}}\bar{\tilde{u}}_{\tilde{x}\tilde{x}}-\alpha(\bar{\tilde{u}}_{\tilde{x}})^2)+\frac{\alpha\beta}{2}\tilde{h}^2(\alpha\tilde{b}_{\tilde{x}\tilde{x}}\bar{\tilde{u}}^2+\tilde{b}_{\tilde{x}}(\alpha\bar{\tilde{u}}\bar{\tilde{u}}_{\tilde{x}}+\bar{\tilde{u}}_{\tilde{t}}))$$

then the momentum balance equation can be written as

$$\frac{\partial\tilde{I}}{\partial\tilde{t}}+\frac{\partial\tilde{q}_I}{\partial\tilde{x}}=-\tilde{P}_b\tilde{b}_{\tilde{x}}+\mathcal{O}(\alpha\beta^2).$$

Using the scaling $I=\rho c_0 b_0\tilde{I}$ and $q_I=\rho c_0^2 b_0\tilde{q}_I$, the dimensional forms of the momentum density and momentum flux per unit span are given by

$$I=\rho\bar{u}h,\tag{32}$$

and

$$q_I=\rho\bar{u}^2h+\frac{\rho g}{2}h^2-\frac{\rho}{3}(\bar{u}_{xt}+\bar{u}\bar{u}_{xx}-\bar{u}_x^2)h^3-\frac{\rho}{2}\left(b_{xx}\bar{u}^2+b_x(\bar{u}\bar{u}_x+\bar{u}_t)\right)h^2,\tag{33}$$

respectively.

It turns out that the momentum conservation law is also an exact consequence of the SGN system (25a)–(25b). Indeed, if the momentum density is defined by (32), the momentum flux plus pressure force is defined by (33), and the pressure is defined by (27), then solutions of the SGN system also satisfy exactly the equation

$$\frac{\partial I}{\partial t}+\frac{\partial q_I}{\partial x}=b_x p.$$

Note that if the bottom $z = -b = -b_0$ is horizontal, then the last equation is homogeneous and does not depend on the pressure p.

Taking $\beta \to 0$ in the momentum balance equations (31), and using dimensional variables and horizontal bottom $b = b_0$, the momentum density is unchanged, but the flux reduces to

$$q_I^{sw} = \rho \bar{u}^2 h + \frac{\rho g}{2} h^2. \tag{34}$$

Thus it is plain that both the momentum density I and flux q_I reduce correctly to the nonlinear shallow water approximation. In the case $\beta \sim \alpha$ and a flat bottom, the quantities for the momentum balance law are $I = \rho \bar{u}(b_0 + \eta)$ and $q_I = \rho b_0 \bar{u}^2 + \frac{\rho g}{2} h^2 - \frac{\rho}{3} b_0^3 \bar{u}_{xt}$, which agree with the corresponding quantities of the classical Boussinesq system.

3.3. Energy balance

The total mechanical energy inside a control volume can be written as the sum of the kinetic and potential energy as

$$\mathcal{E} = \int_{x_1}^{x_2} \int_{-b}^{\eta} \left\{ \frac{\rho}{2}(u^2 + v^2) + \rho g z \right\} dz\, dx.$$

The conservation energy can be expressed as

$$\begin{aligned} &\frac{d}{dt} \int_{x_1}^{x_2} \int_{-b}^{\eta} \left\{ \frac{\rho}{2}(u^2 + v^2) + \rho g z \right\} dz\, dx \\ &== \left[\int_{-b}^{\eta} \left\{ \left(\frac{\rho}{2}(u^2 + v^2) + \rho g z \right) u + uP \right\} dz \right]_{x_2}^{x_1}, \end{aligned} \tag{35}$$

and in non-dimensional variables as

$$\begin{aligned} &\frac{d}{d\tilde{t}} \int_{\tilde{x}_1}^{\tilde{x}_2} \int_{\tilde{b}}^{\alpha\tilde{\eta}} \left\{ \frac{\alpha^2}{2}(\tilde{u}^2 + \beta \tilde{v}^2) + \tilde{z} \right\} d\tilde{z}\, d\tilde{x} \\ &= \alpha \left[\int_{\tilde{b}}^{\alpha\tilde{\eta}} \left\{ \frac{\alpha^2}{2}(\tilde{u}^3 + \beta \tilde{v}^2 \tilde{u}) + \tilde{z}\tilde{u} + \tilde{p}\tilde{u} \right\} d\tilde{z} \right]_{\tilde{x}_2}^{\tilde{x}_1}. \end{aligned} \tag{36}$$

By substituting the expressions (17), (18) and (27) for $\tilde{u}$, $\tilde{v}$ and $\tilde{p}$ respectively, the energy balance equation takes the form

$$\begin{aligned} &\frac{d}{d\tilde{t}} \int_{\tilde{x}_1}^{\tilde{x}_2} \left(\frac{\alpha^2}{2}\left(\bar{\tilde{u}}^2 + \beta \tilde{b}_{\tilde{x}}^2 \bar{\tilde{u}}^2 \right) \tilde{h} - \frac{\alpha^2 \beta}{2} \tilde{b}_{\tilde{x}} \tilde{h}^2 \bar{\tilde{u}} \bar{\tilde{u}}_{\tilde{x}} \right. \\ &\quad \left. + \frac{\alpha^2 \beta}{6} \tilde{h}^3 \bar{\tilde{u}}_{\tilde{x}}^2 + \frac{\tilde{h}^2}{2} + \tilde{b}\tilde{h} \right) d\tilde{x} \\ &= \left[\frac{\alpha^3}{2} \bar{\tilde{u}}^3 \left(1 + \beta \tilde{b}_{\tilde{x}}^2 \right) \tilde{h} + \frac{\alpha}{2} \tilde{h}^2 \bar{\tilde{u}} \right. \\ &\quad + \alpha \tilde{b} \bar{\tilde{u}} \tilde{h} - \frac{\alpha^3 \beta}{2} \tilde{b}_{\tilde{x}} \bar{\tilde{u}}_{\tilde{x}} \bar{\tilde{u}}^2 \tilde{h}^2 + \frac{\alpha^3 \beta}{6} \bar{\tilde{u}} \bar{\tilde{u}}_{\tilde{x}}^2 \tilde{h}^3 \Big]_{\tilde{x}_2}^{\tilde{x}_1} \\ &\quad + \left[\frac{\alpha}{2} \bar{\tilde{u}} \tilde{h}^2 - \frac{\alpha^2 \beta}{3} \tilde{h}^3 \bar{\tilde{u}} \left(\bar{\tilde{u}}_{\tilde{x}\tilde{t}} + \alpha \bar{\tilde{u}} \bar{\tilde{u}}_{\tilde{x}\tilde{x}} - \alpha \bar{\tilde{u}}_{\tilde{x}}^2 \right) \right. \\ &\quad \left. - \frac{\alpha^2 \beta}{2} \left(\alpha \tilde{b}_{\tilde{x}\tilde{x}} \bar{\tilde{u}}^2 + \tilde{b}_{\tilde{x}} (\alpha \bar{\tilde{u}} \bar{\tilde{u}}_{\tilde{x}} + \bar{\tilde{u}}_{\tilde{t}}) \right) \tilde{h}^2 \Big]_{\tilde{x}_2}^{\tilde{x}_1} + \mathcal{O}(\alpha \beta^2). \end{aligned} \tag{37}$$

The differential form of the energy balance equation is given by

$$\begin{aligned} &\left(\frac{\alpha^2}{2}\left(\bar{\tilde{u}}^2 + \beta \tilde{b}_{\tilde{x}}^2 \bar{\tilde{u}}^2 \right) \tilde{h} - \frac{\alpha^2 \beta}{2} \tilde{b}_{\tilde{x}} \tilde{h}^2 \bar{\tilde{u}} \bar{\tilde{u}}_{\tilde{x}} + \frac{\alpha^2 \beta}{6} \tilde{h}^3 \bar{\tilde{u}}_{\tilde{x}}^2 + \frac{\tilde{h}^2}{2} + \tilde{b}\tilde{h} \right)_{\tilde{t}} \\ &\quad + \left(\frac{\alpha^3}{2} \bar{\tilde{u}}^3 \tilde{h} + \frac{\alpha^3 \beta}{3} \tilde{b}_{\tilde{x}}^2 \bar{\tilde{u}}^3 + \alpha \bar{\tilde{u}} \tilde{h}^2 + \alpha \tilde{b} \bar{\tilde{u}} \tilde{h} - \frac{\alpha^2 \beta}{3} \tilde{h}^3 \bar{\tilde{u}} \right. \\ &\quad \times \left. \left(\bar{\tilde{u}}_{\tilde{x}\tilde{t}} + \alpha \bar{\tilde{u}} \bar{\tilde{u}}_{\tilde{x}\tilde{x}} - \frac{3}{2} \alpha \bar{\tilde{u}}_{\tilde{x}}^2 \right) - \frac{\alpha^3 \beta}{2} \tilde{b}_{\tilde{x}} \bar{\tilde{u}}_{\tilde{x}} \bar{\tilde{u}}^2 \tilde{h}^2 \right)_{\tilde{x}} \\ &\quad - \left(\frac{\alpha^2 \beta}{2} \tilde{h}^2 \left(\alpha \tilde{b}_{\tilde{x}\tilde{x}} \bar{\tilde{u}}^2 + \tilde{b}_{\tilde{x}} (\alpha \bar{\tilde{u}} \bar{\tilde{u}}_{\tilde{x}} + \bar{\tilde{u}}_{\tilde{t}}) \right) \right)_{\tilde{x}} = \mathcal{O}(\alpha \beta^2). \end{aligned}$$

Considering the appropriate terms in the energy density and flux in (36) which are of order zero or one in the differential energy balance (37), we find that the non-dimensional energy density is

$$\begin{aligned} \tilde{E} = &\frac{\alpha^2}{2}(\bar{\tilde{u}}^2 + \beta \tilde{b}_{\tilde{x}}^2 \bar{\tilde{u}}^2) \tilde{h} - \frac{\alpha^2 \beta}{2} \tilde{b}_{\tilde{x}} \tilde{h}^2 \bar{\tilde{u}} \bar{\tilde{u}}_{\tilde{x}} \\ &+ \frac{\alpha^2 \beta}{6} \tilde{h}^3 \bar{\tilde{u}}_{\tilde{x}}^2 + \frac{\tilde{h}^2}{2} + \tilde{b}\tilde{h}, \end{aligned}$$

while the non-dimensional energy flux plus the work rate due to pressure forces is written as

$$\begin{aligned} \tilde{q}_E = &\frac{\alpha^3}{2} \bar{\tilde{u}}^3 \tilde{h} + \frac{\alpha^3 \beta}{2} \tilde{b}_{\tilde{x}}^2 \bar{\tilde{u}}^3 + \alpha \tilde{b} \bar{\tilde{u}} \tilde{h} + \alpha \bar{\tilde{u}} \tilde{h}^2 \\ &- \frac{\alpha^2 \beta}{3} \tilde{h}^3 \bar{\tilde{u}} \left(\bar{\tilde{u}}_{\tilde{x}\tilde{t}} + \alpha \bar{\tilde{u}} \bar{\tilde{u}}_{\tilde{x}\tilde{x}} - \frac{3}{2} \alpha \bar{\tilde{u}}_{\tilde{x}}^2 \right) - \frac{\alpha^3 \beta}{2} \tilde{b}_{\tilde{x}} \bar{\tilde{u}}_{\tilde{x}} \bar{\tilde{u}}^2 \tilde{h}^2 \\ &- \frac{\alpha^2 \beta}{2} \tilde{h}^2 \bar{\tilde{u}} \left(\alpha \tilde{b}_{\tilde{x}\tilde{x}} \bar{\tilde{u}}^2 + \tilde{b}_{\tilde{x}} (\alpha \bar{\tilde{u}} \bar{\tilde{u}}_{\tilde{x}} + \bar{\tilde{u}}_{\tilde{t}}) \right). \end{aligned}$$

With these definitions, the energy balance is

$$\frac{\partial \tilde{E}}{\partial \tilde{t}} + \frac{\partial \tilde{q}_E}{\partial \tilde{x}} = \mathcal{O}(\alpha \beta^2). \tag{38}$$

Using the scaling $E = \rho c_0^2 b_0 \tilde{E}$ and $q_E = \rho c_0^3 b_0 \tilde{q}_E$, the dimensional form of energy density per unit span in the transverse direction is given as the sum of the kinetic and the potential energy by

$$E = \underbrace{\frac{\rho}{2} \bar{u}^2 (1 + b_x^2) h + \frac{\rho}{2} \bar{u} \bar{u}_x b_x h^2 + \frac{\rho}{6} \bar{u}_x^2 h^3}_{E_k} + \underbrace{\frac{\rho g}{2} h^2 - \rho g b h}_{E_p}, \tag{39}$$

and the dimensional form of energy flux plus work rate due to the pressure force is given by

$$\begin{aligned} q_E = &\rho g \bar{u}(h^2 - bh) + \frac{\rho}{2} \bar{u}^3 h (1 + b_x^2) \\ &- \frac{\rho}{3} h^3 \bar{u} \left(\bar{u}_{xt} + \bar{u} \bar{u}_{xx} - \frac{3}{2} \bar{u}_x^2 \right) \\ &+ \frac{\rho}{2} \bar{u}^2 \bar{u}_x b_x h^2 - \frac{\rho}{2} \bar{u} h^2 \left(b_{xx} \bar{u}^2 + b_x (\bar{u} \bar{u}_x + \bar{u}_t) \right). \end{aligned}$$

For a horizontal bed, it is more convenient to normalize the potential energy of a fluid particle to be zero at the bottom. If this is done, then the dimensional forms of energy density and energy flux plus work rate due to pressure forces are given by

$$E = \frac{\rho g}{2} h^2 + \frac{\rho}{2} h \bar{u}^2 + \frac{\rho}{6} h^3 \bar{u}_x^2, \tag{40}$$

and

$$q_E = \rho g \bar{u} h^2 + \frac{\rho}{2} \bar{u}^3 h - \frac{\rho}{3} h^3 \bar{u} \left(\bar{u}_{xt} + \bar{u} \bar{u}_{xx} - \frac{3}{2} \bar{u}_x^2 \right), \tag{41}$$

respectively. Note that as $\beta \to 0$ in Eq. (37), the energy balance reduces to the shallow-water energy conservation with

$$E^{sw} = \frac{\rho g}{2} \left(b_0^2 + 2 b_0 \eta + \eta^2 \right) + \frac{\rho}{2} h \bar{u}^2 \tag{42}$$

and

$$q_E^{sw} = \rho g h^2 \bar{u} + \frac{\rho}{2} h \bar{u}^3. \tag{43}$$

In addition, in the case $\alpha \sim \beta$, the energy balance reduces correctly to the case of the classical Boussinesq system, with $E = \frac{\rho g}{2}(b_0^2 + 2b_0\eta + \eta^2) + \frac{\rho}{2} b_0 \bar{u}^2$ and $q_E = \rho g(b_0^2 + 2\eta b_0)\bar{u}$.

It is worth noting that the conservation of the asymptotic approximation to the total energy with nontrivial bathymetry in the fully nonlinear regime is satisfied by the solutions of the SGN equations exactly. This can be seen by performing lengthy computations using formal integrations by parts, or by recognizing that potential energy is generally only defined up to a constant, and $\mathcal{E} = \int E\, dx$ differs from the Hamiltonian (4) by the constant term $\frac{g}{2}\int b^2\, dx$.

4. Applications

4.1. Evolution of undular bores

In free surface flow, the transition between two states of different flow depth is called a hydraulic jump if the transition region is stationary, and a bore if it is moving. Bores are routinely generated by tidal forces in several rivers around the world, and may also be generated in wavetank experiments [49,50].

The experimental studies of [49] show that when the ratio between the difference in flow depths to the undisturbed water depth is smaller than 0.28, then the bore will feature oscillations in the downstream part. If this ratio is greater than approximately 0.75, then a so-called turbulent bore ensues. If the ratio is between 0.28 and 0.75, the bore will be partially turbulent, but will also feature some oscillations. The bore strength can also be expressed in terms of the Froude number $Fr = \sqrt{[(2h_1/h_0 + 1)^2 - 1]/8}$, and more recent studies, such as [50] have found that when $Fr \geq 1.4$ approximately, the bore consists of a steep front, while undulations are growing at the bore front only in the near-critical state $Fr \approx 1$. The different shapes and a transition from the subcritical to the supercritical regime is described in [51], and in [52] an empirical critical value $Fr_{crit} = 1.3$ is suggested in order to determine the breaking of an undular bore. However the exact characterization of the transition between these states still remains unclear.

Some of the divergence in the results on the critical bore strength might be explained by the observation that one single nondimensional number may not be sufficient to classify all bores. For example, in [53], a hyperbolic shear-flow model is suggested which allows the classification of bores with an additional parameter depending on the strength of the developing shear flow near the bore front.

The connection between the initial bore strength and the ensuing highest undulation is fairly well understood. Using Whitham modulation theory [54], it can be shown that if viscosity is neglected, the amplitude of the leading wave behind the bore front is exactly twice the initial ratio of flow depths [47,55]. This result agrees well with experimental findings. For example, the amplitude of the leading wave found experimentally in [49] was 2.06 times the initial amplitude ratio.

In this section, we present a numerical study of the energy balance of undular bores for the SGN equations. The classical theory of bores relies on an inviscid shallow-water theory and the examination of exact weak solutions of the shallow-water equations [34]. It is well known that due to the simplifications inherent in long-wave shallow-water models, a sharp transition in both flow depth and flow velocity which respects conservation of both mass and momentum necessitates a loss of energy across the front.

Given these assumptions, it is natural to explain the energy loss across the bore front by pointing to the physical effects neglected in the shallow-water theory, such as viscosity, frequency dispersion, and turbulent flow. Indeed, in strong bores, turbulent dissipation accounts for the lion's share of energy dissipation, and a long-wave model can only give a first approximation of the dynamics. Most of the work investigating the energy loss has focused on weak undular bores, where long-wave models can be expected to yield an accurate description of the flow. The loss of energy in weak bores has been explained by the creation of oscillations in the free surface behind the front, but it was noted in [35] that an additional dissipation mechanism is needed. In [36], the bottom boundary layer was invoked to explain this required additional energy loss, but it was noted in [37,38] that invoking frictional effects to explain the energy loss experienced by a conservative system was not consistent.

However, as already mentioned, there was a slight technical problem in the analysis of [38], since the energy functional

$$\mathcal{E}_{Bous} = \frac{1}{2}\int_{\tilde{x}_1}^{\tilde{x}_2} \left[\alpha^2 \tilde{w}^2 \tilde{h} + \frac{\alpha^2\beta}{3}\left(\tilde{w}\tilde{w}_{\tilde{x}\tilde{x}} + \tilde{w}_{\tilde{x}}^2\right) + \tilde{h}^2\right] d\tilde{x}, \tag{44}$$

used in that work could not be obtained in the framework of the asymptotically correct mechanical balance laws derived in [31]. Indeed, the expressions for the energy and energy flux associated to the Boussinesq system which were derived in [31] are

$$\tilde{E} = \frac{1}{2} + \alpha\tilde{\eta} + \frac{\alpha^2}{2}\tilde{\eta}^2 + \frac{\alpha^2}{2}\tilde{w}^2 = \frac{\alpha}{2}\tilde{h}^2 + \frac{\alpha^2}{2}\tilde{w}^2,$$

and the non-dimensional energy flux (corrected for the work rate due to pressure forces) as

$$\begin{aligned}\tilde{q}_E &= \alpha\tilde{w} + 2\alpha^2\tilde{w}\tilde{\eta} + \frac{\alpha\beta}{2}\left(\theta^2 - \frac{1}{3}\right)\tilde{w}_{\tilde{x}\tilde{x}} \\ &= \alpha\tilde{w} + 2\alpha^2\tilde{w}\tilde{\eta} + \frac{\alpha\beta}{6}\tilde{w}_{\tilde{x}\tilde{x}},\end{aligned}$$

where $\tilde{w}$ is the nondimensional horizontal velocity component at height $\theta = b_0\sqrt{2/3}$ in the water column. It is apparent that as $\beta \to 0$, these expressions do not reduce correctly to the corresponding expressions of the shallow-water theory. However, since the expressions (40) and (41) do reduce to the correct shallow-water equivalents, the analysis of the energy loss in the undular bore can be made precise in the context of the SGN system. Nevertheless, the SGN system is an approximation, and ideally, a study of undular bores should include short-wave effects, bottom friction and vorticity.

The numerical method that was used to perform the numerical simulations in this paper is detailed in the Appendix. It is also noted that for simplicity's sake we consider the water density $\rho = 1\, kg/m^3$. The numerical experiments require initial data. An initial surface condition that triggers the generation of undular bores is

$$h(x,0) = h_0 + \frac{1}{2}(h_1 - h_0)\tanh(\kappa x),$$

where κ is the parameter that determines the steepness of the undular bore. Here we take $\kappa = 1/2$. In order to generate a simple undular bore, i.e. a wave that propagates mainly in one direction, we consider an initial flow given by the following velocity profile:

$$\begin{aligned}u(x,0) = \frac{\delta h}{h_1}&\left(\frac{g}{2h_0}\left(2h_0^2 + 3(\delta h)h_0 + (\delta h)^2\right)\right)^{1/2} \\ &\times\left(1 - \tanh(\kappa x)\right),\end{aligned}$$

where $\delta h = h_1 - h_0$. One may envision other numerical methods to create an undular bore, such as the addition of a line source in the upstream part, such as used in [56]. Nevertheless, the initial

Table 1
Energy conservation.

h_1/h_0	Fr	$q_E(x_1) - q_E(x_2)$	$d\mathcal{E}/dt$
1.1	1.07	3.6481059	3.6481059
1.2	1.15	8.6017456	8.6017456
1.3	1.22	15.100378	15.100378
1.4	1.30	23.394470	23.394470
1.5	1.37	33.746103	33.746103
1.6	1.44	46.429376	46.429376
1.7	1.51	61.730669	61.730669

Table 2
Momentum conservation.

h_1/h_0	Fr	$q_I(x_1) - q_I(x_2)$	$d\mathcal{I}/dt$
1.1	1.07	1.1330550	1.1330549
1.2	1.15	2.5898340	2.5898399
1.3	1.22	4.3997850	4.3997849
1.4	1.30	6.5923199	6.5923198
1.5	1.37	9.1968749	9.1968748
1.6	1.44	12.242880	12.242879
1.7	1.51	15.759764	15.759764

conditions described above were sufficient for our purposes. First we present the computation of the energy budget in an undular bore for various bore strengths. We consider the control volume $[x_1, x_2]$, where x_1 is far to the left of the bore front, and x_2 is far to the right. In Table 1 the bore strength is shown in the first column, and the corresponding Froude number is shown in the second column. Taking $h_0 = 1$ and h_1 between 1.1 and 1.7 we monitor the energy flux and work rate due to the pressure force, given by $q_E(x_1) - q_E(x_2)$ as defined in (41), and these values are shown in the third column of the table. We also monitor the gain in energy in the control interval as given by $\mathcal{E}(t) = \int_{x_1}^{x_2} E\, dx$. These values are shown in the fourth column. The particular figures shown in the table are for $T = 30$, but the values are nearly constant over time. It is apparent from the table that energy conservation holds to at least eight digits, even for large bore strengths. These numbers confirm our previous finding that the energy is exactly conserved in the SGN model, and also validates the implementation of the numerical method. In addition, these results confirm our claim that no dissipation mechanism is necessary to explain the energy loss in an undular bore.

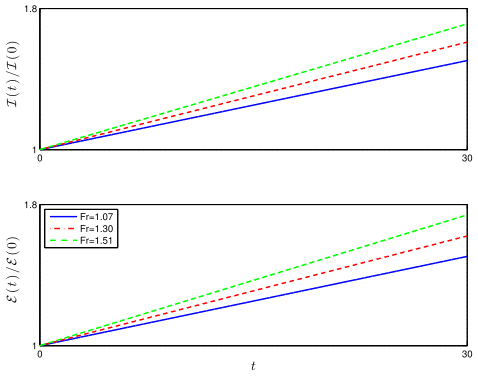

Fig. A.2. The momentum and the energy of the undular bore for $Fr = 1.07$, 1.30 and 1.51.

As noted in the previous section, the expression (41) for the energy flux and work rate due to pressure forces reduces to the corresponding formula for the shallow-water theory in the case of very long waves. Since x_1 and x_2 are relatively far from the bore front, shallow-water theory should be valid at these points. Therefore, the usual formula for the energy loss in an undular bore in the shallow-water theory is valid:

$$\frac{dE^{sw}}{dt} + q_E^{sw}(x_2, t) - q_E^{sw}(x_1, t) = -\frac{\rho}{4}(h_1 - h_0)^3 \sqrt{\frac{1}{2}g^3\left(\frac{1}{h_0} + \frac{1}{h_1}\right)}. \tag{45}$$

Since there is no energy loss in a dispersive system, one may conclude that the excess energy is fed into oscillations of the free surface, and the formula (45) furnishes an estimate of the amount of energy which is residing in the oscillatory motion.

A similar study can be performed on the momentum balance. Momentum gain in the control interval is given by the momentum flux through the lateral boundaries and the pressure force as $q_I(x_1) - q_I(x_2)$, with q_I given in (33) up to $T = 30$. Table 2 presents the momentum rates. As in the case of the energy, the corresponding values agree to about eight digits. In Fig. A.2, we present the normalized values $\mathcal{I}(t)/\mathcal{I}(0)$ of the momentum and $\mathcal{E}(t)/\mathcal{E}(0)$ of the total energy for the values of the Froude number $Fr = 1.07$, 1.30 and 1.51. The slopes of the lines can be found in Tables 1 and 2.

Fig. A.3 shows the profiles of the undular bores generated when $h_1/h_0 = 1.3$, 1.5 and 1.7. From these figures, we observe that as the Froude number Fr increases, the peak amplitude of the leading wave becomes larger, and the shape of the wave envelope is changing. For example the shape of the wave envelope of Fig. A.3(a) can be described by a linear function while the shape of the wave envelope of Fig. A.3(c) can be described by a square-root function. For the various shapes of the undular bores we refer to [57].

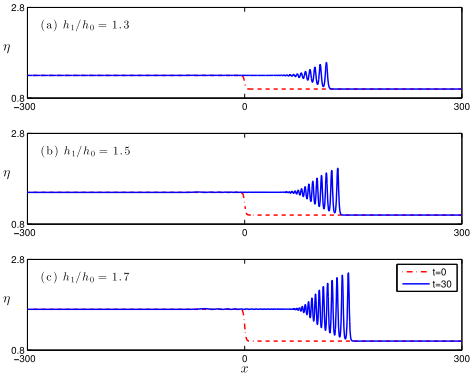

Fig. A.3. Undular bores profiles for various Fr values.

4.2. Shoaling of solitary waves

In this section, we study the conservation of energy in the case of a nonuniform bathymetry. Specifically, we consider the experiments proposed in [58,59] related to the shoaling of solitary waves on a beach of slope 1:35. The shoaling of solitary waves has been studied theoretically and experimentally in many works, such as in [58–61]. Next, we study the shoaling of solitary waves with normalized amplitude $A = 0.1$, 0.15, 0.2 and 0.25 in the domain $[-100, 34]$. In the numerical experiments we take $\Delta x = 0.05$ while we translate the solitary waves such that the peak amplitude

Table 3
Conserved values of energy (in Joules) and Hamiltonian for shoaling of solitary waves on a plane beach of slope 1:35.

A	$\mathcal{E}$	$\mathcal{H}$
0.10	62.4704607870	0.05202930490
0.15	62.7102258381	0.09856973753
0.20	62.9401348199	0.15627417412
0.25	63.1680884219	0.22460417742

is achieved at $x = -20.1171$ while the bottom is described by the function

$$b(x) = \begin{cases} 1, & x \le 0 \\ 1 - x/35, & x > 0, \end{cases}$$

but modified appropriately around $x = 0$ so as to be smooth enough and to satisfy the regularity requirements of the model.

A comparison between the experimental results on shoaling waves from [58], and the shoaling solitary waves computed with numerical approximation of (1) and (A.1) is presented in Fig. A.4. Overall, we observe a very good agreement between the numerical results and the experimental data.

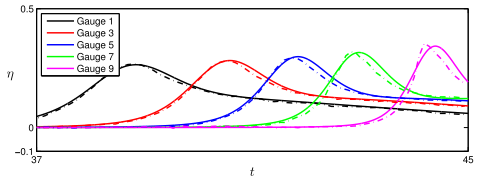

Fig. A.4. Comparison of the numerical solution and the experimental data on wave gauges of [59]. —: Numerical solution; — · —: Experimental data.

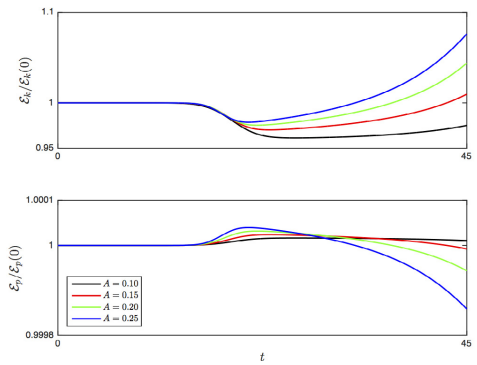

Fig. A.5. Normalized kinetic and potential energy for shoaling of solitary waves on a plane beach of slope 1:35.

Table 3 presents the conserved values of the total energy $\mathcal{E}$ and of the Hamiltonian $\mathcal{H}$ for $t \in [0, 45]$ for the computations shown in Fig. A.4. We observe that the energy is conserved with more than ten decimal digits. Due to the small values of Δx and Δt no energy dissipation can be observed verifying the efficacy of the numerical method.

Although the total energy is conserved the kinetic and the potential energy are not constant with time. Fig. A.5 presents the normalized kinetic energy $\mathcal{E}_k(t)/\mathcal{E}_k(0)$ and normalized potential energy $\mathcal{E}_p(t)/\mathcal{E}_p(0)$ evaluated in the spatial interval $[-100, 34]$. As can be seen in Fig. A.5 the kinetic energy is decreasing at the early stages of shoaling due to the slight decrease in the wave speed while the potential energy is initially increasing due to the increase of the wave height. At later stages of the shoaling, the kinetic energy increases again, due to the increase in particle velocities, and the potential energy decreases again, due to the rising bottom, and narrowing wave peak. Nevertheless, the total energy is constant over time.

5. Summary and conclusions

We have detailed the derivation of mechanical balance laws for the SGN equations in the case of a horizontal bed and also in the case of varying bathymetry. The mechanical balance laws derived here, including the mass, momentum and energy balance laws, are valid to the same asymptotic order as the SGN system, providing a firm link between conservation laws associated to the governing SGN equations, and the above mechanical quantities. Finally, applications to the energy budget of undular bores and the development of potential and kinetic energy in shoaling solitary waves have been presented. In particular, it has been shown that the energy loss in undular bores is fully compensated for by the development of surface oscillations, since the energy in the SGN with a flat bottom is exactly conserved. Indeed, exact conservation of energy to near machine precision was observed in our numerical computations, and this gave an additional check on the implementation of the numerical algorithm.

Acknowledgments

Part of this research was conducted during a visit of Zahra Khorsand to the University of California, Merced, and the authors would like to express their gratitude for hospitality and support. HK and ZK also acknowledge support by the Research Council of Norway (Grant number RCN: 213474/F20). Dimitrios Mitsotakis was supported by the Marsden Fund administered by the Royal Society of New Zealand (Contract number: VUW1418). Dimitrios Mitsotakis also thanks the participants of the "Dispersive Hydrodynamics meeting at BIRS, 2015", and especially Professors Gavin Esler, Sergey Gavrilyuk and Edward Johnson for fruitful discussions on the SGN equations.

Appendix. The numerical method

In this appendix, we consider the initial–boundary value problem (IBVP) comprised of system (25a)–(25b) subject to reflective boundary conditions. Rewriting the system in terms of $(h,\ u)$, and dropping the bar over the symbol of the horizontal velocity, yields the IBVP

$$\begin{aligned} &h_t + (hu)_x = 0, \\ &hu_t + huu_x + gh(h-b)_x \\ &\quad + \left[h^2\left(\frac{1}{3}\mathcal{P} + \frac{1}{2}\mathcal{Q}\right)\right]_x - hb_x\left(\frac{1}{2}\mathcal{P} + \mathcal{Q}\right) = 0, \\ &u(A,t) = u(B,t) = 0, \\ &h(x,0) = h_0(x), \\ &u(x,0) = u_0(x), \end{aligned} \tag{A.1}$$

where $\mathcal{P} = h\left[u_x^2 - u_{xt} - uu_{xx}\right]$, $\mathcal{Q} = -b_x(u_t + uu_x) - b_{xx}u^2$, $x \in [A, B] \subset \mathbb{R}$ and $t \in [0,\ T]$. Considering a spatial grid $x_i = A + i\,\Delta x$, for $i = 0,\ 1, \ldots, N$, where Δx is the spatial mesh-length, such that $\Delta x = (B - A)/N$, $N \in \mathbb{N}$. We define the space of cubic splines

$$S = \left\{\phi \in C^2[A,B] \,\middle|\, \phi|_{[x_i, x_{i+1}]} \in \mathbb{P}^3,\ 0 \le i \le N-1\right\},$$

where $\mathbb{P}^k$ is the space of polynomials of degree k. We also consider the space

$$S_0 = S \cap \left\{ \phi \in C([A, B]) \middle| \phi(A) = \phi(B) = 0 \right\}.$$

The basis functions of the space S and S_0 consist of the usual B-splines described in [63].

The semi-discrete scheme is reduced in finding $\hat{h} \in S$ and $\hat{u} \in S_0$ such that

$$\begin{aligned} &(\hat{h}_t, \phi) + \left((\hat{h}\hat{u})_x, \phi\right) = 0, \\ &\mathcal{B}(\hat{u}_t, \psi; \hat{h}) + \left(\hat{h}\hat{u}\hat{u}_x + g\hat{h}(\hat{h} - b)_x, \psi\right) \\ &\quad + \left(\hat{h}^2\left(\frac{1}{3}\hat{\mathcal{P}} + \frac{1}{2}\hat{\mathcal{Q}}\right), \psi_x\right) - \left(\hat{h}b_x\left(\frac{1}{2}\hat{\mathcal{P}} + \hat{\mathcal{Q}}\right), \psi\right) = 0, \end{aligned} \tag{A.2}$$

for $\phi \in S$, and $\psi \in S_0$, and $\hat{\mathcal{P}} = \hat{h}\left[\hat{u}_x^2 - \hat{u}\hat{u}_{xx}\right]$ and $\hat{\mathcal{Q}} = -b_x\hat{u}\hat{u}_x - b_{xx}\hat{u}^2$. $\mathcal{B}$ is defined as the bilinear form that for fixed $\hat{h}$ is given by

$$\begin{aligned} \mathcal{B}(\psi, \chi; \hat{h}) = &\left(\hat{h}\left[1 - \hat{h}_x b_x - \frac{1}{2}\hat{h}b_{xx} + b_x^2\right]\psi, \chi\right) \\ &+ \frac{1}{3}\left(\hat{h}^3\psi_x, \chi_x\right) \quad \text{for } \psi, \chi \in S_0. \end{aligned} \tag{A.3}$$

The system of Eqs. (A.2) is accompanied by the initial conditions

$$\hat{h}(x, 0) = \mathcal{P}\{h_0(x)\}, \qquad \hat{u}(x, 0) = \mathcal{P}_0\{u_0(x)\}, \tag{A.4}$$

where $\mathcal{P}$ and $\mathcal{P}_0$ are the L^2-projections onto S and S_0 respectively, satisfying $(\mathcal{P}v, \phi) = (v, \phi)$ for all $\phi \in S$ and $(\mathcal{P}_0 v, \psi) = (v, \psi)$ for all $\psi \in S_0$. Upon choosing basis functions ϕ_j and ψ_j for the spaces S and S_0, (A.2) is reduced to a system of ordinary differential equations (ODEs). For the integration in time of this system we employ the Dormand–Prince adaptive time-stepping methods, [64,62]. One may apply the same numerical method to solve the IBVP with non-homogeneous Dirichlet boundary conditions. For example if $u(A, t) = u_A$ then the change of variables $u(x, t) = w(x, t) + u_0(x)$ reduces the non-homogeneous system to a homogeneous IBVP system for the variable w. In all the numerical experiments we took $\Delta x = 0.1$, while the tolerance for the relative error of the adaptive Runge–Kutta scheme was taken $5 \cdot 10^{-14}$. For the computations of the integrals, the Gauss–Legendre quadrature rule with 8 nodes was employed.

The convergence properties of the standard Galerkin method for the SGN system are very similar to those of the classical Boussinesq system studied in detail in [65,66]. In order to compute the convergence rates in various norms, we consider the nonhomogeneous SGN system with flat bottom admitting the exact solution $h(x, t) = 1 + e^{2t}(\cos(\pi x) + x + 2)$ and $u(x, t) = e^{-t}x\sin(\pi x)$ for $0 \le x \le 1$, and for $t \in (0, T]$ with $T = 1$. We compute the normalized errors

$$E_s[F] \doteq \frac{\|F(x, T; \Delta x) - F_{\text{exact}}(x, T)\|_s}{\|F_{\text{exact}}(x, T)\|_s}, \tag{A.5}$$

where $F = F(\cdot; \Delta x)$ is the computed solution, i.e., either $H \approx h(x, T)$ or $U \approx u(x, T)$, F_{exact} is the corresponding exact solution and $s = 0, 1, 2, \infty$ correspond to the L^2, H^1, H^2 and L^∞ norms, respectively. The analogous rates of convergence are defined as

$$\text{rate for } E_s[F] \doteq \frac{\ln(E_s[F(\cdot; \Delta x_{k-1})]/E_s[F(\cdot; \Delta x_k)])}{\ln(\Delta x_{k-1}/\Delta x_k)}, \tag{A.6}$$

where Δx_k is the grid size listed in row k in Table A.4. To ensure that the errors incurred by the temporal integration do not affect the rates of convergence we use $\Delta t \ll \Delta x$ while we take $\Delta x = 1/N$.

Table A.4 presents the spatial convergence rates in the L^2 norm. We observe that the convergence is optimal for the u variable but suboptimal for the h variable. Specifically, it appears that $\|h - \hat{h}\| \sim \Delta x^{3.5}$, while $\|u - \hat{u}\| \sim \Delta x^4$. More precisely, as in the case of the classical Boussinesq system [65], and because the rate of convergence in h appears to be less that 3.5 yields that the error should be of $O(\Delta x^{3.5}\sqrt{\ln(1/\Delta x)})$. Similar results obtained for the convergence in the H^1, H^2 and L^∞ norms. Specifically it was observed numerically that $\|h - \hat{h}\|_s \sim \Delta x^{3.5-s}$, $\|u - \hat{u}\|_1 \sim \Delta x^{4-s}$, for $s = 0, 1, 2$ and $\|h - \hat{h}\|_\infty \sim \Delta x^3$, while $\|u - \hat{u}\|_\infty \sim \Delta x^4$ approximately.

Table A.4
Spatial errors and rates of convergence in the L^2 norm.

N	$E_0[H]$	Rate for $E_0[H]$	$E_0[U]$	Rate for $E_0[U]$
300	0.1211×10^{-8}	–	0.6127×10^{-11}	–
320	0.9674×10^{-9}	3.4793	0.4733×10^{-11}	3.9983
340	0.7836×10^{-9}	3.4772	0.3714×10^{-11}	3.9999
360	0.6422×10^{-9}	3.4797	0.2955×10^{-11}	3.9977
380	0.5322×10^{-9}	3.4754	0.2382×10^{-11}	3.9885
400	0.4452×10^{-9}	3.4793	0.1939×10^{-11}	4.0099

References

[1] F. Serre, Contribution á l' étude des écoulements permanents et variables dans les canaux, Houille Blanche 8 (1953) 374–388.
[2] F. Serre, Contribution á l' étude des écoulements permanents et variables dans les canaux, Houille Blanche 8 (1953) 830–872.
[3] C.H. Su, C.S. Gardner, Korteweg–de Vries equation and generalizations. III. Derivation of the Korteweg–de Vries equation and Burgers equation, J. Math. Phys. 10 (1969) 536–539.
[4] A. Green, P. Naghdi, A derivation of equations for wave propagation in water of variable depth, J. Fluid Mech. 78 (1976) 237–246.
[5] F. Seabra-Santos, D. Renouard, A. Temperville, Numerical and experimental study of the transformation of a solitary wave over a shelf or isolated obstacle, J. Fluid Mech. 176 (1987) 117–134.
[6] G. El, R. Grimshaw, N. Smyth, Transcritical shallow-water flow past topography: finite-amplitude theory, J. Fluid Mech. 640 (2009) 187–214.
[7] D. Lannes, P. Bonneton, Derivation of asymptotic two-dimensional time-dependent equations for surface water wave propagation, Phys. Fluids 21 (2009) 016601.
[8] D. Lannes, The Water Waves Problem: Mathematical Analysis and Asymptotics, American Mathematical Society, 2013.
[9] E. Barthelemy, Nonlinear shallow water theories for coastal waves, Surv. Geophys. 25 (2004) 315–337.
[10] G. Wei, J.T. Kirby, S.T. Grilli, R. Subramanya, A fully nonlinear boussinesq model for surface waves. part 1. highly nonlinear unsteady waves, J. Fluid Mech. 294 (1995) 71–92.
[11] P.A. Madsen, D.R. Fuhrman, B. Wang, A boussinesq-type method for fully nonlinear waves interacting with a rapidly varying bathymetry, Coast. Eng. 53 (5) (2006) 487–504.
[12] M. Brocchini, A reasoned overview on Boussinesq-type models: the interplay between physics, mathematics and numerics, Proc. R. Soc. Lond. Ser. A Math. Phys. Eng. Sci. 469 (0496) (2013) 1–27.
[13] G. El, R. Grimshaw, N. Smyth, Asymptotic description of solitary wave trains in fully nonlinear shallow-water theory, Physica D 237 (19) (2008) 2423–2435.
[14] J.W. Miles, R. Salmon, Weakly dispersive nonlinear gravity waves, J. Fluid Mech. 157 (1985) 519–531.
[15] T. Benjamin, P. Olver, Hamiltonian structure, symmetries and conservation laws for water waves, J. Fluid Mech. 125 (1982) 137–185.
[16] W. Choi, R. Camassa, Fully nonlinear internal waves in a two-fluid system, J. Fluid Mech. 396 (1999) 1–36.
[17] S. Gavrilyuk, H. Kalisch, Z. Khorsand, A kinematic conservation law in free surface flow, Nonlinearity 28 (6) (2015) 1805–1821.
[18] G. Whitham, Variational methods and applications to water waves, Proc. R. Soc. Lond. Ser. A 299 (1967) 6–25.
[19] M. Ehrnström, H. Kalisch, Traveling waves for the Whitham equation, Differential Integral Equations 22 (11–12) (2009) 1193–1210.
[20] R. Cienfuegos, E. Barthelemy, P. Bonneton, A fourth-order compact finite volume scheme for fully nonlinear and weakly dispersive Boussinesq-type equations. Part I: Model development and analysis, Internat. J. Numer. Methods Fluids 51 (2006) 1217–1253.
[21] D. Peregrine, Long waves on beaches, J. Fluid Mech. 27 (1967) 815–827.
[22] J. Carter, R. Cienfuegos, The kinematics and stability of solitary and cnoidal wave solutions of the Serre equations, Eur. J. Mech. B Fluids 30 (2011) 259–268.
[23] Y. Li, Linear stability of solitary waves of the Green–Naghdi equations, Comm. Pure Appl. Math. 54 (2001) 501–536.
[24] Y. Li, Hamiltonian structure and linear stability of solitary waves of the Green–Naghdi equations, J. Nonlinear Math. Phys. 9 (2002) 99–105.
[25] D. Mitsotakis, J. Carter, D. Dutykh, On the nonlinear dynamics of the traveling wave solutions of the serre equations, Preprint arXiv:1404.6725.

[26] Z. Khorsand, Particle trajectories in the Serre equations, Appl. Math. Comput. 230 (0496) (2014) 35–42.
[27] R. Camassa, D. Holm, C. Levermore, Long-time effects of bottom topography in shallow water, Physica D 98 (2) (1996) 258–286.
[28] R.S. Johnson, Camassa–Holm, Korteweg–de Vries and related models for water waves, J. Fluid Mech. 455 (2002) 63–82.
[29] S. Israwi, Large time existence for 1D Green–Naghdi equations, Nonlinear Anal. 74 (2011) 81–93.
[30] H. Kalisch, Mechanical balance laws in long wave models, Oberwolfach Rep. 2015 (19) (2015) 28–31.
[31] A. Ali, H. Kalisch, Mechanical balance laws for Boussinesq models of surface water waves, J. Nonlinear Sci. 22 (2012) 371–398.
[32] A. Ali, H. Kalisch, On the formulation of mass, momentum and energy conservation in the KdV equation, Acta Appl. Math. 133 (1) (2014) 113–131.
[33] Z.I. Fedotova, G.S. Khakimzyanov, D. Dutykh, Energy equation for certain approximate models of long-wave hydrodynamics, Russian J. Numer. Anal. Math. Modelling 29 (3) (2014) 167–178.
[34] L. Rayleigh, On the theory of long waves and bores, Proc. R. Soc. Lond. Ser. A Math. Phys. Eng. Sci. 90 (1914) 324–328.
[35] T. Benjamin, J. Lighthill, On cnoidal waves and bores, Proc. R. Soc. Lond. Ser. A Math. Phys. Eng. Sci. 224 (1954) 448–460.
[36] B. Sturtevant, Implications of experiments on the weak undular bore, Phys. Fluids 8 (1965) 1052–1055.
[37] A. Ali, H. Kalisch, Energy balance for undular bores, C. R. Mec. 338 (2010) 67–70.
[38] A. Ali, H. Kalisch, A dispersive model for undular bores, Anal. Math. Phys. 2 (2012) 347–366.
[39] D. Mitsotakis, B. Ilan, D. Dutykh, On the Galerkin/finite-element method for the Serre equations, J. Sci. Comput. 61 (2014) 166–195.
[40] O.L. Métayer, S. Gavrilyuk, S. Hank, A numerical scheme for the Green–Naghdi model, J. Comput. Phys. 229 (6) (2010) 2034–2045.
[41] D. Dutykh, D. Clamond, P. Milewski, D. Mitsotakis, Finite volume and pseudo-spectral schemes for the fully nonlinear 1D Serre equations, European J. Appl. Math. 24 (2013) 761–787.
[42] P. Bonneton, F. Chazel, D. Lannes, F. Marche, M. Tissier, A splitting approach for the fully nonlinear and weakly dispersive Green–Naghdi model, J. Comput. Phys. 230 (2011) 1479–1498.
[43] R. Cienfuegos, E. Barthelemy, P. Bonneton, A fourth-order compact finite volume scheme for fully nonlinear and weakly dispersive Boussinesq-type equations. Part II: Boundary conditions and model validation, Internat. J. Numer. Methods Fluids 53 (2007) 1423–1455.
[44] G. El, R. Grimshaw, N. Smyth, Unsteady undular bores in fully nonlinear shallow-water theory, Phys. Fluids 18 (2006) 027104.
[45] J. Pearce, J. Esler, A pseudo-spectral algorithm and test cases for the numerical solution of the two-dimensional rotating Green–Naghdi shallow water equations, J. Comput. Phys. 229 (20) (2010) 7594–7608.
[46] D. Mitsotakis, C. Synolakis, M. McGuinness, A modified galerkin/finite element method for the numerical solution of the Serre–Green–Naghdi system, Preprint arXiv: 1505.07795.
[47] G.B. Whitham, Linear and Nonlinear Waves, John Wiley & Sons Inc., New York, 1999.
[48] E.N. Pelinovsky, H.S. Choi, A mathematical model for non-linear waves due to moving disturbances in a basin of variable depth, J. Korean Soc. Coast. Ocean Eng. 5 (1993) 191–197.
[49] H. Favre, Ondes de Translation, Dunond, Paris, 1935.
[50] H. Chanson, Current knowledge in hydraulic jumps and related phenomena: A survey of experimental results, Eur. J. Mech. B Fluids 28 (2) (2009) 191–210.
[51] M. Tissier, P. Bonneton, F. Marche, F. Chazel, D. Lannes, Nearshore dynamics of Tsunami-like undular bores using a fully-nonlinear Boussinesq model, J. Coast. Res. 64 (2011) 603–607.
[52] M. Tissier, P. Bonneton, F. Marche, F. Chazel, D. Lannes, A new approach to handle wave breaking in fully non-linear Boussinesq models, Coast. Eng. 67 (2012) 54–66.
[53] G. Richard, S. Gavrilyuk, The classical hydraulic jump in a model of shear shallow-water flows, J. Fluid Mech. 725 (2013) 492–521.
[54] G.B. Whitham, A general approach to linear and non-linear dispersive waves using a Lagrangian, J. Fluid Mech. 22 (1965) 273–283.
[55] R. Grimshaw, Solitary waves in fluids, Adv. Fluid Mech. 47 (2007) 208.
[56] M. Bestehorn, P. Tyvand, Merging and colliding bores, Phys. Fluids 21 (042107) (2009) 1–11.
[57] M. Hoefer, Shock waves in dispersive Eulerian fluids, J. Nonlinear Sci. 24 (2014) 525–577.
[58] S. Grilli, R. Subramanya, I. Svendsen, J. Veeramony, Shoaling of solitary waves on plane beaches, J. Waterw. Port Coast. Ocean Eng. 120 (1994) 609–628.
[59] S. Grilli, I. Svendsen, R. Subramanya, Breaking criterion and characteristics for solitary waves on slopes, J. Waterw. Port Coast. Ocean Eng. 123 (1997) 102–112.
[60] C. Synolakis, Green's law and the evolution of solitary waves, Phys. Fluids 3 (1991) 490–491.
[61] C. Synolakis, J. Skjelbreia, Evolution of maximum amplitude of solitary waves on plane beaches, J. Waterw. Port Coast. Ocean Eng. 119 (1993) 323–342.
[62] E. Hairer, S.P. Nørsett, G. Wanner, Solving Ordinary Differential Equations: Nonstiff Problems, Springer, 2009.
[63] M.H. Schultz, Spline Analysis, first ed., Prentice Hall, 1973.
[64] J. Butcher, Numerical Methods for Ordinary Differential Equations, John Wiley and Sons Ltd, 2008.
[65] D. Antonopoulos, V. Dougalis, Numerical solution of the 'classical' Boussinesq system, Math. Comput. Simulation 82 (2012) 984–1007.
[66] D. Antonopoulos, V. Dougalis, Error estimates for Galerkin approximations of the "classical" Boussinesq system, Math. Comp. 82 (2013) 689–717.

Paper D

On the shoaling of solitary waves in the KdV equation *

* *Published in Proc. 34th Conf. Coastal Engng, Seoul, 2014*

D

ON THE SHOALING OF SOLITARY WAVES IN THE KDV EQUATION

Zahra Khorsand[1], Henrik Kalisch[2]

The evolution of the form of surface waves with a sufficiently slow variation in depth is examined. This study is made of the development of cnoidal Korteweg-de Vries wave on a shoal region. Reconstructing a system based on the wave height and water depth by using the preservation of energy flux, mass and constant period.

Keywords: Solitary wave propagation; wave shoaling; long wave theory; KdV equation

INTRODUCTION

Depending on the magnitude of the forces acting on the water and different speeds of impact, waves occur in different sizes and forms. The study of long waves is of importance to the engineer in the design of harbors and in studying estuaries and lagoons. The literature on long waves shows a considerable number of experimental and numerical investigations of the slow deformation of waves over a sloping bottom.

Although, the classical shoaling solution was first considered for linear waves on an intuitive physical basis by Rayleigh (1911), the theory of cnoidal wave shoaling has been described by several authors. Ostrovskiy and Pelinovskiy (1970) considered a stationary cnoidal Korteweg-de Vries wave (KdV) to evaluate surface-wave deformation with a sufficiently slow variation in depth. As indicated in Ostrovskiy and Pelinovskiy, a sinusoidal wave height, when the modulus of elliptic function m remains small, increases as $h^{\frac{-1}{4}}$ (Green's law). Then m grows rapidly and the wave profile changes from sinusoidal to soliton. For a solitary wave, the wave height increases as h^{-1} (Boussinesq's law).

Svendsen and Brink-Kjær (1972) represented that the variation of the cnoidal wave height are connected to deep water data by the assumption that the energy flux determined by the linear theory and the cnoidal theory is the same at the matching point of $\frac{h}{L_0} = 0.10$, where this point is a deep water limit for cnoidal waves, which gives a discontinuity in wave height. Svendsen and Hansen (1977) considered continuity in wave height thus the calculated relative height values were increased significantly. Sakai and Battjes (1980) applied Cokelet's numerical nonlinear theory to investigate shoaling process and compared their result with existing shoaling curves calculated from different finite amplitude waves theories. They found the shoaling curves calculated from Cokelet's theory predict higher wave height than other curves. Svendsen and Hansen (1978) employed a time-periodic solution of the KdV equation of the second-order approximation to represent the deformation of periodic long waves due to the sloping bottom. In that case the wave deformation at any point of the slope would be determined by the local water depth and bottom slope. To confirm the resulting waves comparison was done with experimental results.

The propagation of a solitary wave in a shoal area has also been investigated by several authors. Numerical solutions to the solitary wave problem have been developed by Hibberd and Peregrine (1979), and analytic solutions were obtained by Synolakis (1987). The evolution of solitary waves over gentle slop depth have been studied by Grimshaw (1971) where he observed that for small values of initial waveheight, the shoaling rates are not exactly given by Boussinesq's law. He found that the shoaling rates approach Boussinesq's law in the limit of zero waveheight. Recently, Kalisch and Senthilkumar (2013) have analyzed shoaling of solitary waves by using conservation of energy in the Boussinesq scaling and their result recover Boussinesq's law.

The propagation of a solitary wave in experiments for gentle slops has also been observed by Ippen and Kulin (1954), and Camfield and Street (1969). Grilli et al. (1994) employed two-dimensional fully nonlinear wave models based on potential flow theory (FNPM) to calculate shoaling of solitary waves over a 1:35 slope. Their results show that exact shoaling rates significantly differ from prediction of both Green's and Boussinesq's laws. An advanced version of this model was used to compute solitary wave variation in over plane slopes by Grilli et al. (1997). Their experiments show that, wave height initially decreases and the rate is lower than predicted by Green's law, and then increases.

In this study we consider the evolution of a cnoidal KdV which agrees well with observations about shoal conditions. The KdV equation was derived in 1895 by Korteweg and de Vries (1895), in dimensional variables is given by

$$\eta_t + c_0\eta_x + \frac{3}{2}\frac{c_0}{h_0}\eta\eta_x + \frac{c_0h_0^2}{6}\eta_{xxx} = 0, \tag{1}$$

[1]Department of Mathematics, University of Bergen, Norway
[2]Department of Mathematics, University of Bergen, Norway

where $\eta(x,t)$ stands for the excursion of the free surface, h_0 denotes the undisturbed water depth, g is the gravitational acceleration and $c_0 = \sqrt{gh_0}$ is taken as the limiting long-wave speed. In the classical long-wave assumptions this equation reveals that $\beta = \frac{h_0^2}{l^2}$ and $\alpha = \frac{a}{h_0}$ are small parameters and $\frac{\alpha}{\beta} = O(1)$, where l represents a typical wave length and a a typical wave amplitude. Equation (1) has stationary solutions, the cnoidal waves

$$\eta = f_2 + (f_1 - f_2)\mathrm{cn}^2\left(\sqrt{\frac{3(f_1 - f_3)}{4h_0^3}}; m\right), \tag{2}$$

are given in terms of the Jacobian elliptic function cn with modulus $m = \frac{f_1 - f_2}{f_1 - f_3}$ and span the range from sinusoidal wave in deep water to solitary wave in shallow water. These solutions depend on three parameters f_1, f_2 and f_3 which can choose to be ordered as $f_3 < f_2 < f_1$. The wave speed C and the wavelength L are given by

$$C = c_0\left(1 + \frac{f_1 + f_2 + f_3}{2h_0}\right), \qquad L = K(m)\sqrt{\frac{16h_0^3}{3(f_1 - f_3)}}$$

where $K(m)$ is the complete elliptic integral of the first kind. In this setup, f_1 and f_2 represent the wave crest and the wave trough, respectively and f_3 appears in both the wave length and wave speed. The aim of the present investigation has been to develop a system related to the wave amplitude at two points of interest as wave shoals by using the energy flux for the KdV equation introduced by Ali and Kalisch (2014). The variation of the height of shoaling can be computed in a straightforward manner.

The paper is made up as follows. First, a brief resume is given of the energy balance for the KdV equation. In the third section, an outline is given of our method and calculations. In the forth section, the calculated waveheight variation is compared with linear theory, Svendsen and Brink-Kjær (1972), Svendsen and Hansen (1977), and Sakai and Battjes (1980) for the case of cnoidal wave and with Grilli et al. (1997) for the solitary wave. Finally, the conclusion is given.

ENERGY BALANCE

For the convenience of the reader, a brief review of the energy balance in the fluid is given here and we refer the reader to Ali and Kalisch (2014) for details.

Consider an inviscid, incompressible fluid of unit density. With Cartesian coordinates (x,z) chosen so that the horizontal $x-$axis is in the direction of wave propagation and with the $z-$axis pointing vertically upwards, the equation of the free surface is $z = \eta(x,t)$, and the fluid domain at time $t \geq 0$ is $\{(x,z) \in \mathbb{R}^2 \,|\, x \in \mathbb{R},\ -h_0 < z < \eta(x,z)\}$. Let $\mathbf{u} = (u(x,z,t), w(x,z,t))$ be the velocity field and $P(x,z,t)$ represents the pressure. The surface water-wave problem is generally given by the Euler equations

$$\mathbf{u}_t + (\mathbf{u}\cdot\nabla)\mathbf{u} + \nabla P = g, \tag{3}$$

$$\nabla\cdot\mathbf{u} = 0, \tag{4}$$

with no-flow conditions at the bottom and kinematic and dynamic boundary conditions at the free surface. From the incompressibility of the fluid and assuming irrotational flow, the problem can be written in terms of the Laplace equation for a velocity potential ϕ. Therefore, the complete problem is given by

$$\eta_t + \phi_x\eta_x - \phi_z = 0, \text{ on } z = \eta(x,t), \tag{5}$$

$$\phi_t + \frac{1}{2}(\phi_x^2 + \phi_z^2) + g\eta = 0, \text{ on } z = \eta(x,t). \tag{6}$$

We perform the following change of variables

$$\tilde{x} = \frac{x}{l}, \qquad \tilde{z} = \frac{z + h_0}{h_0}, \qquad \tilde{\eta} = \frac{\eta}{a}, \qquad \tilde{t} = \frac{c_0 t}{l}, \qquad \tilde{\phi} = \frac{c_0}{gal}\phi$$

yielding the non-dimensionalization of the problem. Following the method explained in Bona and Saut (2002) and Whitham (1974), the non-dimensional KdV equation is

$$\tilde{\eta}_{\tilde{t}} + \tilde{\eta}_{\tilde{x}} + \frac{3}{2}\alpha\tilde{\eta}\tilde{\eta}_{\tilde{x}} + \frac{1}{6}\beta\tilde{\eta}_{\tilde{x}\tilde{x}\tilde{x}} = O(\alpha^2, \alpha\beta, \beta^2)$$

and the non-dimensional velocity field $(\tilde{\phi}_{\tilde{x}}, \tilde{\phi}_{\tilde{z}})$ is given by

$$\tilde{\phi}_{\tilde{x}}(\tilde{x},\tilde{z},\tilde{t}) = \tilde{\eta} + \frac{1}{4}\alpha\tilde{\eta}^2 + \beta(\frac{1}{3} - \frac{\tilde{z}^2}{2})\tilde{\eta}_{\tilde{x}\tilde{x}} + O(\alpha^2, \alpha\beta, \beta^2), \tag{7}$$

$$\tilde{\phi}_{\tilde{z}}(\tilde{x},\tilde{z},\tilde{t}) = \beta\tilde{z}\tilde{\eta}_{\tilde{x}} + O(\alpha\beta, \beta^2). \tag{8}$$

The dynamic pressure P', which measures the deviation from hydrostatic pressure, is given by

$$P' = P - P_{atm} + \rho g z = -\rho\phi_t - \frac{\rho}{2}|\nabla\phi|^2.$$

Using the scaling $\rho g a\tilde{P}' = P'$, the dynamic pressure becomes

$$\tilde{P}' = \tilde{\eta} + \frac{1}{2}\beta(\tilde{z}^2 - 1)\tilde{w}_{\tilde{x}\tilde{t}} + O(\alpha\beta, \beta^2).$$

Now, we examine energy balance of the KdV equation. If it is assumed that the potential energy of a particle is zero at the undisturbed free surface, further the potential energy is zero when there is no wave motion, then the energy balance can be fined by the equation

$$\frac{\partial}{\partial t}\left\{\int_{-h_0}^{\eta}\frac{1}{2}|\nabla\phi|^2 dz + \int_0^{\eta} g z dz\right\} + \frac{\partial}{\partial x}\int_{-h_0}^{\eta}\{\frac{1}{2}|\nabla\phi|^2 + gz + P\}\phi_x dz = 0.$$

Using non-dimensional variables and performing an integration with respect to $\tilde{z}$, the equation becomes

$$\frac{\partial}{\partial\tilde{t}}\left(\alpha^2\tilde{\eta}^2 + \frac{\alpha^3}{4}\tilde{\eta}^3 + \frac{\alpha^2\beta}{6}\tilde{\eta}\tilde{\eta}_{\tilde{x}\tilde{x}} + \frac{\alpha^2\beta}{6}\tilde{\eta}_{\tilde{x}}^2\right) + \frac{\partial}{\partial\tilde{x}}\left(\pm\alpha^2\tilde{\eta}^2 \pm\frac{5}{4}\alpha^3\tilde{\eta}^3 \pm \frac{\alpha^2\beta}{2}\tilde{\eta}\tilde{\eta}_{\tilde{x}\tilde{x}}\right) = O(\alpha^4, \alpha^3\beta, \alpha^2\beta^2).$$

Consequently, the energy density could be written as

$$\tilde{E}^* = \alpha^2\tilde{\eta}^2 + \frac{\alpha^3}{4}\tilde{\eta}^3 + \frac{\alpha^2\beta}{6}\tilde{\eta}\tilde{\eta}_{\tilde{x}\tilde{x}} + \frac{\alpha^2\beta}{6}\tilde{\eta}_{\tilde{x}}^2,$$

and the energy flux becomes

$$\tilde{q}_E^* = \pm\alpha^2\tilde{\eta}^2 \pm \frac{5}{4}\alpha^3\tilde{\eta}^3 \pm \frac{\alpha^2\beta}{2}\tilde{\eta}\tilde{\eta}_{\tilde{x}\tilde{x}}.$$

The dimensional forms are given by

$$E^* = c_0^2\left(\frac{1}{h_0}\eta^2 + \frac{1}{4h_0^2}\eta^3 + \frac{h_0}{6}\eta\eta_{xx} + \frac{h_0}{6}\eta_x^2\right),$$

and

$$q_E^* = \pm c_0^3\left(\frac{1}{h_0}\eta^2 + \frac{5}{4h_0^2}\eta^3 + \frac{h_0}{2}\eta\eta_{xx}\right). \tag{9}$$

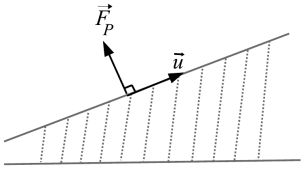

DETERMINATION OF WAVE HEIGHT H

We can follow the variation in wave parameters by considering a constant period and preservation of the energy flux and mass. We assume that the wave motion at water depth h_A is given, then we will find the wave height and other parameters at water depth h by using the following equations:

$$\frac{C_A}{L_A} = \frac{C}{L}, \tag{10}$$

$$\int_0^T q^*_{E_A} dt = \int_0^T q^*_E dt, \tag{11}$$

$$\int_0^L \eta_A dx = \int_0^L \eta dx. \tag{12}$$

Using the expression (9) for q^*_E and introducing for η Equation (2) and noting that

$$\int \mathrm{cn}^2(u)du = u - \frac{u}{m^2} + \frac{E(\mathrm{am}(u), m^2)}{m^2},$$

$$\int \mathrm{cn}^4(u)du = \frac{1}{3m^4}[(2-3m^2)(1-m^2)u + 2(2m^2-1)E(u)$$

$$+m^2 \mathrm{sn}(u)\mathrm{cn}(u)\mathrm{dn}(u)],$$

$$\int \mathrm{cn}^6(u)du = \frac{1}{5m^2}[4(2m^2-1)\int \mathrm{cn}^4(u)du + 3(1-m^2)\int \mathrm{cn}^2(u)du$$

$$+\mathrm{cn}^3(u)\mathrm{sn}(u)\mathrm{dn}(u)],$$

we arrive at the three nonlinear equations. As mentioned before, the wave motion parameters at water depth h_A are given, therefore the expressions in the left-hand side of equations (10),(11) and (12) are known. We consider

$$A_0 = \int_0^T q^*_{E_A} dt, \qquad A_1 = \frac{C_A}{L_A}, \qquad A_2 = \int_0^L \eta_A dx,$$

thus the equation (10) becomes

$$A_1 = \frac{c_0\left(1 + \frac{f_1+f_2+f_3}{2h_0}\right)}{K(m)\sqrt{\frac{16h_0^3}{3(f_1-f_3)}}},$$

and the equation (11) becomes

$$A_0 = c_0^3[T(B_0 + \frac{(m^2-1)}{m^2}B_2 + \frac{B_4}{3m^4}(2-3m^2)(1-m^2) + B_6(\frac{-3}{5m^2}(m^2-1)^2 +$$

$$\frac{4}{15m^6}(2m^2-1)(2-3m^2)(1-m^2))) - (B_2 + \frac{3}{5m^2}(1-m^2) + \frac{2B_4}{3m^2}(2m^2-1)$$

$$+\frac{8B_6}{15m^2}(2m^2-1)^2)\frac{E\sqrt{4h^3}}{c_0 m^2\left(1+\frac{f_1+f_2+f_3}{2h_0}\right)\sqrt{3(f_1-f_3)}}],$$

also the equation (12) reads

$$A_2 = K(m)\sqrt{\frac{16h_0^3}{3(f_1-f_3)}}\left(f_2 + \frac{(m^2-1)(f_1-f_2)}{m^2} + \frac{(f_1-f_2)E_1\sqrt{4h^3}}{m^2\sqrt{3(f_1-f_3)}}\right),$$

where

$$B_0 = \frac{f_1}{h} + \frac{5f_2^3}{4h^2} + \frac{3f_2}{4h^2}(1-m^2)(f_1-f_2)(f_1-f_3),$$
$$B_2 = \frac{2f_2}{h}(f_1-f_2) + \frac{15f_2^2}{4h^2}(f_1-f_2) + \frac{3}{4h^2}(f_1-f_2)$$
$$(f_1-f_3)(2f_2(2m^2-1) + (1-m^2)(f_1-f_2)),$$
$$B_4 = \frac{(f_1-f_2)^2}{h} + \frac{15f_2}{4h^2}(f_1-f_2)^2 + \frac{3}{4h^2}(f_1-f_2)$$
$$(f_1-f_3)(2(2m^2-1)(f_1-f_2) - 3m^2f_2),$$
$$B_6 = \frac{(f_1-f_2)^2}{4h^2}(5(f_1-f_2) - 9m^2(f_1-f_3)),$$

also E and E_1 denote the incomplete elliptic integrals of the second kind over one period and one wave length, respectively. This system of equations has been solved numerically and the parameters for the incident wave at arbitrary water depth h will be obtained. If the depth varies slowly enough, we expect that the wave height H will be a function of depth h. In order to find the variation of wave height, we start with initial data for the cnoidal wave which satisfies the system of equations introduced above and to find the variation of solitary wave height, initial data are chosen in such a way m approaches to one.

RESULTS

The calculation were performed for different values of the deep-water steepness $\frac{H_0}{L_0}$. The curve for $\frac{H_0}{L_0} = 0$ is corresponds to the linear wave theory. The initial data have been chosen in such a way to compare the work done by Svendsen and Brink-Kjær (1972), Svendsen and Hansen (1977), and Sakai and Battjes (1980).

Figure 1 shows three profiles and the corresponding shoaling curves for which $\frac{H}{L}$ is 0.004, 0.002 and 0.001. The parameter $\frac{L}{h}$ is also given for each profile. It may be seen that the wavelength is more than 10 times the water depth, which means that in all cases we are in cnoidal region. As we see in the shoaling panels, the curves presented by Svendsen and Brink-Kjær, which were obtained by matching the calculated energy flux values of the cnoidal theory and linear theory at $\frac{h}{L_0} = 0.1$, have a discontinuity in wave height. We can see variation in wave height given by Svendsen and Brink-Kjær is almost the same as those of the present paper. These panels also show the comparison with curves given by Svendsen and Buhr Hansen, and Sakai and Battjes. Svendsen and Buhr Hansen considered that the wave heights of the cnoidal theory and the linear theory are matched at $\frac{h}{L_0} = 0.1$, therefore the calculated relative wave height values increased significantly and these values are higher than those of the present shoaling curves and the other two curves. The shoaling curves calculated from Cokelet's theory by Sakai and Battjes show the largest growth for all initial steepness and relative depth except for the curves obtained by Svendsen and Buhr Hansen. However, the approach presented in the present paper is much more logical and straightforward.

In Figure 2, we can see a wave profile close to solitary wave for which the initial wave height H_0 is 0.2. Comparison between the present shoaling result and the numerical result obtained by Grilli et al. (1997) and also Boussinesq's law, $H \propto h^{-1}$, and Green's law, $H \propto h^{-1/4}$ is shown in the right panel. As we can see the wave height rate starts lower than both Green's law and the numerical result and then starts diverging from them. In Figure 3, we consider higher wave, $H_0 = 0.4$, and as we see in the right panel close agreement is obtained between the present result and the numerical result. Finally in Figure 4, we consider a wave with the initial height $H_0 = 0.6$ and the corresponding shoaling cure of the present work which is illustrated in the right panel, is in good agreement with the numerical result.

CONCLUSION

The cnoidal wave theory was used to calculate changes in wave height owing to the shoaling of waves. It was shown that there is an increase in wave height according to the decrease in water depth and the variation in wave height for a long wave with small initial amplitude starts diverging from the Green's law curve. The calculation were performed for different values of the deep water steepness $\frac{H}{L_0}$. The calculated values of $\frac{H}{H_0}$ were plotted versus $\frac{h}{L_0}$ for the case of cnoidal theory and $\frac{h}{h_0}$ for the solitary waves. The

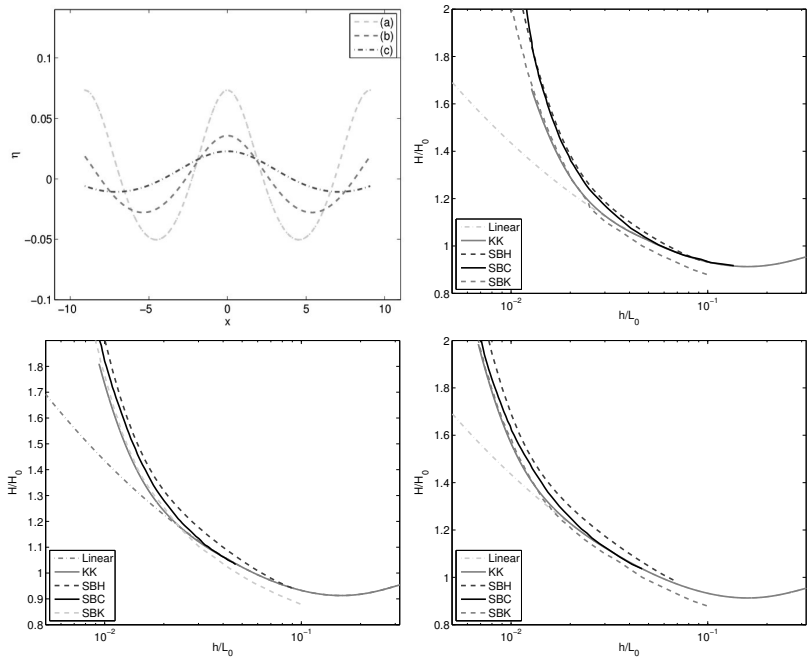

Figure 1: Wave profile and the corresponding shoaling curves.
$(a)\ \frac{H_0}{L_0} = 0.004,\ \frac{L_0}{h_0} = 10.84.\ (b)\ \frac{H_0}{L_0} = 0.002,\ \frac{L_0}{h_0} = 11.9.\ (c)\ \frac{H_0}{L_0} = 0.001,\ \frac{L_0}{h_0} = 13.8.$ **In the upper right panel** $\frac{H_0}{L_0} = 0.004$**, in the lower left panel** $\frac{H_0}{L_0} = 0.002$**, and in the lower right panel** $\frac{H_0}{L_0} = 0.001$ **. The black solid curve, KK, is shoaling curve based on the present paper. The light solid curve, SBC, is shoaling curve after Sakai and Battjes calculated from Cokelet's theory. The light dashed curve, SBK, is shoaling curve after Svendsen and Brink-Kjær. The dashed-datted curve, SBH, is shoaling curve after Svendsen and Buhr Hansen.**

result have been compared with three kinds of previous results which calculated by using different finite-amplitude wave theories: Svendsen and Brink-Kjær (1972), Svendsen and Hansen (1977), and Sakai and Battjes (1980). It was shown the wave height ratio $\frac{H}{H_0}$ of the present curves increases slower than those of the other three kinds of curves. However, the differences were small with curves given by Svendsen and Brink-Kjær (1972) without any discontinuity in wave height.

The shoaling curves of the present paper in the limit of solitary wave were compared with the numerical results obtained by Grilli et al. (1997) and the agreement with the numerical results is good for larger initial wave height.

References

Ali, A. and Kalisch, H. (2014), 'On the formulation of mass, momentum and energy conservation in the kdv equation', *Acta. Appl. Math.* .

Bona, J.L., M. C. and Saut, J.-C. (2002), 'Boussinesq equations and other systems for small-amplitude long waves in nonlinear dispersive media. i: Derivation and linear theory', *J. Nonlinear Sci.* **12**, 283–318.

Camfield, F. and Street, R. (1969), 'Shoaling of solitary waves on small slopes', *J. Wtrwy., Port, Coast., and Oc. Engrg, ASCE* **95**(1), 1–22.

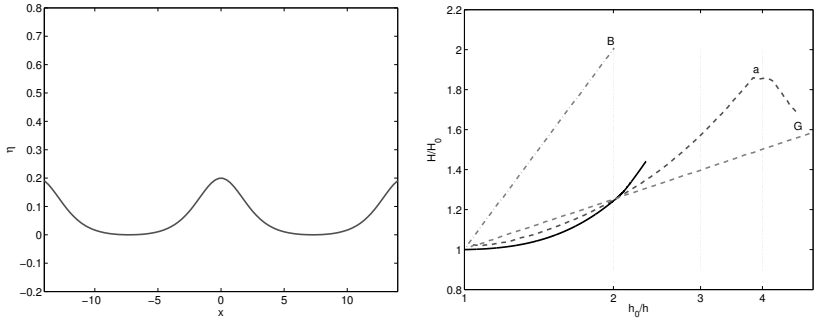

Figure 2: Wave profile and the corresponding shoaling curve with $\frac{L}{h}$ = 14.5, $\frac{H}{h}$ = 0.2, $\frac{H}{L}$ = 0.013. a: shoaling curve after Grilli et al., black solid curve: shoaling curve of the present paper, G: Green's law and B: Boussinesq's law.

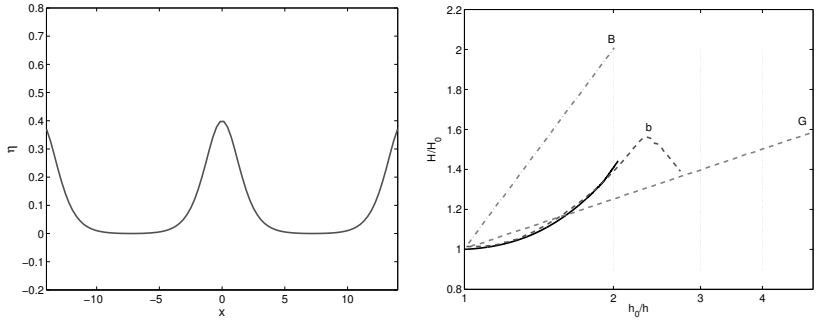

Figure 3: Wave profile and the corresponding shoaling curve with $\frac{L}{h}$ = 14.5, $\frac{H}{h}$ = 0.4, $\frac{H}{L}$ = 0.027. b: shoaling curve after Grilli et al., black solid curve: shoaling curve of the present paper, G: Green's law and B: Boussinesq's law.

Grimshaw, R. (1971), 'The solitary wave in water of variable depth. part 2', *J. Fluid Mech.* **46**, 611–622.

Hibberd, S. and Peregrine, D. (1979), 'Surf and runup on a beach: a uniform bore', *J. Fluid Mech.* **95**(2), 323–345.

Ippen, A. and Kulin, G. (1954), 'The shoaling and breaking of the solitary wave', *Proc. 5th Conf. On Coast. Eng., Grenoble* pp. 27–47.

Kalisch, H. and Senthilkumar, A. (2013), 'Derivation of boussinesq's shoaling law using a coupled bbm system', *Nonlin. Processes Geophys.* **20**(1–7).

Korteweg, D. and de Vries, G. (1895), 'On the change of form of long waves advancing in a rectangular channel and on a new type of long stationary wave', *Philos. Mag.* **39**, 422–443.

Ostrovskiy, L. and Pelinovskiy, E. (1970), 'Wave transformation on the surface of a fluid oa variable depth', *Atmos. Ocean. Phys.* **6**, 552–555.

Rayleigh, L. (1911), 'Wave breaking in boussinesq models for undular bores', *Phil. Mag.* **6**, 177–187.

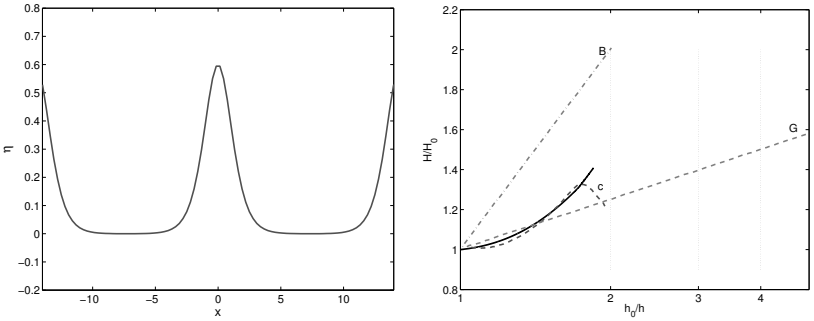

Figure 4: Wave profile and the corresponding shoaling curve with $\frac{L}{h}$ = 14.5, $\frac{H}{h}$ = 0.6, $\frac{H}{L}$ = 0.041. c: shoaling curve after Grilli et al., black solid curve: shoaling curve of the present paper, G: Green's law and B: Boussinesq's law.

Sakai, T. and Battjes, J. (1980), 'Wave shoaling calculated from cokelet's theory', *Coastal Engineering* **4**, 65–84.

Svendsen, I. and Brink-Kjær, O. (1972), 'Shoaling of cnoidal waves', *Proc. 13th Conf. Coastal Engng, Vancouver* pp. 365–383.

Svendsen, I. and Hansen, J. B. (1977), 'The wave height variation for regular waves in shoaling water', *Coastal Engineering* **1**, 261–284.

Svendsen, I. and Hansen, J. B. (1978), 'On the deformation of periodic long waves over a gently sloping bottom', *J. Fluid Mech.* **87**(3), 433–448.

Synolakis, C. (1987), 'The runup of solitary wave', *J. Fluid Mech.* **185**, 523–545.

Whitham, G. (1974), *Linear and Nonlinear Waves*, Wiley, New York.